

Hydrogen sorption properties of the composite system $2\text{NaBH}_4 + \text{MgH}_2$

Vom Promotionsausschuss der
Technischen Universität Hamburg-Harburg
zur Erlangung des akademischen Grades
Doktor der Naturwissenschaften (Dr. rer. nat.)
genehmigte Dissertation

von
Claudio Pistidda

aus
Sassari, Italien

2011

Vorsitzender des Prüfungsausschusses : Prof. Dr. J. Weißmüller

1. Gutachter: Prof. Dr. R. Bormann

2. Gutachter: Prof. Dr. T. Klassen

Tag der mündlichen Prüfung: 9.12.2011

Abstract of the PhD Thesis

Hydrogen sorption properties of the composite system $2\text{NaBH}_4+\text{MgH}_2$

Claudio Pistidda

The hydrogen storage properties of the system $2\text{NaBH}_4+\text{MgH}_2$ are investigated as a model system for the class of Reactive Hydride Composites based on MgB_2 . The hydrogen absorption and desorption mechanisms are thoroughly elucidated. The effect of the applied hydrogen pressure and temperature on the hydrogen absorption mechanism is studied. For a given set of hydrogen pressure and temperature the dependence of the absorption reaction mechanism on the ratio of the starting reactants is also investigated. For the desorption reaction, considerable kinetic improvements are achieved by heating the as milled material in hydrogen pressure. The possibility to improve the desorption reaction by an innovative method of enhancing the effective contact area between reactants is also proposed. This method opens a new path for the kinetic enhancement of multi-compound reaction in the solid state.

Abstract der Dissertation

Wasserstoffspeichereigenschaften des Kompositen-Systems $2\text{NaBH}_4+\text{MgH}_2$

Claudio Pistidda

In dieser Arbeit wurden die Wasserstoffspeichereigenschaften von $2\text{NaBH}_4 + \text{MgH}_2$ als Modellsystem für die so genannten Reaktiven Hydrid Komposite untersucht. Der allgemeine Reaktionsmechanismus der Wasserstoffabsorption und -desorption wird ausführlich erläutert. Zudem wird der Einfluss von Temperatur und Wasserstoffdruck auf den Mechanismus der Absorption untersucht. Für bestimmte Temperaturen und Wasserstoffdrücke konnte eine Abhängigkeit des Mechanismus vom Verhältnis der Edukte gezeigt werden. Die Kinetik des Desorptionsprozess konnte signifikant verbessert werden, indem das Material nach dem Mahlvorgang unter Wasserstoffatmosphäre erhitzt wurde. Weitere Verbesserungen der Desorption konnten durch ein innovatives Verfahren zur Steigerung der effektiven Kontaktfläche zwischen den Edukten erreicht werden. Dieses Verfahren ermöglicht einen neuen Weg zur Verbesserung der Kinetik von Multi-Komponenten-Festphase Reaktionen.

Contents

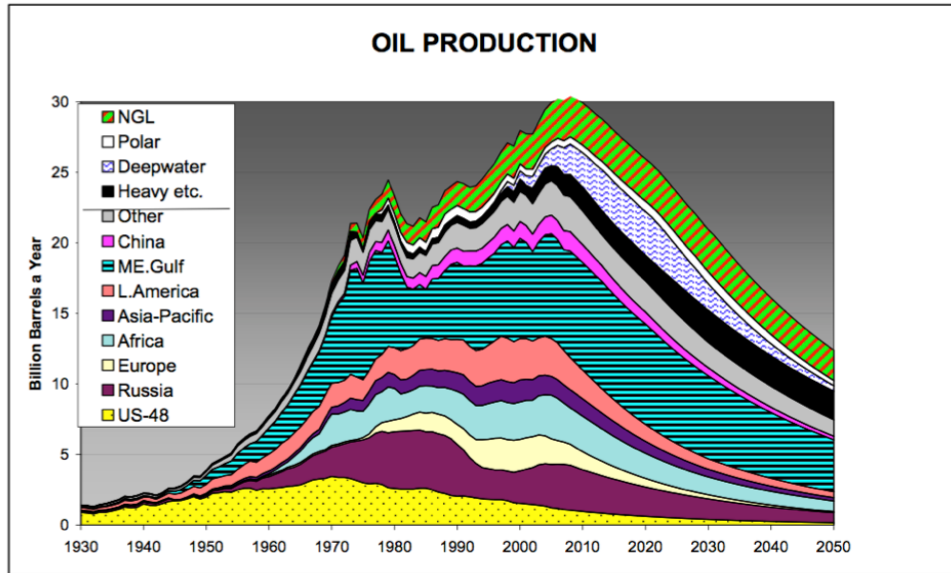
1	Introduction.....	1
1.1	Complex hydrides for hydrogen storage.....	4
1.2	Scope of the work	7
2	Experimental section	9
2.1	Materials.....	9
2.2	Sample preparation.....	10
2.3	Kinetic characterization	11
2.4	Thermal analysis	11
2.5	Ex situ X-ray diffraction	12
2.6	In situ synchrotron radiation powder X-ray diffraction	12
2.7	Electron microscopy.....	13
2.8	Solid state nuclear magnetic resonance.....	14
3	Results.....	17
3.1	The first hydrogen absorption	17
3.1.1	Volumetric analysis.....	17
3.1.2	Thermal analysis	21
3.1.3	In situ SR-PXD characterization.....	23
3.1.4	TEM investigation	25
3.1.5	MAS NMR analysis.....	27
3.2	Effect of the hydrogen pressure on the absorption reaction.....	30
3.2.1	Volumetric analysis.....	31
3.2.2	Thermal analysis	34
3.2.3	In situ SR-PXD characterization.....	35
3.2.4	MAS NMR analysis.....	36
3.3	Effect of NaH/MgB ₂ ratio on the absorption kinetics.....	38

3.3.1	Volumetric analysis.....	38
3.3.2	XRD characterization	39
3.3.3	Thermal analysis	42
3.3.4	In situ SR-PXD characterization.....	43
3.4	The first hydrogen desorption	45
3.4.1	Hydrogen desorption of the as milled system	45
3.4.1.1	Microstructure and phase distribution.....	45
3.4.1.2	Volumetric analysis	46
3.4.1.3	Simultaneous thermal analysis and mass spectroscopy.....	47
3.4.1.4	In situ SR-PXD characterization	48
3.4.2	Optimization of the $2\text{NaBH}_4 + \text{MgH}_2$ desorption properties	50
3.4.2.1	Volumetric analysis.....	50
3.4.2.2	In situ SR-PXD characterization	51
3.4.2.3	MAS NMR analysis.....	53
3.4.2.4	Morphological and microstructural characterization	54
3.4.3	Hydrogen desorption properties of the material exposed to the moist atmosphere	59
3.4.3.1	Volumetric analysis.....	59
3.4.3.2	MAS NMR analysis.....	60
3.4.3.3	Microstructure and phase distribution.....	61
3.4.3.4	In situ SR-PXD characterization	63
4	Discussion	65
4.1	Hydrogen absorption mechanism	65
4.1.1	MgH_2 and NaMgH_3 formation.....	74
4.1.2	Effect of the NaH-NaBH_4 molten phase on the absorption reaction	77
4.2	Hydrogen desorption mechanism	80
4.2.1	Hydrogen treatment effect.....	83
4.2.2	Exposure to the moist atmosphere effect.....	85
5	Outlook	88
6	Summary	93
7	Bibliography.....	96

1 Introduction

Since the late 19th century, humankind has known an uninterrupted period of industrial and economic growth. Discovery of fossil fuels, which provide easy and rapid access to energy, has been the main factor making this possible. However, continuation of this trend of growth is becoming increasingly problematic. According to recent studies ^[1, 2] in the next few decades the fossil fuels, on which almost the total world energy supply relies, will certainly reach a peak (figure 1.1). After that point and without economically suitable alternatives, the economy will suffer an inevitable crisis. From the environmental point of view, excessive use of fossil fuels has disturbed the global climate equilibrium, due to the damaging greenhouse gas emissions ^[3, 4]. In addition, oil recovery from bituminous sands or out of the deep sea carries high environmental risks as clearly shown by the oil spill disaster caused by the Deep water Horizon drilling rig explosion in April 2010.

As an alternative to fossil fuels, hydrogen is widely regarded as a key element for a potential energy solution, capable of solving the issues of both environmental emissions and energy sustainability. Differently from fossil fuels such oil, gas and coal, hydrogen is not a primary energy source, but rather a secondary energy source since it must be produced itself using energy. However, the possibility to produce hydrogen utilizing several and different intermittent renewable resources such as solar energy, wind energy, etc. shows several advantages. On the one hand it will contribute to a drastic reduction of pollutants released in the air, and on the other hand it will significantly contribute to the security of energy supply. In addition, the implementation of the hydrogen as “energy carrier” would result in an effective and synergic utilization of the renewable energy resources. A major obstacle for the use of hydrogen as energy vector is represented by its utilization in the transportation sector. In fact, although for a given amount of energy, hydrogen has the highest energy density by weight if compared to any common fuel, it needs a storing volume which is several times bigger than that requested by common fossil fuels.

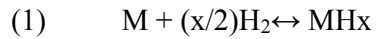


Source: Association for the Study of Peak Oil and Gas

Figure 1.1: Production of: natural gas liquids extraction (NGL), polar crude oil extraction (Polar), offshore crude oil extraction (Deepwater), heavy crude oil extraction (Heavy etc.); Oil extraction in: China (China), in the gulf of Mexico (ME.Gulf), in south America (L.America), in the Asia and Pacific ocean area (Asia-Pacific), in Africa (Africa), in Europe (Europe), in Russia (Russia), in the contiguous United States (US-48), in countries different from the above mentioned (Other).

In this respect, hydrogen storage technology is considered a key roadblock towards the use of H₂ as an effective energy carrier for vehicular applications. So far three main options for storing hydrogen exist: highly pressurized gas, liquefied hydrogen and in metal hydrides chemically bonded hydrogen. The most common method to store hydrogen is to compress it to high pressure gas cylinders. However, pressures in the range of more than 700 bar are required in order to achieve reasonable volumetric storage capacities. Liquid hydrogen offers a gravimetric density higher than compressed gas at ambient temperature. In fact 1 kg of hydrogen gas at atmospheric pressure (1 bar) and ambient temperature (295 K) occupies 11.125 m³, whereas in case of liquid hydrogen it is possible to store 754.275 kg of hydrogen in the same volume at ambient pressure. Unfortunately, the condensation temperature of hydrogen at 1 bar is 20 K only and cryogenic vessels require very efficient thermal insulation

in order to keep the hydrogen liquid. Moreover, despite good insulation, a daily boil-off rate of not less than 1% is inevitable if no additional energy is used to cool the system. On the other hand it is well known that several metals, and in particular transition metals, have a high affinity for the hydrogen. This high affinity leads to the reaction between hydrogen (H₂) and the metal (M) with consequent formation of a metal hydride (MH_x) phase. This process can be described as follows:



Depending on the reacting metal, different types of metal hydrides can be formed. In case of metals like Pd^[5], V, Nb and U, in the hydrogenation process the hydrogen atoms occupy only interstitial sites without causing the topological structure of the metal to change. These hydrides are called interstitial hydrides. In metals such Mg, Pd, Zr and Ti the absorption of hydrogen leads to the formation of crystalline hydride phases^[6]. Several hydrides like those of Mg^[7-11] and Pd^[12-15] have been studied for decades as possible hydrogen storage materials. However, for vehicular applications the gravimetric capacity of these systems is generally too low. In addition, in those cases with higher gravimetric storage capacity the heat of reaction i.e. the value of reaction enthalpy of the hydrogenation reaction is either too strong or too weak for practical applications. Two examples are the hydrides AlH₃ and MgH₂. In the first case the value of reaction enthalpy appears to be too small, in the latter too high. Alane (AlH₃) has a gravimetric hydrogen capacity of ~10 wt.%, however, due to the weak hydrogen binding energy (enthalpy desorption = 5-8 kJ/mol H₂), its direct formation from Al and H₂ is impossible. Magnesium hydride possesses a high hydrogen gravimetric capacity of about 8 wt.% as well, however, in contrast to AlH₃ its strong binding energy (enthalpy desorption = 75 kJ/mol H₂) leads to an equilibrium pressure of only 1 bar at 300 °C. Therefore the tailoring of the reaction enthalpies is a key issue for developing suitable metal hydrides for hydrogen storage. A widely used approach to tune the thermodynamic properties of conventional metal hydrides is the alloying with other elements. However, as main drawback the alloying causes a drastic reduction of the hydrogen storage capacity.

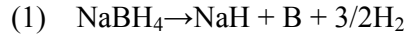
1.1 Complex hydrides for hydrogen storage

Recently, because of their high hydrogen storage capacity, “complex hydrides” attracted considerable attention as potential hydrogen storage materials. This class of material consists of hydride species composed by metal cations (e.g. often lightweight alkali or alkaline earth such Li, Na, Mg or Ca cations) and hydrogen-containing “complex” anions such as alanates^[16], amides^[17] and borohydrides^[18]. Although this class of hydrides has been known for a long time (the first report on pure metal borohydride was published in the beginning of the last century^[19, 20]) they were initially not considered suitable for reversible hydrogen storage purposes. This lack of initial interest can be traced to their apparent irreversibility. In fact, the products of their thermally activated hydrogen desorption could not be rehydrogenated unless very harsh conditions were applied^[21, 22]. In addition, though the possibility to employ them as “one pass” hydrogen-storage system was widely investigated, the on-board irreversibility of the rehydrogenation process made these materials not suitable for automotive applications.

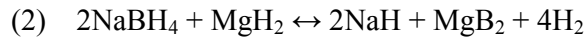
In the 1996 Bogdanovic and Schwickardi^[16] were the first to demonstrate the concrete possibility of reversibly store hydrogen in titanium-based doped NaAlH₄ at moderate temperature and pressure conditions. Since then, many efforts have been made to optimize complex hydrides as potential hydrogen storage materials for vehicular applications. However, before complex hydrides can be efficiently employed in the transportation sector, the issues connected with their high thermodynamic stability and sluggish sorption kinetics still have to be addressed.

In 1967 Reilly et al. discovered the possibility to change the reaction enthalpy of hydride containing composites by mixing them with additives which react reversibly with the hydride during desorption to form a stable compound. He could show that at the expense of hydrogen capacity the reaction enthalpy of a 3MgH₂+MgCu₂ composite is lowered if compared to pure MgH₂^[23]. Recently, this approach of Reilly et al. has been modified by the Chen et al.^[24] and later Vajo et al.^[25] and Barkhordarian et al.^[26] by using mutually destabilizing hydride mixtures which are also called Reactive Hydride Composites. This concept offers the advantage that the high gravimetric storage capacity of the single hydrides is maintained. Very interesting examples for such hydride mixtures are 2NaBH₄ + MgH₂, 2LiBH₄+MgH₂ and Ca(BH₄)₂+MgH₂. One clear illustration of the advantages of using a

hydride mixture instead of a single complex hydride, can be given using as prototype systems NaBH_4 and $2\text{NaBH}_4 + \text{MgH}_2$ (figure 1.2). Pure NaBH_4 has a gravimetric hydrogen capacity of roughly 8 wt.% and dehydrogenates according the following reaction:



The enthalpy change for reaction 1 is equal to 90 KJ/mol H_2 , resulting in an equilibrium pressure of 1 bar at $\sim 500^\circ\text{C}$ [27]. Instead, the dehydrogenation of the corresponding composite system $2\text{NaBH}_4 + \text{MgH}_2$ proceeds as follows:



In this case the gravimetric hydrogen storage capacity is equal to 7.8 wt.% but the reaction enthalpy is only 62 kJ/mol H_2 , which results in an estimated equilibrium pressure of 1 bar at 350°C . The formation of MgB_2 alongside with the decomposition of NaBH_4 results in a significant decrease of the overall desorption reaction enthalpy. The enthalpy decrement is mirrored in a lowering of the estimated equilibrium temperature by roughly 150°C . In addition, the reduced amount of heat which has to be led away from or led in of a potential tank system strongly contributes to improve the energy efficiency of the system.

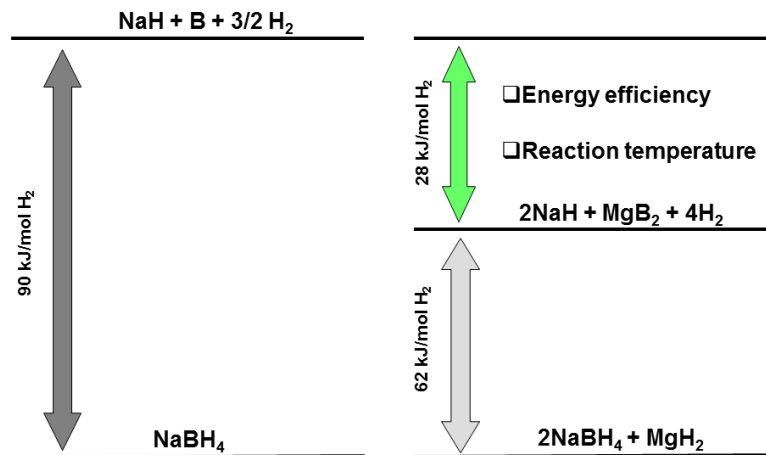


Figure 1.2: Enthalpy diagram for the systems NaBH_4 and $2\text{NaBH}_4 + \text{MgH}_2$.

Although, alloying and the use of selected hydride mixture are powerful tools for tuning the thermodynamic properties of a certain hydrogen storage system, the issue of sluggish kinetics is perhaps the primary challenge associated with this class of materials. Hydrogenation and dehydrogenation reactions in complex hydrides and mixtures of complex hydrides are generally more complicate than in conventional metal hydrides. This difference is mostly due to the involvements of the constituent elements in various reaction steps. For example, the hydrogen desorption from a complex hydride such as a borohydride, requires the bond-breaking of anionic complexes ($[BH_4]^-$) and recombination of the H atoms to form H_2 molecules. In addition, the constituent metal elements may have to undergo long range diffusion before the next reaction step can occur or before a final product can be formed. In the last decades several catalysts or additives have been investigated and employed in order to enhance the sorption properties of complex hydrides. Significant kinetic improvements were reported, however only in a few cases it was possible to clearly identify the atomistic mechanism responsible for the enhancement. As in case of conventional metal hydrides for the complex hydride also the particle-crystallite size distribution of the reactants plays a crucial role on determining the sorption properties of the system. Although, ball milling is a well-known technique and is widely employed on downsizing materials for hydrogen storage, the advantages gained by the use of such method in certain cases vanish upon the material cycling. A method recently applied in order to ensure a fine and stable particle size distribution, is the confinement of the hydride materials, in high surface area scaffolds. Examples of hydrides to which this method was successfully applied are $LiBH_4$ ^[28] and $NaAlH_4$ ^[29]. However, although this approach effectively improves the hydrogen sorption properties of the hydride material it drastically reduces the overall hydrogen capacity of the system ^[30].

1.2 Scope of the work

In the present work, the hydrogen sorption properties of the Reactive Hydride Composite system (RHC) $\text{NaBH}_4/\text{MgH}_2$ are investigated in detail. As pointed out above, the system $2\text{NaBH}_4\text{-MgH}_2$ has a theoretical gravimetric hydrogen capacity of 7.8 wt.%, and an overall reaction enthalpy of $62 \text{ kJmol}^{-1}\text{H}_2$ which results in an estimated equilibrium pressure of 1 bar at $350 \text{ }^\circ\text{C}$ ^[31]. Although for this system the reaction enthalpy value is higher than the required for onboard applications, its study is of primary importance for achieving a basic understanding of the sorption properties of Reactive Hydride Composites. In order to achieve such knowledge both the absorption and desorption were characterized stepwise by means of volumetric analysis, X-ray diffraction, calorimetric technique and solid state nuclear magnetic resonance method.

As stated before, in the Reactive Hydride Composite systems the absorption/desorption processes are characterized by the involvement of the constituent elements in various reaction steps. The reaction steps in which hydrogen is involved, are characterized by specific equilibrium conditions (temperature and pressure). Therefore, since hydrogen takes part in the most of the reaction steps, it is likely that the hydrogen pressure influences the course of the absorption/desorption processes. Clear evidences of the applied hydrogen pressure effect on the sorption reaction mechanism of the Reactive Hydride Composites were recently reported by Vajo et al. ^[32], Bosenberg et al. ^[33] and Price et al. ^[34] regarding the desorption properties of the system $2\text{LiBH}_4+\text{MgH}_2\leftrightarrow 2\text{LiH}+\text{MgB}_2$.

One of the aims of this work is to understand the impact of the applied hydrogen pressure on the pathway and reaction products of $2\text{NaH}+\text{MgB}_2$ absorption process. In order to address this task, the first part of this work focuses on the absorption reaction performed under the pressures of 50, 25 and 5 bar H_2 . Moreover, for the hydrogen absorption performed under 50 bar H_2 , the effect of the NaH/MgB_2 molar ratio on reaction pathway and reaction products was studied. In particular the following compositions were investigated: $1.5\text{Na}/\text{MgB}_2$, NaH/MgB_2 and $0.5\text{NaH}/\text{MgB}_2$.

As pointed out above a problem associated with the use complex hydrides and mixtures of complex hydrides is their high kinetic stability. In this work, the possibility to enhance the $2\text{NaBH}_4+\text{MgH}_2$ hydrogen desorption reaction, by surface modifications is proposed. In a first step, the observed kinetic enhancement subsequent to a combined heat and

hydrogen treatment of the as milled $2\text{NaBH}_4+\text{MgH}_2$ is reported and discussed. Then, the discovery of a new approach which allows achieving fast desorption reaction improving the contact area between reactants in the mixed Reactive Hydride Composite system $2\text{NaBH}_4+\text{MgH}_2$ is also proposed.

2 Experimental section

In this section a brief description of the materials, techniques and utilized instrumentations is given. Due to the multiplicity of the experimental conditions the detailed experimental parameters will be reported later in the corresponding sections.

2.1 Materials

Hereunder the materials used throughout the present work are reported. They are described in terms of purity, and provenance (Table 2.1):

Material	Purity	Company
NaBH ₄	98%	Alfa-Aesar
NaH	95%	Sigma-Aldrich
MgH ₂	95%	Goldschmidt
MgB ₂	99.999%	Alfa-Aesar

Table 2.1: Materials description.

The powder mixture 2NaBH₄+MgH₂ was prepared using NaBH₄ (98% purity) and MgH₂ (95% purity) purchased from Alfa-Aesar and Goldschmidt, respectively.

The powder mixture 2NaH+MgB₂ was prepared using NaH (95% purity) and MgB₂ (99.99% purity) purchased from Sigma-Aldrich and Alfa Aesar, respectively.

During the compilation of this work we observed a sensible variation of the 2NaBH₄+MgH₂ sorption properties for different NaBH₄ batches.

2.2 Sample preparation

All the investigated materials were prepared at the Helmholtz-Zentrum Geesthacht by high-energy ball milling using a Spex 8000 shaker mill or a Fritsch P5 mill. In both cases, hardened stainless steel vials and balls were used. The $2\text{NaBH}_4+\text{MgH}_2$ samples were prepared by first pre-milling MgH_2 for 20 hours in a Fritsch P5 planetary ball mill, with a ball to powder ratio of 10:1. Then NaBH_4 was added to the pre-milled MgH_2 and the mixture milled for additional 20 hours in the planetary ball mill with a ball to powder ratio of 10:1. The ball milled ($2\text{NaBH}_4+\text{MgH}_2$) mixture was divided in three batches. A first batch of material was directly employed for the desorption studies of the as milled system. The second portion of the material was heated in a Sievert's type apparatus up to $300\text{ }^\circ\text{C}$ and then kept one hour under isothermal conditions at 50 bar of hydrogen pressure. For this sample also the desorption properties were investigated (section 3.4.2.1). The last batch of material was furtherly divided into two parts to study the effect of exposure to moistened atmosphere on the desorption properties of the $2\text{NaBH}_4+\text{MgH}_2$ mixture. For this purpose, the milled $2\text{NaBH}_4 + \text{MgH}_2$ (500 mg) was charged in a 100 ml double neck round-bottom flask, which was then evacuated. Subsequently, 2 ml of distilled water were poured in a 100 ml single neck round-bottom flask. The two flasks were connected by means of a 10 cm rubber tube. At this point, the evacuated vessel containing the powder was open leaving the total system at a pressure lower than the atmospheric pressure (the flask containing the powder and the flask containing the water). A first batch of material was prepared exposing the milled powder for one hour to the water moisture, and a second one increasing the exposure time to two hours. The exposed materials were then dried under dynamic vacuum (10^{-2} bar) for 12 hours at room temperature.

The $x\text{NaH}+\text{MgB}_2$ samples were prepared charging simultaneously NaH and MgB_2 into a hardened steel vial and subsequently milling them for 1 hour in a Spex 8000 ball mill, with a ball to powder ratio of 10:1. Handling and milling was always performed in a dedicated glove box under a continuously purified argon atmosphere.

2.3 Kinetic characterization

To evaluate the hydrogen sorption properties of the investigated materials two Sievert's apparatus designed by HERA Hydrogen System and Advanced Materials Corporation were used respectively at the Helmholtz-Zentrum Geesthacht and at the JRC's Institute for Energy in Petten (Netherland). The measurements performed at JRC's were carried out by Dr. Francesco Dolci. The amount of material utilized for each measurement is about 100 mg for the Hera volumetric apparatus and approximately 600 mg for the Advanced Materials Corporation apparatus. The hydrogen absorption measurements were carried out in a range of applied pressures between 5 and 50 bar, by heating up the samples from room temperature (heating rate of 3 °C/min) to the desired final temperatures and then keeping it under isothermal conditions until the end of the experiment. The hydrogen desorption measurements were performed under static vacuum conditions (starting pressure 10^{-2} mbar) heating up the sample from room temperature to 450 °C (heating rate of 3 °C/min) which was then kept under isothermal conditions. The hydrogen release and uptake was determined by measuring the differential pressure between sample holder and an empty reference. Sample holder and reference are of identical design and are subjected to identical pressure and temperature conditions. The measured change in differential pressure is a measure of the amount of released or absorbed hydrogen.

2.4 Thermal analysis

Thermodynamic investigations during hydrogen absorption on the system $2\text{NaH}+\text{MgB}_2$ were performed by HPDSC Netzsch DSC 204 HP Phoenix at the Karlsruhe Institute of Technology. The HPDSC measurements were carried out in dynamic mode under constant pressure in a range of temperature of 25-400 °C, with a constant heating rate of 5 °C/min. The amount of material used for each measurement was roughly 20 mg. The crucibles and lids used as sample holder and reference are made of Al_2O_3 and were directly provided by Netzsch. The measured The HP-DSC apparatus was placed in a dedicated glove box under a continuously purified argon atmosphere.

2.5 Ex situ X-ray diffraction

X-ray diffraction is a powerful technique to gain a wide range of structural information regarding the investigated materials. In fact quantitative and qualitative analysis of the crystallite phase compositions, crystallographic structures and crystallite domain sizes are possible by means of a normal laboratory X-ray diffractometer. In this work X-ray diffraction analysis were carried out using a Siemens D5000 X-ray diffractometer, a Philips XPERT diffractometer (Bragg-Brentano configuration) with XCellerator RTMS detector and a Bruker D8 Advance X-ray diffractometer all using Cu K α radiation ($\lambda = 1.5406 \text{ \AA}$). In order to avoid the exposure of the sample to the air a particular sample holder equipped with an airtight Kapton foil was used. A part of the XRD characterization was performed outside of Helmholtz-ZentrumGeesthacht at the JRC's Institute for Energy in Petten (Netherland). The measurements performed at JRC's were carried out by Dr. Francesco Dolci. For these measurements the material was dispersed in high vacuum grease and deposited on a aluminum plate.

2.6 In situ synchrotron radiation powder X-ray diffraction

The phase evolution during the absorption/desorption process were investigated by *in situ* synchrotron radiation powder X-ray diffraction (SR-PXD). The measurements were performed in transmission mode at the beamline I711 at the Max II synchrotron in Lund. The radiation source was a 1.8 T multipole wiggler. The beam was focused vertically by a bendable mirror and horizontally by an asymmetrically cut Si (111) monochromator^[35]. The range of available wavelength was 0.08-0.155 nm. The I711 beamline was equipped with a MAR 165 charge coupled device (CCD) plate detector, with a pattern recording time of 15-20 seconds. A special sample holder designed for in-situ monitoring of solid/gas reactions was utilized^[33, 36, 37]. Hydrogen pressures up to 150 bar and temperatures up to 600 °C could be applied.

2.7 Electron microscopy

The microstructure of the system $2\text{NaBH}_4+\text{MgH}_2$ was investigated upon hydrogen desorption and absorption by means of electron microscopy. Several specimens were prepared at Helmholtz-Zentrum Geesthacht and FZK using Sievert's type apparatus, HP-DSC and then characterized by transmission electron microscopy (TEM) and scanning electron microscopy (SEM). The TEM analyses were performed in the department of materials at the University of Oxford together with Dr. Christopher Nwakwuo, Dr. John Sykes and Dr. John Hutchison. Material handling and sample preparation for TEM were done in a dedicated glove box under a purified argon atmosphere. A ground powder sample was mixed with n-hexane and a drop of the supernatant liquid placed on a lacey-carbon copper TEM grid. TEM and high resolution electron microscopy (HREM) investigation were carried out using the JEOL-JEM-3000F field emission gun (FEG) microscope at 300 kV with a point resolution of 0.16 nm. It is also equipped with a high angle annular dark field (HAADF) detector, Gatan imaging filter (GIF), Mega scan CCD camera and an Oxford Instrument energy dispersive X-ray (EDX) spectrometer.

The materials were analyzed by SEM at Helmholtz-Zentrum Geesthacht. SEM investigations were carried out using the ZEISS DSM 962 Scanning electron microscope. The material was spread onto a double sided adhesive, electrically conductive carbon sheet under a continuously purified argon atmosphere and then transferred in the electron microscope. Although, particular attention in avoiding the oxygen contamination of the specimens was paid, this could not be ensured completely. This is true in particular for the SEM measurements where the samples had to be directly exposed to the atmospheric air for roughly thirty seconds in order to transfer them into the machine.

2.8 Solid state nuclear magnetic resonance

Several specimens with different hydrogenation degree were prepared at Helmholtz-Zentrum Geesthacht and FZK using Sievert's type apparatus, HP-DSC and then characterized by solid state Nuclear Magnetic Resonance (NMR) technique at the Servei de Ressonància Magnètica Nuclear (SeRMN) (Universitat Autònoma de Barcelona, 08193 Bellaterra, Spain). The measurements were performed by Dr. Sebastiano Garroni.

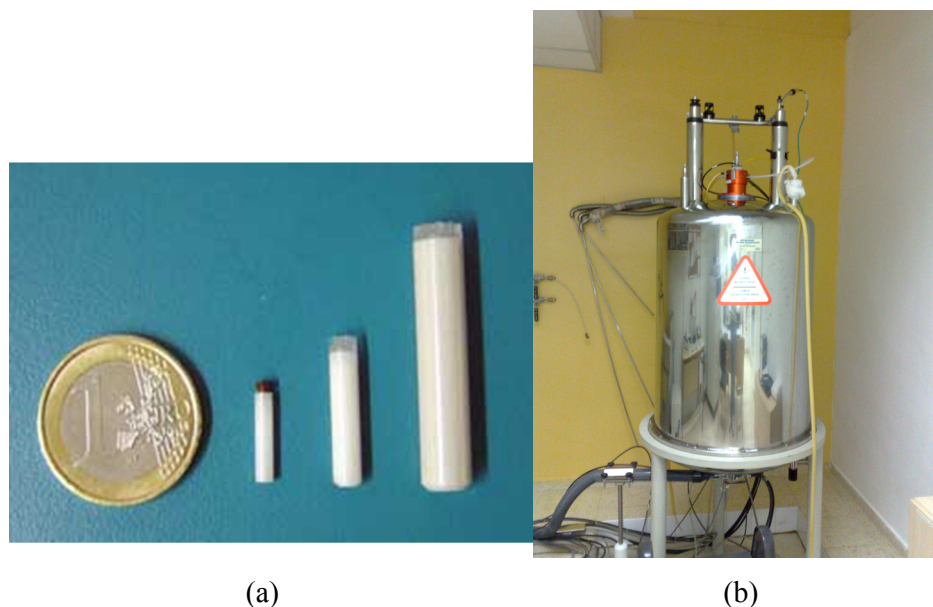


Figure 2.1: (a) ZrO_2 rotors and (b) Bruker Avance 400 MHz spectrometer at the Servei de Ressonància Magnètica Nuclear (SeRMN) Universitat Autònoma de Barcelona, Bellaterra, Spain.

Solid state NMR under Magic Angle Spinning conditions (MAS) has recently been demonstrated to be a powerful technique to study materials for hydrogen storage. Due to the fact that the ^{11}B chemical shift allows a fast identification of the boron containing species, this technique was successfully implemented for the study of metal borohydrides and aluminoboranes [33, 38-40]. In this study, we used single pulse $^{11}B\{^1H\}$ NMR and $^{23}Na\{^1H\}$ NMR under MAS conditions in order to visualize the chemical state of boron and sodium during hydrogen desorption and absorption of the system $2NaBH_4+MgH_2$. Nuclear Magnetic Resonance

(NMR) spectra were measured using a Bruker Avance 400 MHz spectrometer (figure 1.1 b) with a wide bore 9.4 T magnet and employing a boron-free Bruker 4 mm CPMAS probe. The spectral frequencies were 128.33 MHz for ^{11}B nucleus and 105.85 for the ^{23}Na nucleus, the NMR shifts are reported in parts per million (ppm) externally referenced to $\text{BF}_3\cdot\text{O}(\text{CH}_2\text{CH}_3)_2$ and NaCl respectively. In the NMR analysis reported in this work the main peak spinning side bands are indicated with the sign *. The powder materials were packed into 4 mm ZrO_2 rotors (figure 1 A) in an argon-filled glove box and were sealed with tight fitting Kel-F caps. Sample spinning was performed using dry nitrogen gas. The one dimensional (1D) ^{11}B MAS NMR spectra were acquired after a $2.7\ \mu\text{s}$ single $\pi/2$ (corresponding to a radio field strength of 92.6 kHz) and with application of a strong ^1H decoupling by using the two-pulse phase modulation (TPPM) scheme^[41]. The recovery delay was set to 10 seconds. Spectra were acquired at 20°C temperature controlled by a BRUKER BCU unit.

3 Results

The absorption and desorption processes of the system $\text{NaBH}_4\text{-MgH}_2$ were studied in detail by means of volumetric measurements, calorimetric techniques, in and ex situ XRD analysis, electron microscopy (TEM and SEM) and MAS NMR characterization of selected samples.

In this section the hydrogen absorption process will be characterized and the effects of the applied hydrogen pressure and of the NaH/MgB_2 ratio will be investigated in detail. Then, in second part the hydrogen desorption process of the as milled $2\text{NaBH}_4\text{+MgH}_2$ will be analyzed. Regarding the desorption process the beneficial effect of a pretreatment of the as milled material by a heat-hydrogen process or by exposure to water saturated atmosphere will be described also.

3.1 The first hydrogen absorption

A preliminary hydrogen absorption test on the as milled 2NaH+MgB_2 was performed under 50 bar of hydrogen and at a final temperature of 400 °C. These conditions were chosen arbitrarily in order to ensure a fast hydrogen absorption reaction.

3.1.1 Volumetric analysis

The hydrogen absorption kinetics of the as milled 2NaH+MgB_2 is shown in figure 3.1. The measurement was performed at 50 bar of hydrogen pressure, heating the material from RT to 400 °C with a heating rate of 3 °C/min, and subsequently keeping it under isothermal conditions at 400 °C for several hours. The hydrogen absorption starts at roughly 250 °C and in two separate steps of about 0.6 and 3.2 wt.% reaches a total amount of absorbed hydrogen equal to 3.8 wt.%. During the isothermal period at 400 °C the hydrogen uptake apparently stops after ~ 1h without reaching the expected theoretical gravimetric hydrogen storage capacity (7.8 wt.%). Aiming to understand the reasons of the hydrogen uptake stop before

achieving the theoretical storage capacity, the absorption products (roughly 120 mg) were investigated by XRD analysis (figure 3.2). Among the absorption products it is possible to observe the presence of NaBH_4 (43.82 wt.% (± 4)), NaMgH_3 (19.14 wt.% (± 2)) and free Mg (5.88 wt.% (± 1)) in addition to the starting reactants NaH (22.07 wt.% (± 2)) and MgB_2 (5.10 wt.% (± 1)) and a small amount of NaOH (3.54 wt.% (± 1)). Surprisingly, NaMgH_3 and free Mg are present instead of the expected MgH_2 . In fact, at 50 bar of hydrogen and 400 °C MgH_2 is thermodynamically more stable than Mg. The presence of un-reacted material together with NaMgH_3 and free Mg clearly justify the not achieved theoretical hydrogen storage capacity (7.84 wt.%). In addition, the material after absorption appears to “wets” the inner walls of the sample holder. For this reason we assume that one or more absorption reaction steps occur via molten state.

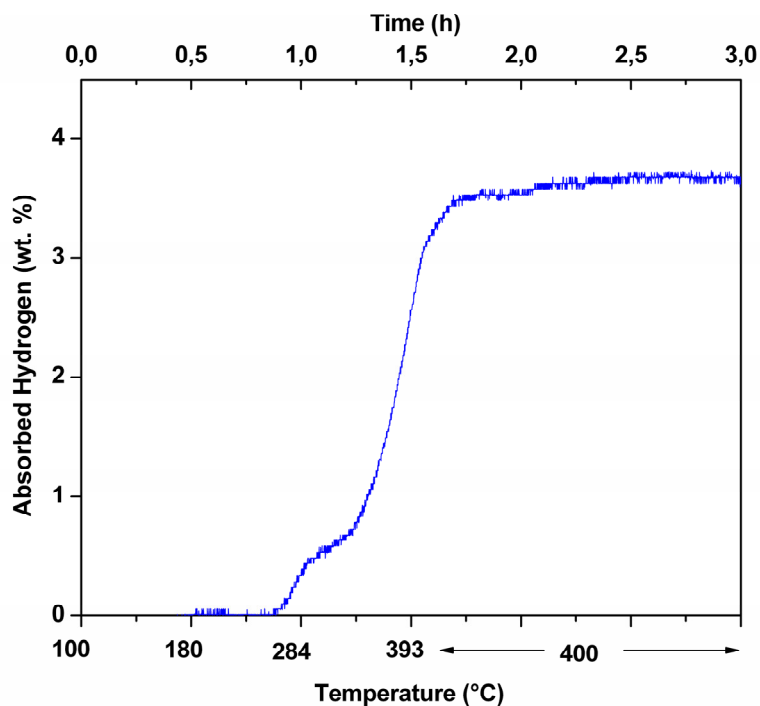


Figure 3.1: Absorption kinetic of as milled $2\text{NaH}+\text{MgB}_2$ measured in a Sievert's -Type apparatus. The sample was heated at 50 bar of hydrogen pressure from RT to 400 °C (heating rate of 3 °C/min) and then kept under isothermal conditions for several hours.

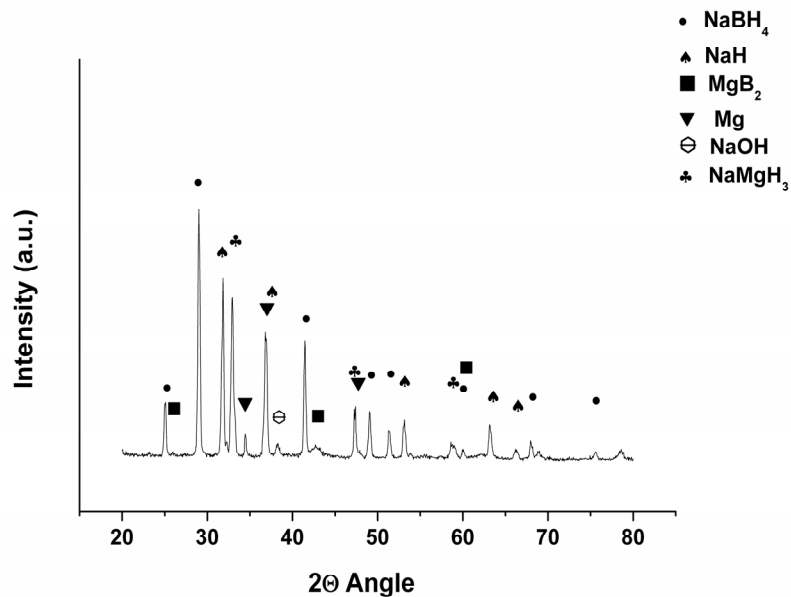


Figure 3.2: XRD pattern of $2\text{NaH}+\text{MgB}_2$ after absorption under 50 bar of hydrogen pressure at $400\text{ }^\circ\text{C}$ (wavelength = 0.154184 nm).

The XRD analyses shown in figure 3.2 describe the average composition of hydrogenated material. However, morphological differences between the material at the topmost and bottom part of the sample holder suggest a possible different material distribution within the same specimen. In fact, the material at the topmost part of the sample holder is dense whereas the material at the bottom of the sample holder is powdery. In order to investigate the material distribution a second batch of $2\text{NaH}+\text{MgB}_2$ was hydrogenated at the same conditions as used for the previous absorption. The material obtained was then divided in several parts. The portions of material at the topmost and bottom of the sample holder (roughly 5 mg each) were analyzed by XRD technique (figure 3.3). The weight fraction of all involved phases was calculated by Rietveld's method and reported in table 3.1. Clearly, the compositions of the two materials are strongly different. The material at the topmost part of the sample holder (figure 3.3 A) includes a mixture of NaBH_4 (19.77 wt.% (± 2)), MgB_2 (36.31 wt.% (± 4)), NaMgH_3 (10.27 wt.% (± 1)), Mg (6.12 wt.% (± 1)), NaH (19.81 wt.% (± 2)), Na (7.31 wt.% (± 1)) and NaOH (3.28 wt.% (± 1)). Differently, the material at the bottom of the sample holder (figure 3.3 B) contains NaBH_4 (57.55 wt.% (± 5)), MgB_2 (22.14 wt.% (± 2)), NaMgH_3 (17.11 wt.% (± 2)) and Mg (3.18 wt.% (± 1)). These results clearly show how the distribution of the

final absorption products results highly inhomogeneous although the composition of the starting material was homogeneous. Interestingly, the material in the upper part of the sample holder appears to be richer of the starting reactants whereas at the bottom of the sample holder the presence of the absorption products is predominant. It must be noticed that although Na is visible among the phases present at the top of the sample holder, its presence in the diffraction pattern of figure 3.2 was not detected. This is due to the fact that whereas the amount of Na present in the portion of sample analyzed (roughly 5 mg) in figure 3.3 A is significant, its amount is negligible when the all sample is considered (roughly 120 mg).

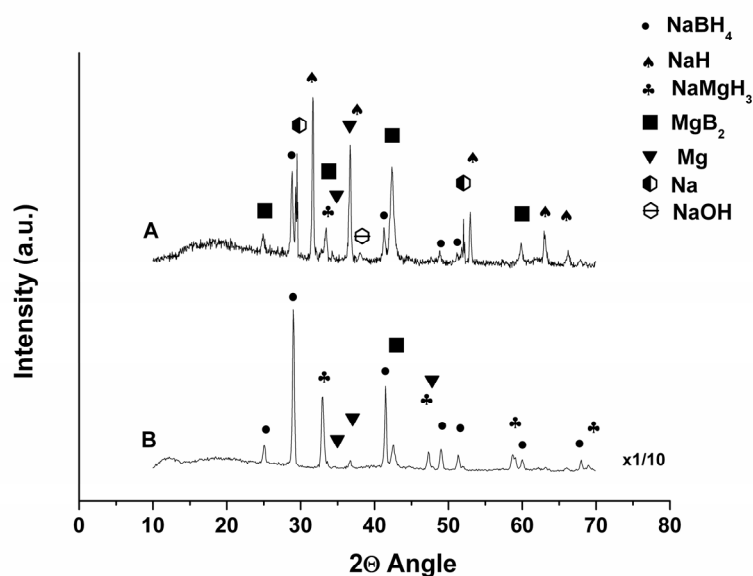


Figure 3.3: XRD pattern of $2\text{NaH} + \text{MgB}_2$ after absorption under 50 bar of hydrogen pressure at 400 °C (wavelength = 0.154184 nm): A) material at the top of the sample holder, B) material at the bottom of the sample holder.

Phase	Material at the top of the sample holder	Material at the bottom of the sample holder
NaBH ₄	19.77 wt.% (±2)	57.55 wt.% (±5)
MgB ₂	36.31 wt.% (±4)	22.14 wt.% (±2)
NaMgH ₃	10.27 wt.% (±1)	17.11 wt.% (±2)
Mg	6.12 wt.% (±1)	3.18 wt.% (±1)
NaH	19.81 wt.% (±2)	0 wt.%
NaOH	3.28 wt.% (±1)	0 wt.%
Na	7.31 wt.% (±1)	0 wt.%

Table 3.1: Phases weight fraction (wt.%).

3.1.2 Thermal analysis

In order to visualize the sequence of events taking place during the heating of the 2NaH+MgB₂ in hydrogen pressure a HP-DSC analysis was performed. Figure 3.4 shows the HP-DSC trace recorded at 50 bar of hydrogen pressure, measured from room temperature to 400 °C and then cooled to room temperature (constant heating/cooling rate 5 °C/min). This measurement shows during heating the presence of three main peaks: two exothermic events with respective onsets at 270 °C and 353 °C and one sharp endothermic peak at 330 °C. During cooling, two exothermic peaks with onset temperature of 367 °C and 316 °C are observed.

Aimed at investigating the whole absorption process, a second HP-DSC analysis was performed (figure 3.5). The material was heated up to 400 °C under 50 bar of hydrogen pressure and then kept at 400 °C for 90 minutes before being cooled down to room temperature (heating/cooling rate of 5 °C/min.). The heating period of the HP-DSC curve shown in figure 3.5 clearly traces out the HP-DSC analysis previously reported in figure 3.4. During the isothermal period at 400 °C no significant further events were observed. However,

the cooling segment (figure 3.5) differently from the trace of figure 3.4 shows the presence of only a single exothermic signal with onset at 367 °C.

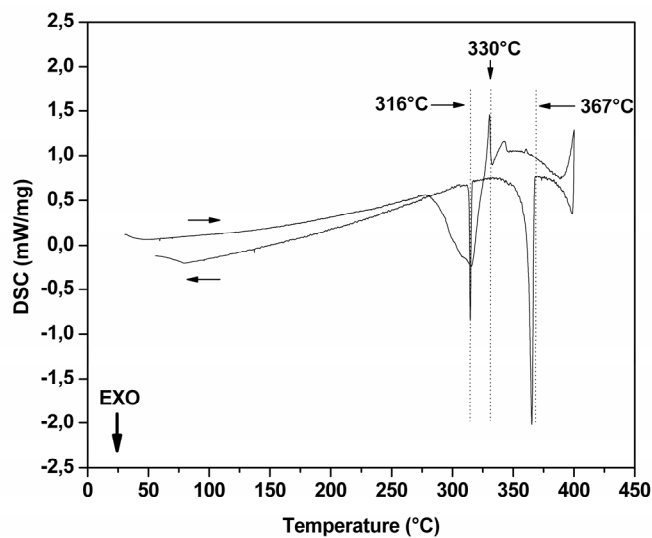


Figure 3.4: HP-DSC trace of the $2\text{NaH}+\text{MgB}_2$ absorption reactions, measured at 50 bar of hydrogen pressure from RT to 400 °C and subsequently cooled (5 °C/min heating/cooling rate).

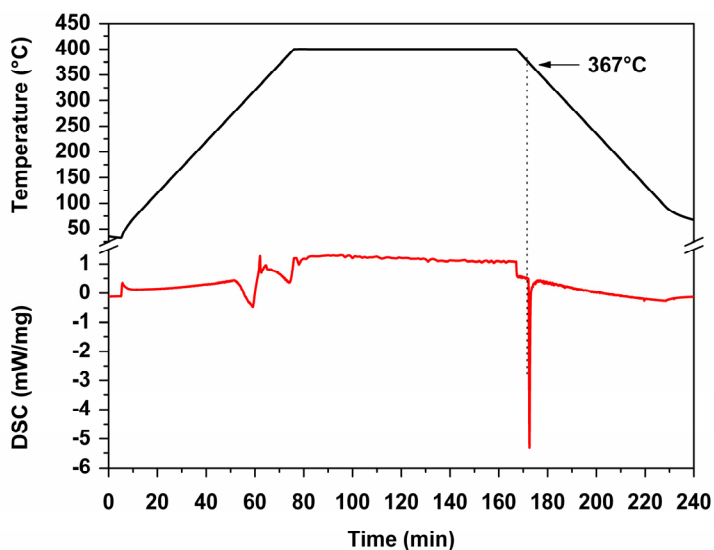


Figure 3.5: HP-DSC trace of the $2\text{NaH}+\text{MgB}_2$ absorption reactions, measured at 50 bar of hydrogen pressure from RT to 400 °C and then kept under isothermal condition at 400 °C for 90 minutes and subsequently cooled (5 °C/min heating/cooling rate).

3.1.3 In situ SR-PXD characterization

With the aim to clarify the undergoing hydrogenation mechanisms *in situ* SR-PXD patterns were measured. Figure 3.6 shows the measurement carried out at 50 bar of hydrogen pressure, in scanning temperature from RT to 400 °C and then cooling to 240 °C with a heating/cooling rate of 5 °C/min. The phases in the starting material are NaH and MgB₂. Upon heating, due to thermal expansion all peaks shift continuously towards lower 2 Θ angles. At roughly 280 °C the formation of an unknown crystalline phase with major reflection at 14.36, 16.59, 19.54, 23.54 and 27.792 Θ angle (wavelength = 0.1072 nm) is observed. This phase is found to be stable up to 325 °C, and then its diffraction peaks disappear. Moreover at roughly 330 °C the formation of NaMgH₃ starts. This is accompanied by a significant decrease of the NaH diffracted intensity. Formation of NaMgH₃ continues up to a temperature of 350 °C. NaMgH₃ formation and the disappearance of NaH are followed by the formation of an amorphous background at 19.50 2 Θ angle. After forming, this amorphous background remains almost constant until the temperature reaches 400 °C. At 380 °C reflections of crystalline NaBH₄ appear and continuously grow until the final temperature 400 °C is reached.

The cooling period is characterized by the progressive intensity rising of the NaH reflections plus two more events, which take place at 370 and 320 °C, respectively. At roughly 370 °C the intensity of NaBH₄ and NaH peaks quickly rise and later at about 320 °C, the peaks related to the unknown phase observed during the heating period reappear. Simultaneously with these two events which are described above, the amorphous background disappears completely. In a second experiment the starting material 2NaH+MgB₂ was heated to 400 °C in 50 bar H₂ and then kept at this temperature. The temperature and pressure at which the measurement was performed were chosen in order to simulate the absorption process carried out in the Sievert's type apparatus (figure 3.7, wavelength = 0.109719 nm). The sequence of events taking place during the heating period, exactly trace out those described for figure 3.6. The isothermal period at 400 °C is characterized by the complete disappearing of the NaH peaks and the growth of NaBH₄ phase, which takes place within the first 30 minutes of the isothermal period. It must be noticed, that NaBH₄ formation is followed by the simultaneous appearance of free Mg.

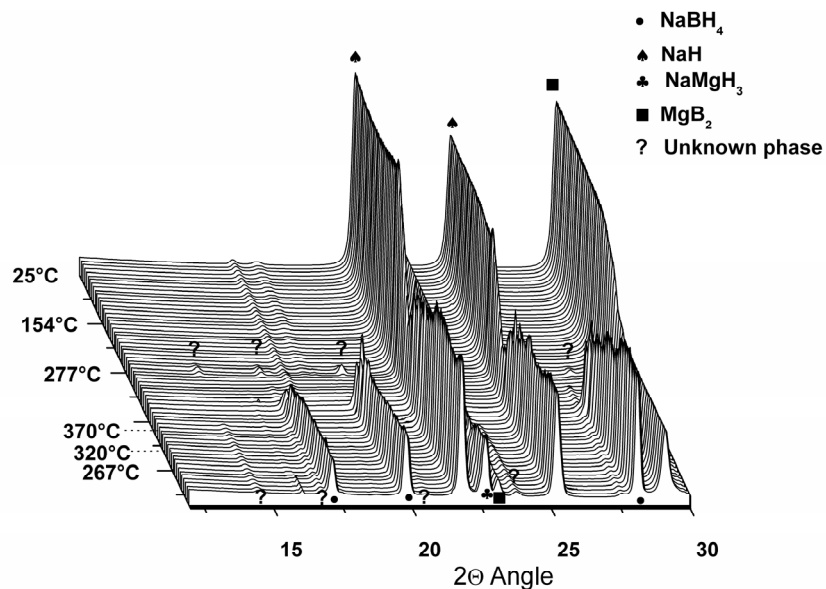


Figure 3.6: Series of SR-PXD patterns of the $2\text{NaH}+\text{MgB}_2$ system heated under 50 bar hydrogen pressure from RT to 400 °C and cooled to 240 °C (5 °C/min, wavelength = 0.1072 nm). The measurement was obtained at the beamline I711 at the Max II synchrotron in Lund.

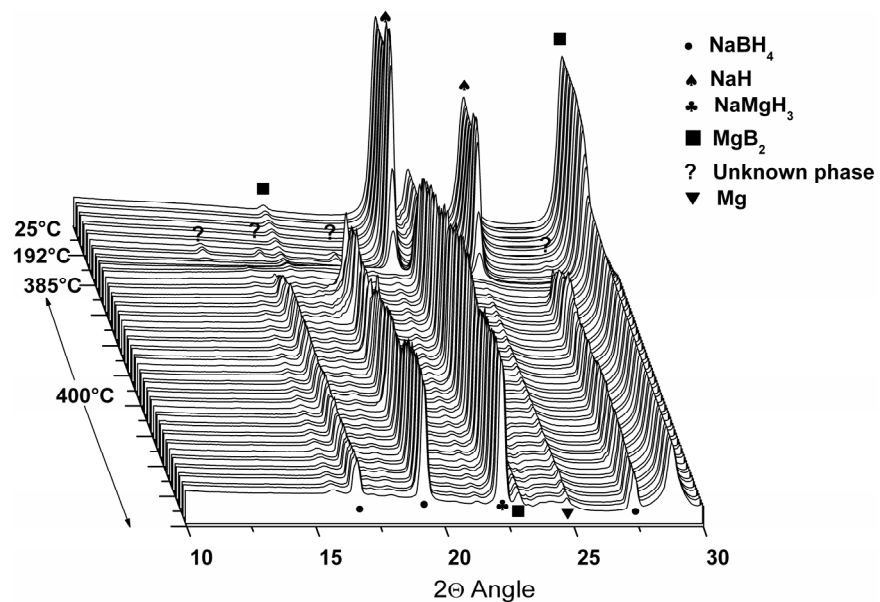


Figure 3.7: Series of SR-PXD patterns of the $2\text{NaH}+\text{MgB}_2$ system heated under 50 bar hydrogen pressure from RT to 400 °C and then kept under isothermal condition (5 °C/min, wavelength = 0.109719 nm). The measurement was obtained at the beamline I711 at the Max II synchrotron in Lund.

3.1.4 TEM investigation

The microstructural evolution of the material during the absorption process was characterized by means of TEM. Figure 3.8 shows the high resolution TEM image (picture a) and the XRD pattern (picture b) of the as milled $2\text{NaH}+\text{MgB}_2$. In the diffraction pattern of figure 3.8 b NaH and MgB_2 are observed as the component phases of the system. Hence, neither significant decomposition nor contamination (e.g. oxygen, iron) of the starting materials took place during the milling period. These two phases are clearly visible also in the high resolution image of figure 3.8 a were based on an inter-planar distance of 0.283 and 0.2127 nm respectively the family of plan (111) for NaH and the (101) for MgB_2 are identified. On the left hand side of figure 3.8 a the presence of an amorphous region is visible. This region is most probably generated by the destructive interaction between the electron beam and the sample. Analyzing the diffraction pattern (figure 3.8 b) by the Rietveld's method using the program MAUD an average crystallite size of 63 and 38 nm respectively for NaH and for MgB_2 was calculated.

The high-resolution TEM image of the material heated at 50 bar of hydrogen pressure up to 310 °C and subsequently cooled to room temperature is shown in figure 3.9 a. The material appears to be constituted in the majority by un-reacted NaH and MgB_2 plus a small fraction of an unidentified phase, which with all probability is the unknown phase observed in the SR-PXD analysis of figure 3.6 and 3.7. In figure 3.9 b the high resolution TEM analysis of material hydrogenated at 400 °C under 50 bar of hydrogen pressure is reported.

In this analysis, NaH, MgB_2 , NaBH_4 and NaMgH_3 are visible. In particular the (111) planes of NaH, the (101) of MgB_2 , the (200) of NaBH_4 (inter-planar distance equal to 0.307 nm) and (111) for NaMgH_3 (inter-planar distance equal to 0.272 nm) are recognizable. Differently from the SR-PXD analysis of figure 3.7 the free Mg is not observed. The phases in figure 3.9 b are distributed in the following way: the top side and the bottom side are occupied respectively by un-reacted NaH and MgB_2 . On the right hand side NaMgH_3 first and the NaBH_4 after are visible. The formation of NaMgH_3 and NaBH_4 seems to take place preferentially around MgB_2 . In fact a high overlapping of the lattice planes of MgB_2 with the

lattice planes of NaMgH_3 and NaBH_4 is noticed. No overlapping between the lattice planes of NaH and NaMgH_3 or NaBH_4 can be observed.

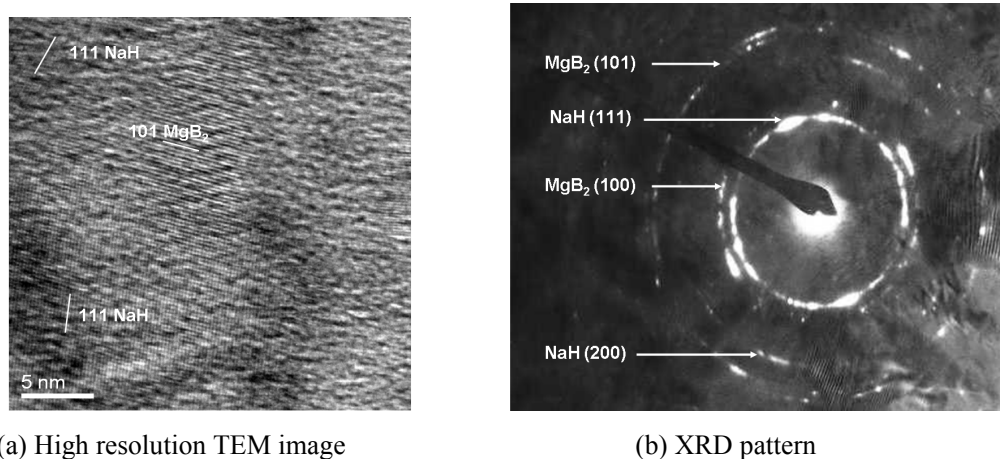


Figure 3.8: (a) High resolution TEM image and (b) XRD patter of the as milled $2\text{NaH}+\text{MgB}_2$. The measurement was obtained at the University of Oxford using the JEOL-JEM-3000F field emission gun (FEG) microscope.

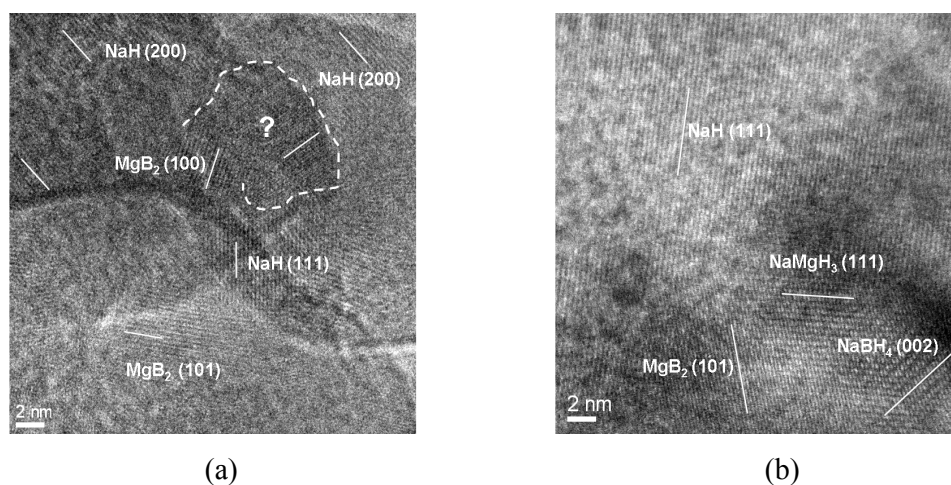


Figure 3.9: TEM image of $2\text{NaH}+\text{MgB}_2$ hydrogenated under 50 bar of hydrogen pressure at $310\text{ }^\circ\text{C}$ (a) and completely hydrogenated at $400\text{ }^\circ\text{C}$ (b). The measurement was obtained at the University of Oxford using the JEOL-JEM-3000F field emission gun (FEG) microscope.

3.1.5 MAS NMR analysis

Due to the possible formation of amorphous compounds, the employment of the MAS NMR technique has been necessary to further elucidate the $2\text{NaH} + \text{MgB}_2$ hydrogen absorption reaction. Several specimens with different hydrogenation degrees were prepared at a hydrogen pressure of 50 bar in a HP-DSC Netzsch DSC 204 HP Phoenix and then characterized. The single pulse $^{11}\text{B}\{^1\text{H}\}$ and $^{23}\text{Na}\{^1\text{H}\}$ NMR analysis are shown in figure 3.10 and figure 3.11 respectively. The $^{11}\text{B}\{^1\text{H}\}$ spectra collected for the as milled material (figure 3.10 A) shows a peak at 96.51 ppm, due to the presence of MgB_2 and although small, a further signal is visible at -42.00 ppm. The presence of this last signal (at -42.00 ppm), suggests a partial formation of NaBH_4 already during milling, however it does not find confirmation in the $^{23}\text{Na}\{^1\text{H}\}$ MAS NMR analysis of figure 3.11 A. In fact, despite the signal observed at -42.00 ppm in figure 3.10 A, the $^{23}\text{Na}\{^1\text{H}\}$ spectrum of the as milled $2\text{NaH} + \text{MgB}_2$ (figure 3.11 A) shows only the signal related to NaH (10.84 ppm). Therefore, the signal at -42 ppm is not due to the formation of NaBH_4 . The investigation of the phase generating the signal at -42.00 ppm (figure 3.11 A) is still in progress.

A first hydrogen charged specimen was prepared by heating the as milled material from room temperature up to a final temperature of 300 °C (heating rate 5 °C/min) under a pressure of 50 bar of hydrogen, and subsequently cooling it down to room temperature. According to the HP-DSC analysis of figure 3.4 and the SR-PXD data shown in figure 3.6, this sample is expected to contain only the observed unknown crystalline phase together with the starting reactants. The presence of this additional phase among the starting reactants is confirmed by both $^{11}\text{B}\{^1\text{H}\}$ and ^{23}Na NMR analysis. In the $^{11}\text{B}\{^1\text{H}\}$ spectra (figure 3.10 B) an intensity increment of the already present peak at -42.00 ppm is clearly visible in addition to the signal at 96.51 ppm of the B- atoms contained in the MgB_2 . Moreover with respect to the as milled material (figure 3.11 A), the $^{23}\text{Na}\{^1\text{H}\}$ spectra (figure 3.11 B) shows the presence of two more signals at -11.71 and at -15.85 ppm. These two new peaks hint to the presence of the unknown crystalline phase. The last sample was prepared by heating the as milled material from room

temperature up to a final temperature of 400 °C (heating rate 5 °C/min) under 50 bar of hydrogen, and finally keeping it at 400 °C for 2 hours. For this material the $^{11}\text{B}\{^1\text{H}\}$ NMR spectra (figure 3.10 C) clearly shows at -42.29 ppm a peak relative to the NaBH_4 presence, plus an additional signal at -15.97 ppm. Analyzing the region of positive shifts, in addition to the peak of the remaining MgB_2 at 96.51 ppm, three more signals are visible. A broad signal at 3.09 ppm (overlapped with the spinning sideband of MgB_2), and two sharp peaks at 6 and 18 ppm. Although, most likely the peak observed at 3.09 ppm is due to the formation of amorphous boron, due to the low signal proportion (less than 1% of total boron signal) an assignment for the three remaining B-containing species (-15.97, 6.16 and 18.20 ppm) is rather difficult. For this reason, a direct spectral sensitivity comparison between, equally recorded, proton decoupled boron experiment $^{11}\text{B}\{^1\text{H}\}$ and proton coupled boron experiment ^{11}B was performed. This analysis allows distinguishing between species which contain boron atoms strongly coupled to protons (directly bonded) and those which are not. Several strategies are known for performing hetero nuclear decoupling. Herein, for CPD (Composite Pulse Decoupling) we employed TPPM technique (Two Pulse Phase Modulation). Figure 3.12 shows the ^{11}B MAS NMR spectra of as milled $2\text{NaH}+\text{MgB}_2$ hydrogenated at 50 bar and 400 °C with proton CDP (blue line) and without proton CDP (black line). Clearly the proton decoupling leads to an enhancement of the signal relative to the $[\text{BH}_4]^-$ anion at -42.29 ppm and of its spinning sidebands at 144.31, 61.62 and -135.33 ppm. Different behaviour is observed for the signals at 18.20, 6.16, 3.09 and -15.97 ppm. For these signals the application of the proton CDP does not influence the intensity of the signals. This behaviour is due to the fact that these species contain B-atoms which are not strongly coupled to hydrogen atoms. This suggests the formation of species without B-H bonds. Spectrum C in figure 3.11 shows the $^{23}\text{Na}\{^1\text{H}\}$ NMR analysis of the material hydrogenated at 400 °C and 50 bar of hydrogen. It is possible to observe the peak of remaining NaH at 10.84 ppm and the signal of the Na contained in NaBH_4 at -15.85 ppm. A further broad signal is observed at 2.32 ppm. Most likely this signal is related with the peaks observed at 18.20, 6.16 and -15.97 ppm in the $^{11}\text{B}\{^1\text{H}\}$ NMR analysis of figure 3.10 spectrum C.

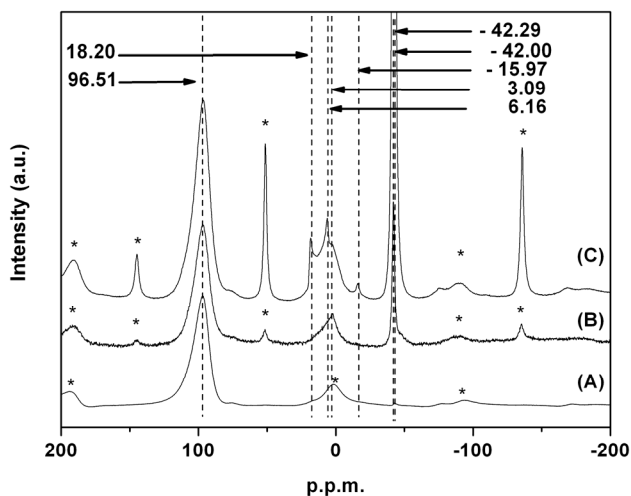


Figure 3.10: A) $^{11}\text{B}\{^1\text{H}\}$ MAS (12 kHz) single pulse NMR spectrum of: as milled $2\text{NaH}+\text{MgB}_2$. B) as milled $2\text{NaH}+\text{MgB}_2$ heated from room temperature up to a final temperature of $300\text{ }^\circ\text{C}$ under a pressure of 50 bar of hydrogen. C) as milled $2\text{NaH}+\text{MgB}_2$ heated from room temperature up to a final temperature of $400\text{ }^\circ\text{C}$ and then kept at $400\text{ }^\circ\text{C}$ for 2 hours under a pressure of 50 bar of hydrogen.

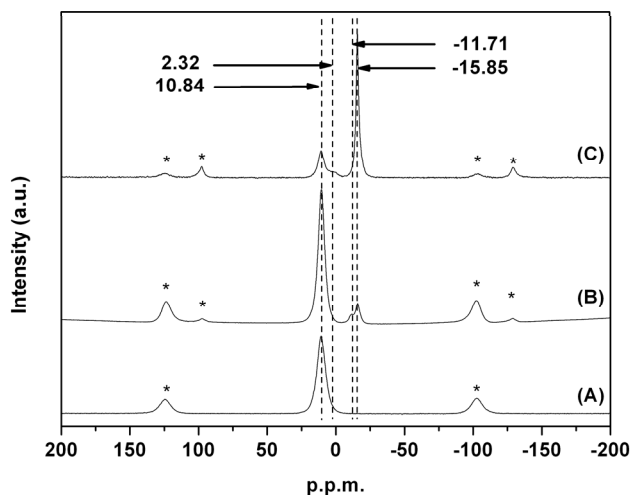


Figure 3.11: A) $^{23}\text{Na}\{^1\text{H}\}$ MAS (12 kHz) single pulse NMR spectrum of: as milled $2\text{NaH}+\text{MgB}_2$. B) as milled $2\text{NaH}+\text{MgB}_2$ heated from room temperature up to a final temperature of $300\text{ }^\circ\text{C}$ under a pressure of 50 bar of hydrogen. C) as milled $2\text{NaH}+\text{MgB}_2$ heated from room temperature up to a final temperature of $400\text{ }^\circ\text{C}$ and then kept at $400\text{ }^\circ\text{C}$ for 2 hours under a pressure of 50 bar of hydrogen.

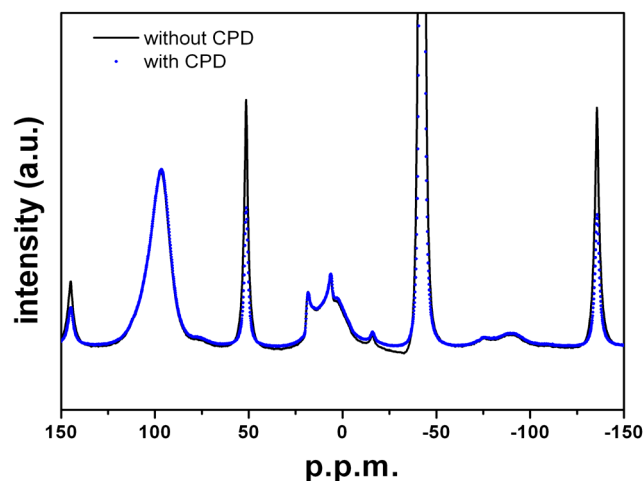


Figure 3.12: $^{11}\text{B}\{^1\text{H}\}$ MAS (12 kHz) single pulse NMR spectrum of as milled $2\text{NaH}+\text{MgB}_2$ heated from room temperature up to a final temperature of $400\text{ }^\circ\text{C}$ and then kept at $400\text{ }^\circ\text{C}$ for 2 hours under a pressure of 50 bar of hydrogen (black line) and ^1H decoupled ^{11}B MAS (12 KHz) single pulse NMR spectrum of as milled $2\text{NaH}+\text{MgB}_2$ heated from room temperature up to a final temperature of $400\text{ }^\circ\text{C}$ and then kept at $400\text{ }^\circ\text{C}$ for 2 hours under a pressure of 50 bar of hydrogen

3.2 Effect of the hydrogen pressure on the absorption reaction

In the previous section the $2\text{NaH}+\text{MgB}_2$ hydrogen absorption at a pressure of 50 bar was investigated. It was observed that at 50 bar H_2 pressure NaBH_4 is not formed directly. Instead, first an unknown crystalline phase is formed, followed upon further heating by the formation of NaMgH_3 and additional unidentified phases. In this section the effect of the applied hydrogen pressure on the hydrogenation process of the system $2\text{NaH}+\text{MgB}_2$ is described. In particular the hydrogen absorption processes at 25 and 5 bar were studied by means of volumetric measurements, HP-DSC technique, *in situ* SR-PXD, MAS NMR and then compared with the hydrogen absorption process carried out at 50 bar.

3.2.1 Volumetric analysis

Figure 3.13 shows the hydrogen absorption kinetics for the system $2\text{NaH}+\text{MgB}_2$ measured under 50, 25 and 5 bar of hydrogen pressure (respectively curve A,B and C) heating the material from RT to 400 °C (heating rate 3 °C/min) and subsequently keeping it under isothermal conditions at 400 °C. The volumetric measurement performed at 50 bar of hydrogen pressure previously discussed (figure 3.1) was added to figure 3.13 for comparison purposes.

The absorption curve of as milled $2\text{NaH}+\text{MgB}_2$ measured at 25 bar of hydrogen pressure (Figure 3.13 B) similarly to curve A (figure 3.13) shows a multi-step hydrogen absorption kinetic. The first step starts at around 300 °C. The amount of hydrogen stored in this stage is equal to 0.7 wt.%. Upon further heating a second hydrogen absorption step starts roughly at 350 °C and continues at 400 °C. The measurement was stopped after 63 hours, when the total amount of hydrogen charged in the system reached 6.2 wt.%. Considering that the measurement was performed at a hydrogen pressure much lower than the previous experiment, the amount of hydrogen stored in the system is rather surprising. A further absorption measurement was performed at a pressure of 5 bar only (Figure 3.13 C). In this case the hydrogen uptake starts at roughly 330 °C, and then continues at 400 °C. After 45 hours an amount of hydrogen equal to 3.8 wt.% was stored in the system. Differently from the first two absorption measurements, the experiment performed at 5 bar hydrogen pressure (figure 3.13 C) does not show a first marked absorption step. The volumetric analysis shows a clear dependence of the absorption kinetics on the hydrogen pressure at which the measurements are performed. However, the causes for this are not yet understood. Therefore, to better understand the effect of the hydrogen pressure on the absorption reaction, XRD measurements of the absorbed materials were performed. The diffraction patterns of the material after hydrogen absorption at 400 °C and 50, 25 and 5 bar of hydrogen pressure respectively (pattern A, B and C) are shown in figure 3.14. The diffraction pattern of the material obtained after hydrogen absorption at 25 bar of hydrogen pressure (figure 3.14 B) shows exactly the same reflections observed for the material synthesized at a pressure of 50 bar (figure 3.14 A).

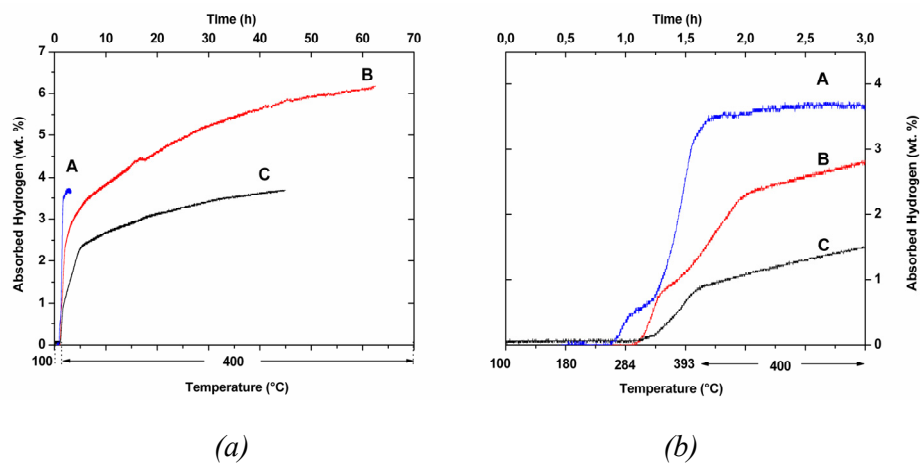


Figure 3.13: Absorption kinetics of as milled $2\text{NaH}+\text{MgB}_2$ measured in a Sievert's -Type apparatus. The samples were heated under 50, 25 and 5 bar hydrogen pressure from RT to 400 °C (curve A,B and C) using a heating rate of 3 °C/min. (a) complete measurements, (b) firsts three hours of absorption.

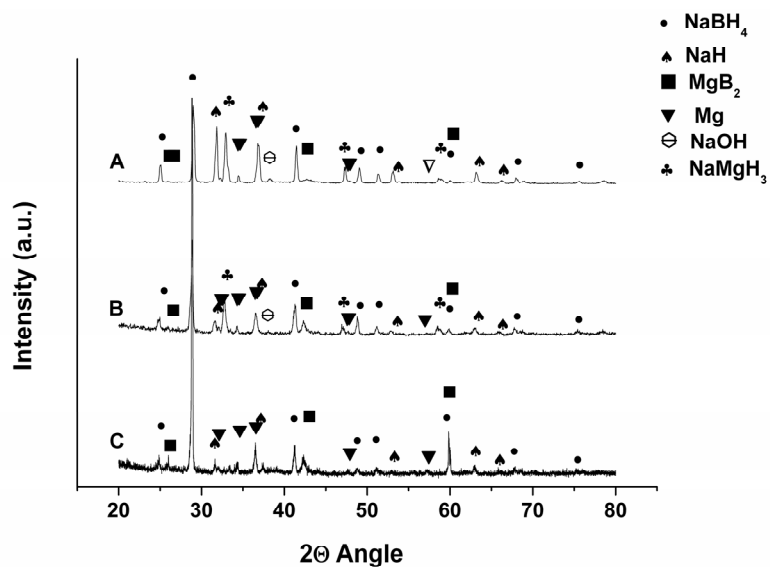


Figure 3.14: XRD patterns of $2\text{NaH}+\text{MgB}_2$ after absorption at 50, 25 and 5 bar of hydrogen pressure and 400 °C (respective patterns A, B and C, wavelength = 0.154184 nm).

Significant differences can be noticed in the respective diffraction phase intensities. In fact, the ratios of peak intensities of NaH and NaMgH₃ reflections to those of NaBH₄, are inferior for the material obtained at a pressure of 25 bar than for the material prepared at 50 bar. For example, the intensity ratio of the peaks NaH (111) at 31.60 2 θ angle and NaMgH₃ (200) at 32.81 2 θ angle to the NaBH₄ peak (220) at 41.26 2 θ angle, changes respectively from 1.49 and 1.31 for the material charged at 50 bar to 0.42 and 1.17 for the material charged at 25 bar H₂ pressure.

This indicates a more marked formation of NaBH₄ for the measurement performed at 25 bar hydrogen pressure. The application of just 5 bar leads to quite different results. Pattern C (figure 3.14) shows the formation of only NaBH₄, and the presence of free Mg together with the starting reactants. NaMgH₃ could not be detected among the final absorption products. Although the simultaneous presence of unreacted materials, together with NaMgH₃ and free Mg, well justify the not achieved theoretical capacity, the reason of the formation of NaMgH₃ and free Mg is an issue which will be addressed later in this work. As for the material absorbed at a pressure of 50 bar of hydrogen the materials hydrogenated at 25 and 5 bar appear to “wet” the inner walls of the sample holder.

3.2.2 Thermal analysis

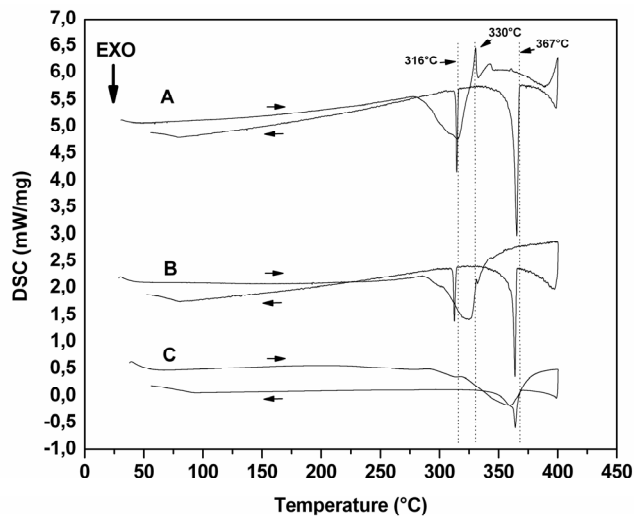


Figure 3.15: HP-DSC traces of the $2\text{NaH}+\text{MgB}_2$ absorption reactions, measured at 50 (pattern A), 25 (pattern B), 5 bar of hydrogen pressure (pattern C) from RT to 400 °C and subsequently cooled (5 °C/min heating/cooling rate).

In order to visualize the sequence of events taking place during absorption at different hydrogen pressures, HP-DSC analyses were performed. Figure 3.15 shows the HP-DSC traces recorded at 50 (A), 25 (B), 5 bar (C) of hydrogen pressure measured from room temperature to 400 °C and then cooled to room temperature (constant heating/cooling rate 5 °C/min). Trace A (figure 3.15) was previously discussed in section 3.1.2 and is here reported for comparison purpose. Curve B (figure 3.15), similarly to the measurement performed under 50 bar hydrogen pressure (Figure 3.15 A), shows a main exothermic peak at 284 °C, and a small endothermic signal at 330 °C. Due to the lowered pressure (25 instead of 50 H₂ bar) the onset of the absorption process is shifted to higher temperatures. Equally to the HP-DSC measurement carried out at 50 bar (figure 3.15 A) the cooling period is characterized by the presence of two strong exothermic signals with onsets at 367 °C and 316 °C. The HP-DSC trace measured at 5 bar hydrogen pressure (figure 3.15 C), shows, upon heating, as in case of the curve measured at 25 bar two exothermic signals. The onset temperature is now shifted to 290 °C and 320 °C. In contrast to the measurements carried out at 50 and 25 bar the cooling period is characterized by the presence of one single exothermic event with an onset

temperature of 367 °C. The second exothermic peak at 316 °C is missing. These findings confirm that the hydrogen absorption process for the 2NaH+MgB₂ system is a multi-steps reaction sensible to the hydrogen pressure at which the measurements is performed. Moreover, the presence of sharp endothermic peaks during heating and sharp exothermic peaks during the cooling-process strengthens our hypothesis that the absorption reaction might occur via molten phase.

Although, the amount of hydrogen stored in the system at 25 bar of hydrogen pressure is sensibly different from that stored at 50 bar, based on the HP-DSC trace (figure 3.15 B) and the XRD analysis (figure 3.14 B) we assume for the two of them a common reaction path.

3.2.3 In situ SR-PXD characterization

In order to investigate the hydrogenation reaction mechanisms of the composite system 2NaH+MgB₂ at 5 bar H₂ pressure an *in situ* SR-PXD analysis was carried out. The material was heated up from room temperature to 400 °C and then held isothermally at this temperature for 3 hours. Finally, the material was cooled down to 60 °C (figure 3.16, heating/cooling rate 5 °C/min). The phases in the starting material are NaH and MgB₂. Apparently, no reaction can be observed below 320 °C. At this temperature the intensity of NaH and MgB₂ peaks start to decrease. Simultaneously an amorphous background starts to form at about 19.50 2 θ angle. Within the first 10 minutes of the isothermal period at 400 °C the complete disappearance of NaH and the formation of free Mg are observed. No significant changes are observed during the remaining part of the isothermal period. During the cooling, at roughly 370 °C the instantaneous formation of NaBH₄ and partial reformation of NaH take place. These two events are followed by the vanishing of the amorphous background (figure 3.16). No further changes occurred during cooling until the measurement was stopped at 60 °C.

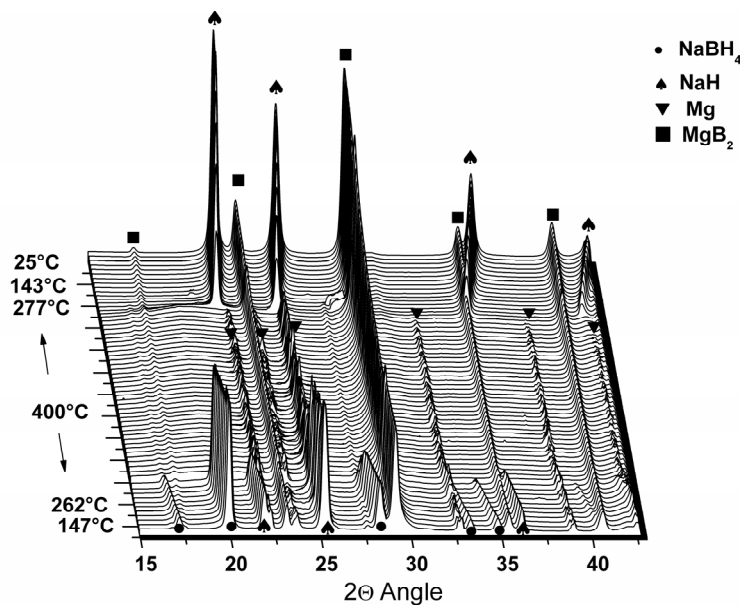


Figure 3.16: Series of SR-PXD patterns of the $2\text{NaH}+\text{MgB}_2$ system heated under 5 bar hydrogen pressure from RT to $400\text{ }^\circ\text{C}$ and kept under isothermal condition for 3 hours before to cool it down to $60\text{ }^\circ\text{C}$ ($5\text{ }^\circ\text{C}/\text{min}$, wavelength = 0.1072 nm). The measurement was obtained at the beamline I711 at the Max II synchrotron in Lund.

3.2.4 MAS NMR analysis

The hydrogen absorption process performed under a pressure of 5 bar was also characterized by MAS NMR technique. The material was prepared heating it up to $400\text{ }^\circ\text{C}$ under a hydrogen pressure of 5 bar and then holding it under isothermal and isobaric conditions for 40 hours. The $^{23}\text{Na}\{^1\text{H}\}$ and the $^{11}\text{B}\{^1\text{H}\}$ NMR spectra of the as milled material are here presented again for comparison purpose. The $^{23}\text{Na}\{^1\text{H}\}$ NMR analysis of the hydrogenated material (figure 3.17 B) shows at 10.88 ppm the signal of the remaining NaH and at -15.65 ppm that due to the NaBH_4 formation. The $^{11}\text{B}\{^1\text{H}\}$ NMR spectra (figure 3.18 B) shows a peak at 96.61 ppm , due to the presence of not reacted MgB_2 and a strong signal at -42.76 ppm , which clearly confirms the formation of NaBH_4 .

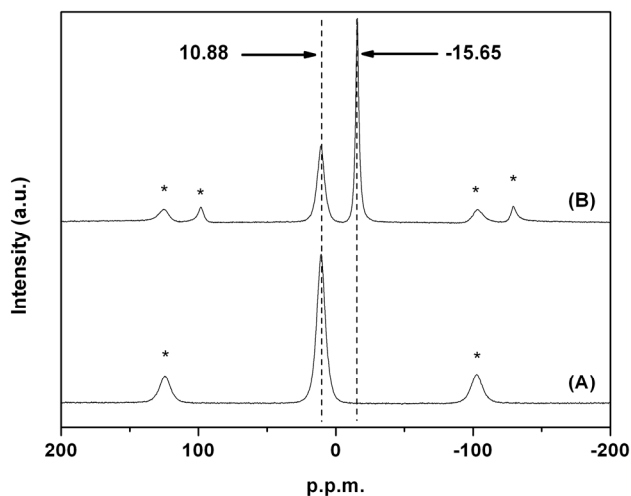


Figure 3.17: A) $^{23}\text{Na}\{^1\text{H}\}$ MAS (12 kHz) single pulse NMR spectrum of: as milled $2\text{NaH}+\text{MgB}_2$. B) as milled $2\text{NaH}+\text{MgB}_2$ heated from room temperature up to a final temperature of $400\text{ }^\circ\text{C}$ under a pressure of 5 and then kept at $400\text{ }^\circ\text{C}$ for 40 hours under a pressure of 50 bar of hydrogen.

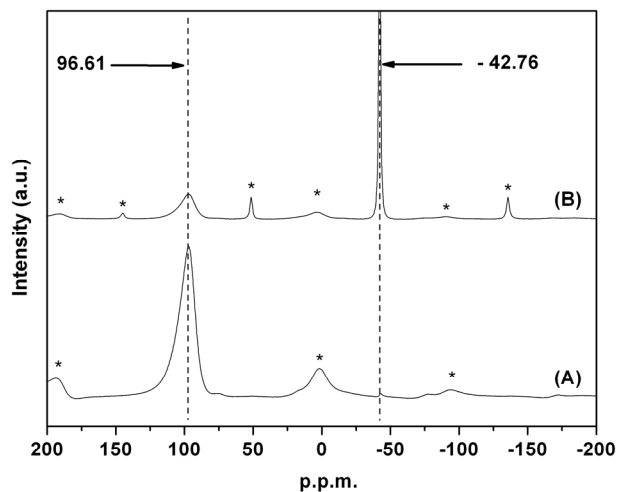


Figure 3.18: A) $^{11}\text{B}\{^1\text{H}\}$ MAS (12 kHz) single pulse NMR spectrum of: as milled $2\text{NaH}+\text{MgB}_2$. B) as milled $2\text{NaH}+\text{MgB}_2$ heated from room temperature up to a final temperature of $400\text{ }^\circ\text{C}$ under a pressure of 5 and then kept at $400\text{ }^\circ\text{C}$ for 40 hours under a pressure of 50 bar of hydrogen.

3.3 Effect of NaH/MgB₂ ratio on the absorption kinetics

In this chapter the possible effect which a different ratio between reactants could trigger on the absorption properties of the NaH-MgB₂ system is investigated. Regarding this topic, two works were recently published by Price et al. [34] and Garroni et al. . In their works, they investigated the effect of the reactants ratio on the sorption properties of the systems LiBH₄-MgH₂ and NaBH₄-MgH₂. However, no clear understanding of the physical effects which lie behind the changed sorption properties was obtained. In order to achieve such a fundamental knowledge the hydrogen absorption behavior of the compositions 1.5Na/MgB₂, NaH/MgB₂ and 0.5NaH/MgB₂ were studied by means of volumetric, HP-DSC and *in situ* – *ex situ* XRD techniques.

3.3.1 Volumetric analysis

The measurements reported here were done at the JRC'S Institute for Energy in Petten. The absorption kinetics were measured at 50 bar of hydrogen pressure, heating the material from room temperature up to 400 °C (heating rate 3 °C/min) and then keeping the material under constant temperature at 400 °C. Figure 3.19 shows the absorption measurements performed for the compositions 2NaH/MgB₂ (A), 1.5Na/MgB₂ (B), NaH/MgB₂ (C) and 0.5NaH/MgB₂ (D). Differently from the measurement reported in figure 3.1 curve A, the absorption reaction reported in figure 3.19 A shows a three steps absorption kinetic. As in case of figure 3.1 curve A the first absorption step starts at roughly 300 °C and continues until an amount of approximately 0.6 wt.% hydrogen is stored in the system. Then the second reaction step starts and continues to absorb hydrogen for additional 14 hours. Then, after absorption of 5.3 wt.% hydrogen a last absorption step occurs charging further 0.45 wt.% of hydrogen. The final amount of absorbed hydrogen was 5.75 wt.%. The observed absorption reaction for the system 1.5Na/MgB₂ (figure 3.19 B) traces out the reaction kinetic observed for the system 2NaH/MgB₂ (figure 3.19 A). However, this time the previously observed third absorption step already starts after 9 hours only at a hydrogen content of 4.4 wt.%. The measurement was stopped after 22 hours and the final amount of hydrogen stored in the system was 4.86 wt.%. The observed absorption reaction for the system NaH/MgB₂ (figure 3.19 C) is divided in two

steps. In the first step again around 0.6 wt.% H₂ is stored. During the second step a further 2.5 wt.% of H₂ is absorbed. Finally after 24 hours a final amount of stored hydrogen equal to 5 wt.% was achieved. The last system investigated was 0.5NaH/MgB₂ (figure 3.19 D). Similarly to other systems, the absorption reaction of this system consists of three steps. In the first step the system charged roughly 0.6 wt.% of hydrogen. Then the absorption reaction continues storing in the second step a further 1.7 wt.%. The final absorption step starts at 380 °C and continues at 400 °C. In this last step an additional 0.8 wt.% of hydrogen was loaded in the system. The absorption reaction stopped after 2.5 hours when the hydrogen stored in the system was equal to 3.1 wt.%.

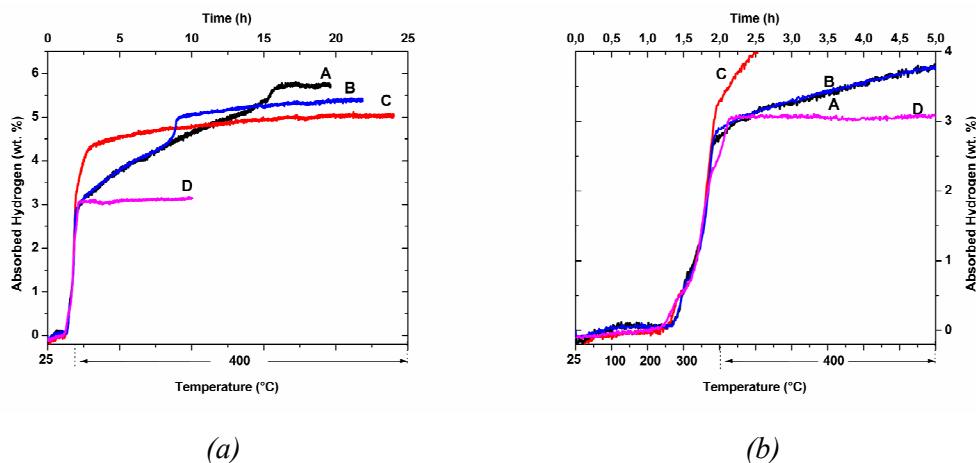


Figure 3.19: Absorption kinetics of as milled material measured in a Sievert's Type apparatus. The samples were heated under 50 bar hydrogen pressure from RT to 400 °C (heating rate 3 °C/min): (A) 2NaH+MgB₂, (B) 1.5NaH+MgB₂, (C) NaH+MgB₂, (D) 0.5NaH+MgB₂. (a) complete measurements, (b) first five hours of absorption.

3.3.2 XRD characterization

The XRD patterns of the as milled 2NaH/MgB₂, 1.5NaH/MgB₂, NaH/MgB₂ and 0.5NaH/MgB₂ are reported in figure 3.20 (respectively pattern A, B, C and D). The four NaH-MgB₂ specimens investigated in figure 3.20 show the presence of NaH and MgB₂ only. This indicates that additional crystalline phases are not formed during milling. In order to further

understand the possible effects of the different NaH-MgB₂ ratios on the hydrogen sorption properties, the diffraction patterns of figure 3.20 were investigated by Rietveld's method. The crystallite sizes for the four NaH-MgB₂ compositions are reported in table 3.2. Interestingly, as a consequence of the reduction of the NaH fraction contained in the NaH-MgB₂ system, the crystallite size of both NaH and MgB₂ phases decrease. In fact, the measured NaH crystallite size for the system 2NaH/MgB₂ is 62.9 (±3.1) nm, whereas it is 55.7 (±2.8) nm for 1.5NaH/MgB₂, 50.0 (±2.3) nm for NaH/MgB₂ and 49.6 (±2.6) nm for 0.5NaH/MgB₂. The crystallite size of MgB₂ measured for the system 2NaH/MgB₂ is 38.3 (±1.9) nm and it decreases to 37.7 (±1.9) nm for 1.5NaH/MgB₂, 33.1 (±1.5) nm for NaH/MgB₂ and 26.9 (±1.4) nm for 0.5NaH/MgB₂. The crystallite size decrement of both NaH and MgB₂ indicates a progressive improvement of the ball milling grain refinement efficiency, what is a consequence of the reduction of NaH amount contained in the NaH-MgB₂ mixture.

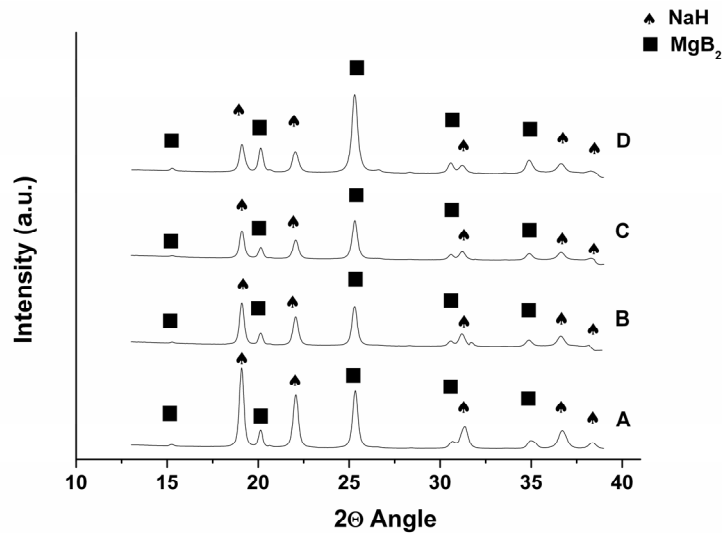


Figure 3.20: XRD patterns of the systems NaH-MgB₂ as milled: 2NaH/MgB₂, 1.5NaH/MgB₂, NaH/MgB₂, 0.5NaH/MgB₂ (respective patterns A, B, C and D, wavelength = 0.0939 nm).

Material	Crystallite Size NaH (nm)	Crystallite Size MgB ₂ (nm)
2NaH+MgB ₂	62.9 (±3.1)	38.3 (±1.9)
1.5NaH+MgB ₂	55.7 (±2.8)	37.7 (±1.9)
NaH+MgB ₂	50.0 (±2.3)	33.1 (±1.5)
0.5NaH+MgB ₂	49.6 (±2.6)	26.9 (±1.4)

Table 3.2: Crystallite size of the systems NaH-MgB₂ as milled.

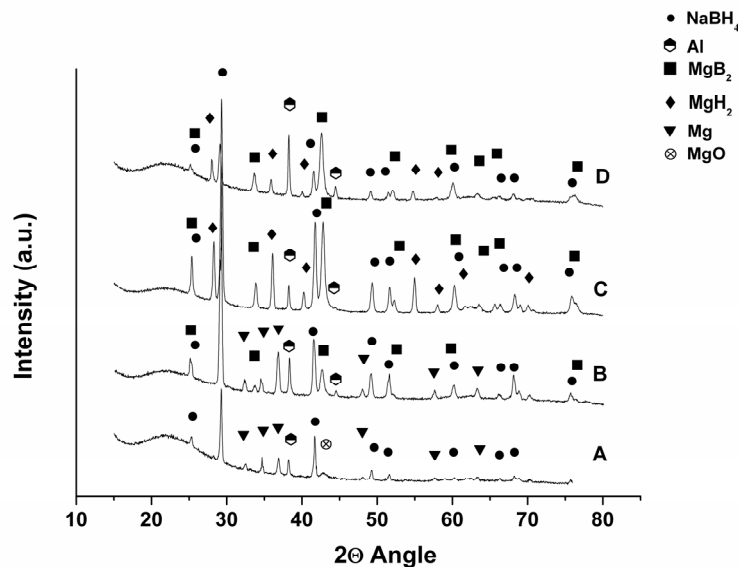


Figure 3.21: XRD patterns of the systems NaH-MgB₂ hydrogenated under 50 bar and 400 °C: 2NaH/MgB₂, 1.5NaH/MgB₂, NaH/MgB₂, 0.5NaH/MgB₂ (respective patterns A, B, C and D, wavelength = 0.154184 nm).

The XRD analysis of the materials after hydrogen absorption is presented in figure 3.21. As previously mentioned (section 2.5) due to different measurement procedure (at the Helmholtz-Zentrum Geesthacht the material was protected by an air tight Kapton foil, whereas for the measurement performed at the JRC's institute the material was dispersed in high vacuum grease) the diffraction patterns collected at the JRC's Institute for Energy show the presence of two peaks derived from the sample holder at 23.26 and 44.42 °2θ angle. In addition, a broad signal with maximum at roughly 22 2θ angle caused by grease as powder support is observed. Pattern A (figure 3.21) shows for the hydrogen charged 2NaH/MgB₂ system the presence of NaBH₄ together with free Mg only. The peak at 42.84° which is close to the theoretical position of the MgB₂ (101) peak is most probably caused by the presence of a small amount of MgO. Interestingly, NaMgH₃ does not appear among the final absorption products. The XRD pattern of the hydrogenated 1.5 NaH/MgB₂ is shown in figure 3.21 B. This sample contains NaBH₄, free Mg and MgB₂. Contrarily to the previously measured

samples the NaH/MgB₂ (figure 3.21 C) does not contain free Mg but MgH₂ together with NaBH₄ and MgB₂. A last XRD analysis was performed on the absorbed 0.5NaH/MgB₂ (figure 3.21 D). Similarly to the system NaH/MgB₂ this material shows the presence of free MgH₂, NaBH₄ and MgB₂. It must be noticed that the increasing fraction of unreacted MgB₂ observed respectively in the patterns B, C, D (figure 3.21) is caused by the different ratio between NaH and MgB₂ in the starting reactants.

3.3.3 Thermal analysis

Figure 3.22 shows the HP-DSC traces for the following compositions: 2NaH/MgB₂ (trace A), 1.5Na/MgB₂ (trace B), NaH/MgB₂ (trace C) and 0.5NaH/MgB₂ (trace D), measured from room temperature to 400 °C and then cooled to room temperature (constant heating/cooling rate 5 °C/min) at 50 bar hydrogen pressure. The analysis performed for the composition 2NaH/MgB₂ (figure 3.22 A) is discussed in section 3.1.2. This measurement is taken as reference. The HP-DSC trace recorded for the system 1.5Na/MgB₂ (figure 3.22 B) shows a trend similar to that observed for the system 2NaH/MgB₂ (figure 3.22 A). However, slight differences can be noticed. The position of the first exothermic peak during heating (figure 3.22 B) is shifted by 6 °C towards lower temperatures (onset temperature 271 °C) with respect to the observed signal in the reference system 2NaH/MgB₂ (onset temperature 277 °C, figure 3.22 A). Although under heating also others signals undergo shift to lower temperature, the magnitude of those shifts is smaller than 5 °C. The cooling period of the HP-DSC trace B (figure 3.22) is characterized by the presence of two main exothermic peaks at 367 and 317 °C plus another smaller exothermic peak at 380 °C. The HP-DSC analysis of the system NaH/MgB₂ (figure 3.22 C) shows during heating a first exothermic event at 248 °C followed by a small endothermic signal with maximum at 328 °C and by a broad exothermic signal split into two parts starting at 330 °C. In contrast to the previous measurements the cooling period does not show any hint for ongoing reactions or phase transitions. Finally, the composition 0.5NaH/MgB₂ was also investigated by means of HP-DSC technique (figure 3.22 D). A first exothermic signal at 240 °C and a small endothermic peak at 328 °C are visible. These signals are followed by a broad exothermic peak at 320 °C split into three parts

with maxima at 352, 356 and 370 °C. Because of the overlaps between them it is not possible to give precise onset temperatures. As for the system NaH/MgB₂ (figure 3.22 C) the cooling period is characterized by the absence of detectable events again.

The HP-DSC analysis of figure 3.22 clearly shows the effect of the ratio of starting reactantson absorption behavior of the system NaH/MgB₂. This change in hydrogen absorption behavior is clearly emphasized in the HP-DSC measurement performed for the system 0.5NaH/MgB₂ (figure 3.22 D).

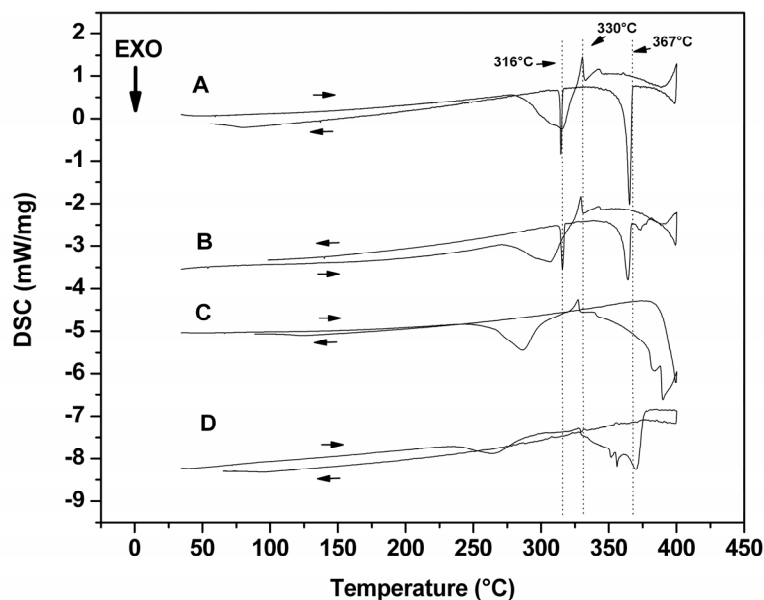


Figure 3.22: HP-DSC traces measured at 50 of the 2NaH+MgB₂ absorption reaction (trace A), 1.5NaH+MgB₂ absorption reaction (trace B), NaH+MgB₂ absorption reaction (trace C) and of 0.5NaH+MgB₂ absorption reaction (trace D), measured from RT to 400 °C and subsequently cooled (5 °C/min heating/cooling rate).

3.3.4 In situ SR-PXD characterization

In order to better understand the effect of the NaH/MgB₂ ratio on the hydrogen absorption reaction, the hydrogenation reaction of the system 0.5NaH/MgB₂ was further characterized by *in situ* SR-PXD analysis (figure 3.23). The measurement was carried out at 50 bar of hydrogen pressure, in scanning temperature from RT to 350 °C and then keeping the

system under isothermal conditions at 350 °C for several hours. The phases in the starting materials are NaH and MgB₂. Due to the reduced amount of NaH in the system the NaH reflections are less intense than those observed for the system 2NaH/MgB₂. During heating at roughly 230 °C the appearance of the previously discussed unknown crystalline phase is observed. Later on at 270 °C the appearance of this phase is followed by the formation of NaMgH₃. With the appearance of the NaMgH₃ phase the NaH phase disappears completely.

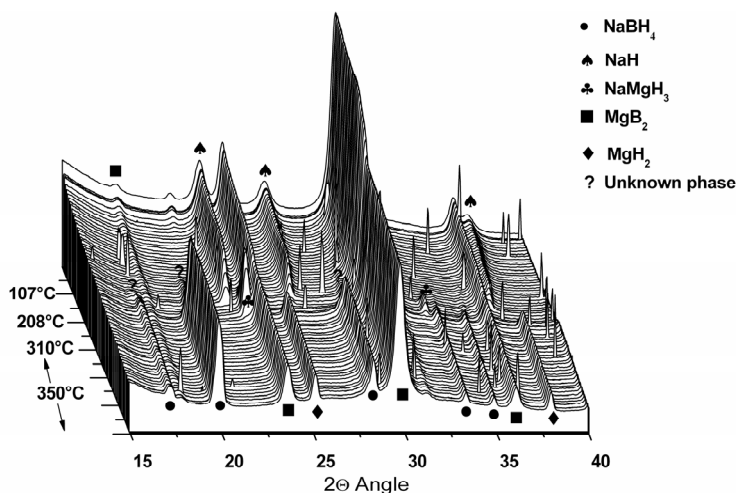


Figure 3.23: Series of SR-PXD patterns of the 2NaH+MgB₂ system heated at 50 bar hydrogen pressure from RT to 350 °C and kept under isothermal condition (5 °C/min, wavelength = 0.1097 nm). The measurement was obtained at the beamline I711 at the Max II synchrotron in Lund.

At 325 °C the formation of NaBH₄ and little later of MgH₂ is observed together with the simultaneous disappearance of both NaMgH₃ and the unknown crystalline phase. The MgB₂ reflections decrease along with the formation of the hydrogenated products, however, without disappearing completely. This is due to the large excess of MgB₂ present in the system 0.5NaH/MgB₂. In contrast to the system 2NaH/MgB₂ (figure 3.4), the system 0.5NaH/MgB₂ (figure 3.23) does not show the formation of the amorphous background. In addition, the formation of MgH₂ was achieved.

3.4 The first hydrogen desorption

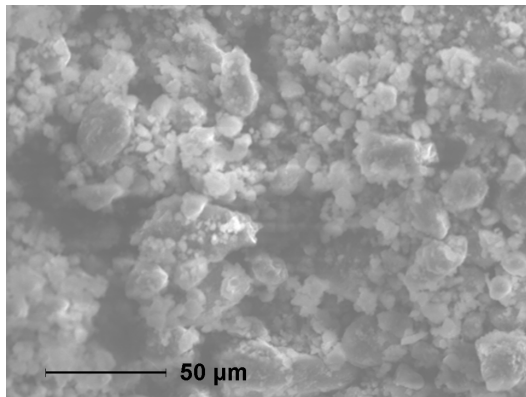
In the following section the study of the hydrogen desorption process for the system $2\text{NaBH}_4+\text{MgH}_2$ is addressed. In section 3.1, it was shown that the complete conversion of the $2\text{NaH}+\text{MgB}_2$ system into $2\text{NaBH}_4+\text{MgH}_2$ could not be achieved for any of the investigated experimental conditions. For this reason in order to study the desorption properties of the $2\text{NaBH}_4+\text{MgH}_2$ system we focused our attention on the material prepared by ball milling of commercially available NaBH_4 and MgH_2 .

3.4.1 Hydrogen desorption of the as milled system

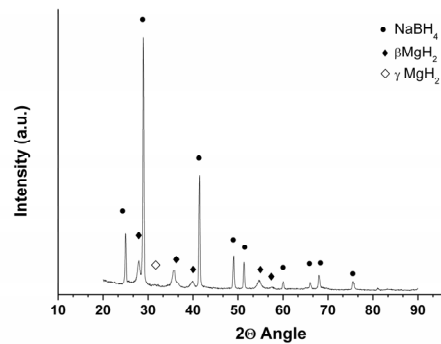
3.4.1.1 Microstructure and phase distribution

Figure 3.24 a shows the SEM image of the as milled $2\text{NaBH}_4+\text{MgH}_2$ system. The particle size distribution of the material appears to be divided in two main domain sizes. In particular in figure 3.24 a it is possible to observe a portion of material having a particle size of 5 to 10 μm and another part constituted of much larger particle diameters of 20 and 30 μm . In spite of several attempts to identify the component phases through SEM-EDX technique, no clear results were obtained. Considering that in the system $2\text{NaBH}_4+\text{MgH}_2$ the NaBH_4 volume fraction is roughly 80% of the total volume, it is reasonable to assume that MgH_2 particles are mostly surrounded by the NaBH_4 .

The XRD analysis of the as milled material ($2\text{NaBH}_4+\text{MgH}_2$) in figure 3.24 b, shows the presence of NaBH_4 , $\beta\text{-MgH}_2$ and a small amount of $\gamma\text{-MgH}_2$. The presence of the $\gamma\text{-MgH}_2$ is due to the high mechanical attrition generated during the ball milling, which partially converted the starting $\beta\text{-MgH}_2$ into the high-pressure polymorph $\gamma\text{-MgH}_2$ ^[42]. From the Rietveld's analysis of the diffraction pattern presented in figure 3.24 bit is possible to attribute to the NaBH_4 and the $\beta\text{-MgH}_2$ a crystallite size of 105 and 17 nm respectively.



(a) SEM image



(b) XRD pattern

Figure 3.24: SEM image and XRD pattern of as milled $2\text{NaBH}_4+\text{MgH}_2$ system.

3.4.1.2 Volumetric analysis

The desorption reaction measured for the as milled $2\text{NaBH}_4+\text{MgH}_2$ by volumetric analysis is reported in figure 3.25. The measurement was carried out under static vacuum conditions (starting value 10^{-2} bar), heating the material from RT up to $450\text{ }^\circ\text{C}$ (constant heating rate $3\text{ }^\circ\text{C}/\text{min}$) and subsequently keeping it at $450\text{ }^\circ\text{C}$ for 14 hours. The hydrogen desorption starts at roughly $300\text{ }^\circ\text{C}$ and continues at higher temperature. The hydrogen release proceeds via single step reaction, reaching a maximum amount of desorbed hydrogen equal to 1.8 wt.%. Further hydrogen release during the isothermal period at $450\text{ }^\circ\text{C}$ is not observed. Despite an estimated equilibrium hydrogen pressure of 1 bar at $350\text{ }^\circ\text{C}$ ^[31], the complete hydrogen desorption was not achieved under the applied conditions. Moreover, the comparison between the achieved hydrogen desorption (1.8 wt.%) and the theoretical hydrogen capacity (7.84 wt.%) suggests a partial dehydrogenation involving only the MgH_2 phases.

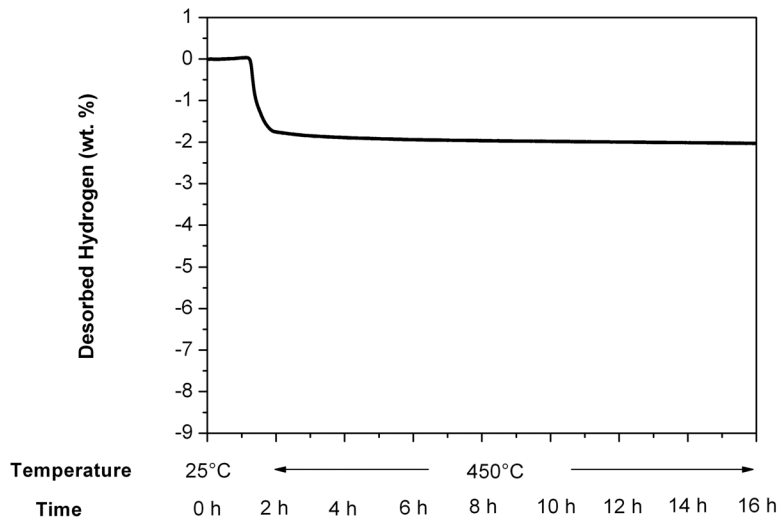


Figure 3.25: Desorption reaction kinetics of the material $2\text{NaBH}_4+\text{MgH}_2$ as milled measured in a Sievert's-Type apparatus. The sample was heated in vacuum up to $450\text{ }^\circ\text{C}$ ($3\text{ }^\circ\text{C}/\text{min}$ heating rate) and kept under isothermal condition for 12 hours.

3.4.1.3 Simultaneous thermal analysis and mass spectroscopy

In order to better understand the dehydrogenation process, the system $2\text{NaBH}_4+\text{MgH}_2$ was investigated by means of coupled calorimetric and mass spectroscopy technique (figure 3.26). The DSC analysis (figure 3.26) was acquired by heating the $2\text{NaBH}_4+\text{MgH}_2$ sample from room temperature up to $550\text{ }^\circ\text{C}$ (constant heating rate $5\text{ }^\circ\text{C}/\text{min}$) under a continuous argon flow of $150\text{ ml}/\text{min}$. For the mass spectroscopic analysis of the evolving gases we focused our attention on the intensity of $m/z = 2$ amu for hydrogen. The possibility to monitor simultaneously the heat flow and the possible release of hydrogen allows a fast assignment of the calorimetric signal related to hydrogen desorption. In the DSC trace of figure 3.26 4 different endothermic signals associated with separated hydrogen releases are visible. A first broad endothermic signal starts at $285\text{ }^\circ\text{C}$. The hydrogen release related to this signal begins also at $285\text{ }^\circ\text{C}$ and stops at roughly $350\text{ }^\circ\text{C}$. Upon, further heating, at $400\text{ }^\circ\text{C}$ a second endothermic event coupled with a small hydrogen release is observed. Later at $450\text{ }^\circ\text{C}$ and $475\text{ }^\circ\text{C}$ two further endothermic signals are observed. Although, both signals are rather

intense, only the one with onset at 475 °C is associated with a strong hydrogen release, whereas the signal starting at 450 °C is followed by a small hydrogen evolution.

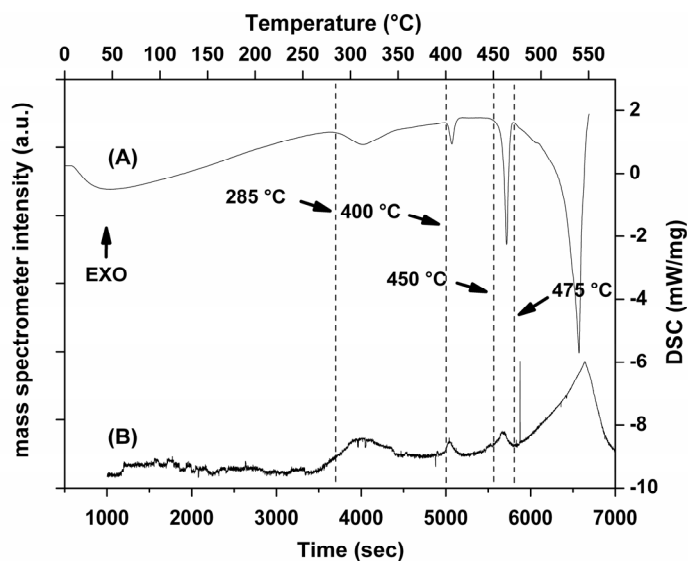


Figure 3.26: Simultaneous calorimetric and mass spectrometric analysis of the system $2\text{NaBH}_4+\text{MgH}_2$ measured in argon flow (150ml/min) from RT to 550 °C (5 °C/min heating). Curve A DSC analysis and curve B mass spectrometer trace for $m/z = 2$ amu.

3.4.1.4 In situ SR-PXD characterization

Aiming to understand the desorption mechanism and to clarify the nature of the occurring events taking place upon heating in vacuum, the desorption reaction of the as milled $2\text{NaBH}_4+\text{MgH}_2$ was investigated by means of *in situ* SR-PXD technique (figure 3.27).

The SR-PXD measurement was performed by heating the ball-milled $2\text{NaBH}_4+\text{MgH}_2$ under dynamic vacuum (10^{-2} bar) from room temperature up to 400 °C and then holding the material under isothermal condition at 400 °C for several hours. The used heating rate was 3 °C/min. Because of technical reasons it was not possible to reach a final temperature equal to that used for the volumetric measurement (450 °C). According to the PXD pattern the starting material in figure 3.27 contains NaBH_4 , $\beta\text{-MgH}_2$, $\gamma\text{-MgH}_2$ and a small amount of MgO . Upon heating, due to thermal cell expansion, a continuous shift of all the diffraction peaks towards lower 2θ angle position is observed. The $\gamma\text{-MgH}_2$ appears to be stable up to 220 °C. At higher

temperature a sensible decrement of the γ -MgH₂ diffracted intensity coupled with an increment in β -MgH₂ signal (indicative of an ongoing $\gamma \rightarrow \beta$ -MgH₂ conversion) is observed. At 300 °C, the formation of free magnesium and the simultaneous decomposition of the two MgH₂ phases start. The formation of Mg is complete at roughly 360 °C. Further reaction can be observed neither during the remaining heating period nor during the isothermal period at 400 °C. In spite of the calculated equilibrium hydrogen pressure of 1 bar at 350 °C for the reaction leading to the formation of MgB₂ during decomposition, even in small amount could not be observed in the *in situ* SR-PXD analysis of figure 3.27.

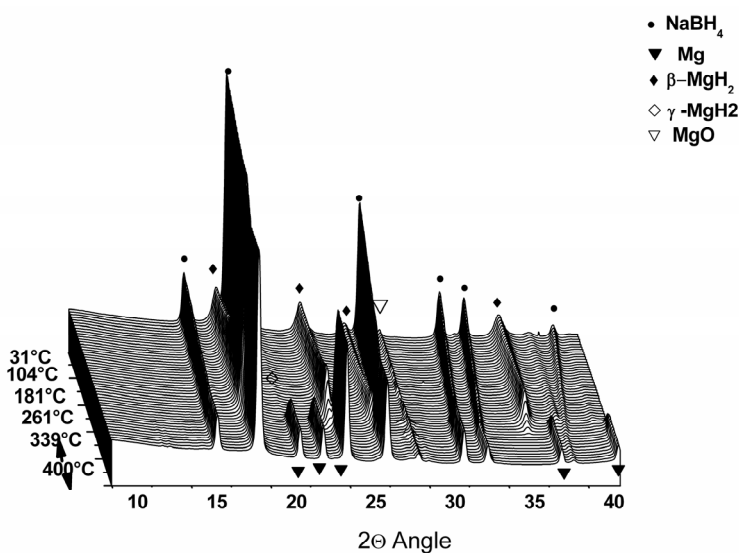


Figure 3.27: Series of SR-PXD patterns of the $2\text{NaBH}_4+\text{MgH}_2$ system heated under 50 bar hydrogen pressure from RT to 300 °C (3 °C/min, wavelength = 0.109719 nm). The measurement was obtained at the beamline I711 at the Max II synchrotron in Lund.

The study of the effect of additives on the desorption properties of the system $2\text{NaBH}_4+\text{MgH}_2$ was behind the scope of this work, however a single attempt was done. The used additive was the titanium isopropoxide. This additive was chosen among the others due to its marked influence on the sorption properties of the systems $2\text{LiBH}_4+\text{MgH}_2$ [33] and $\text{Ca}(\text{BH}_4)_2+\text{MgH}_2$ [43]. The material was prepared by pre-milling MgH₂ with a Spex 8000 mill, using a ball to powder ratio of 10:1. Then NaBH₄ and a 5 wt.% of titanium isopropoxide were added to the pre-milled MgH₂ and the mixture was milled for additional 5 hours always with a ball to powder ratio equal to 10:1. The desorption reaction of the milled material was subsequently

investigated by volumetric analysis and the desorption products characterized by XRD technique. Although the measurements are not reported here, the observed results are worth to be mentioned. The conditions applied for the volumetric analysis are the same as used for the as milled material (figure 3.25). The desorption reaction started at roughly 250 °C and continued at higher temperature. The measurement was stopped after 17 hours when an amount of desorbed hydrogen equal to 3.3 wt.% was reached. The XRD analysis of the desorption products showed the presence of Mg, NaBH₄ and a significant amount of MgO. The formation of MgB₂ even in small quantity was not observed. Most likely the higher desorption capacity achieved for the material milled with the titanium isopropoxide was due to the thermal decomposition of the additive plus a partial NaBH₄ decomposition. These analyses demonstrate that the titanium isopropoxide has not a positive effect on the desorption properties of the system 2NaBH₄+MgH₂ in the as milled condition.

3.4.2 Optimization of the 2NaBH₄+ MgH₂ desorption properties

The following section focuses on the improvement of the 2NaBH₄+MgH₂ hydrogen desorption properties. In particular two different approaches will be introduced. At first, the beneficial effect of pre-treating the as milled 2NaBH₄+MgH₂ by heating it in hydrogen atmosphere is reported. Then, the possibility to improve the desorption process by enhancing the interface conditions between NaBH₄ and MgH₂ will be also proposed. In order to accomplish these tasks volumetric measurements, *in situ* and *ex situ* XRD analysis, MAS NMR, SEM and TEM technique were employed.

3.4.2.1 Volumetric analysis

The heat-hydrogen treated material was prepared by heating the as milled 2NaBH₄+MgH₂ material at 50 bar of hydrogen from RT to 300 °C (constant heating rate 3 °C/min), and then holding it isothermally at 300 °C for one hour. The desorption kinetic measured for the heat-hydrogen treated material is displayed in figure 3.28. The sample was

heated from RT to 450 °C and subsequently kept at 450 °C. Differently from the as milled materials (figure 3.25), this measurement shows a two steps desorption reaction. The reaction steps are characterized by different reaction rates. The first desorption step starts at about 340 °C. Then, after desorbing an amount of hydrogen equal to 1.8 wt.%, at 370 °C the second desorption step starts, and continues at higher temperature reaching after 11 hours of isothermal treatment at 450 °C an amount of desorbed hydrogen equal to 7.8 wt.%.

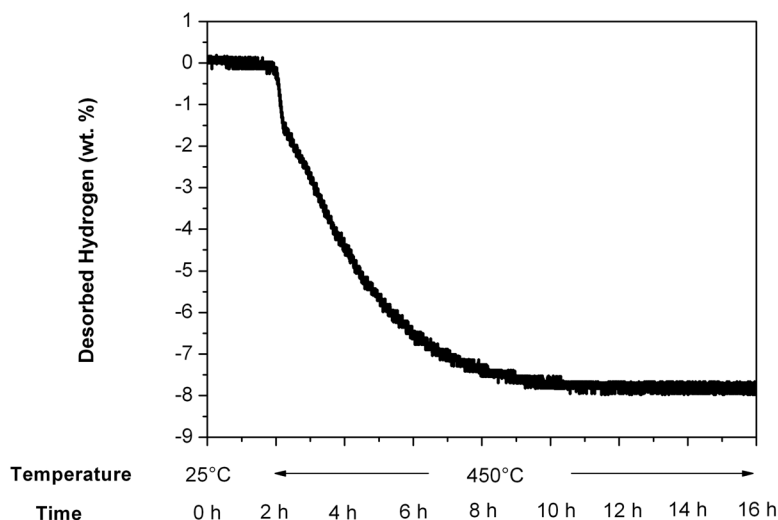


Figure 3.28: Desorption reaction kinetics of the heat-hydrogen treated $2\text{NaBH}_4+\text{MgH}_2$ measured in a Sievert's-Type apparatus. The sample was heated in vacuum from RT up to 450 °C (3 °C/min heating rate) and then kept under isothermal condition for 12 hours.

3.4.2.2 In situ SR-PXD characterization

The desorption reaction of the heat-hydrogen treated $2\text{NaBH}_4+\text{MgH}_2$ was also investigated by means of SR-PXD technique (figure 3.29). The material was heated under static vacuum from RT to 400 °C (constant heating rate 3 °C/min), and then kept under isothermal condition for 2 hours. In the range from RT to 295 °C an intensity decrement of both NaBH_4 and MgH_2 peaks is observed. Although marked, this intensity decrement does not seem to be due to an ongoing reaction between NaBH_4 and MgH_2 , but it is most probably due to a displacement of the sample from the beam focus position during the increase of the temperature. At 300 °C the decomposition of MgH_2 and the simultaneous formation of free

Mg are visible. Then at 350 °C the free Mg starts to react with NaBH₄ to form MgB₂. The reaction is complete at 400 °C. At the best of our knowledge this is the first time that complete hydrogen desorption of the system 2NaBH₄+MgH₂ is achieved at such low temperatures.

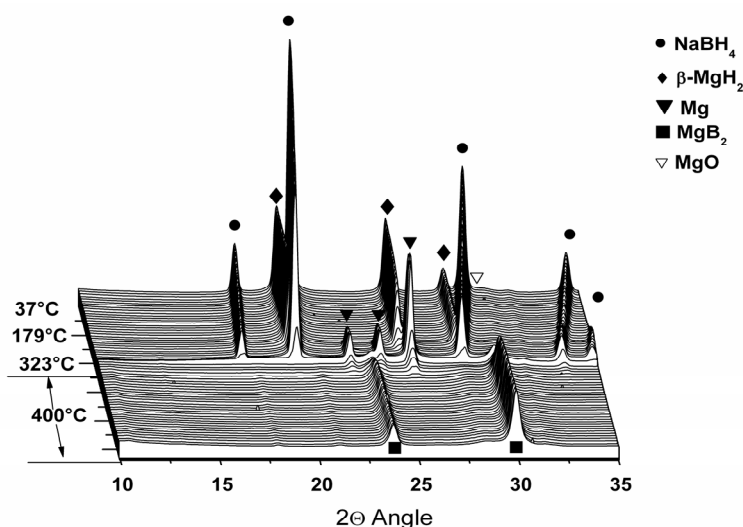


Figure 3.29: Series of SR-PXD patterns of the heat-hydrogen treated 2NaBH₄+MgH₂ heated under vacuum from RT to 400 °C (5 °C/min, wavelength = 0.109719 nm. The measurement was obtained at the beamline I711 at the Max II synchrotron in Lund.

The overall desorption process was further investigated by studying the phase evolutions. In Figure 3.30 the normalized area of selected peaks is plotted as function of time and temperature. As visible in the SR-PXD analysis of figure 3.29 also, the first part of the reaction (from RT to 295 °C) is characterized by a decrement of the NaBH₄ and MgH₂ signals. At temperatures higher than 295 °C a decrement of the MgH₂ integrated area coupled with the rising of the Mg signal is visible. The range of temperature from 350 °C to 400 °C, and the subsequent isothermal period are characterized by the clear decrement of the NaBH₄ and Mg peak intensities as well as the simultaneous rise of the MgB₂ signal. In the temperature range between 350 and 400 °C an anomalous trend of the Mg and MgB₂ curves is also visible. The reaction between free Mg and NaBH₄ does not lead directly toward the formation of the final products. As visible in figure 3.30 at 390 °C the signal of the free Mg stops to decrease before it finally drops away. Simultaneously, the signal of MgB₂ rises very fast, then it halts and continues again after several minutes. Most likely, these unexpected

trends have to be explained by a possible reaction taking place in the liquid state. In fact, although the diffraction peaks of NaBH_4 abruptly drop down this can not be due to a direct decomposition of it, since the hydrogen desorption occurs in a much longer time interval. Furthermore, the different velocity between disappearance of Mg and MgB_2 formation in figure 3.30 suggests the possible presence of one more intermediate reaction step.

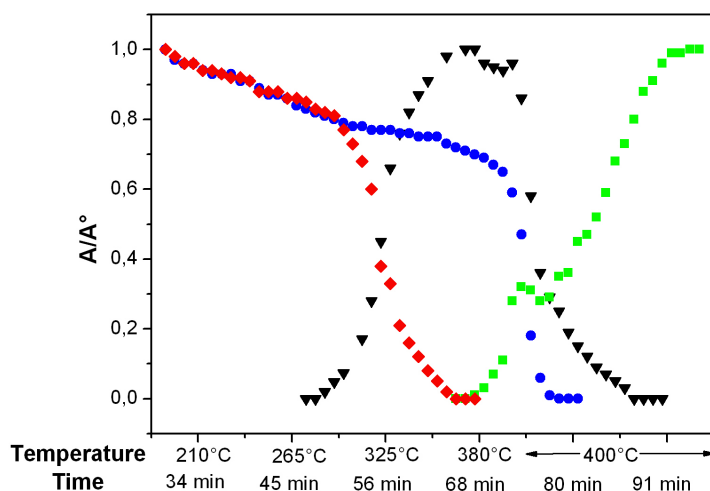


Figure 3.30: Normalized integrated diffracted intensity (A/A°) of selected reflections from the system $2\text{NaBH}_4 + \text{MgH}_2$ heated in vacuum from RT to 400 °C (5 °C/min). Symbols: ● cubic NaBH_4 (111), ◆ tetragonal $\beta\text{-MgH}_2$ (110), ■ hexagonal MgB_2 (001), ▼ hexagonal Mg (100).

3.4.2.3 MAS NMR analysis

Although the positive effect of the heat-hydrogen treatment on the desorption properties of the as milled $2\text{NaBH}_4 + \text{MgH}_2$ is obvious, the reasons which lead to it are not yet understood. In order to shed more light on this issue the desorption process of the system $2\text{NaBH}_4 + \text{MgH}_2$ was investigated by means of $^{11}\text{B}\{^1\text{H}\}$ NMR technique (figure 3.31). The three spectra reported in figure 3.31 are respectively those of the as milled material (spectrum A), the heat-hydrogen treated material (spectrum B) and the material heat-hydrogen treated partially desorbed at 450 °C in vacuum (spectrum C). As for the as milled material the

$^{11}\text{B}\{^1\text{H}\}$ analysis of the heat-hydrogen treated material shows the presence of NaBH_4 only as boron containing species (peak at -42.25 ppm). This demonstrates that no additional boron containing phases are formed during the material treatment. The material partially desorbed at 450°C in vacuum (figure 3.31 C) clearly shows at 97.71 ppm the presence of MgB_2 formed by free Mg and NaBH_4 reaction. In addition, for the material partially desorbed it is possible to notice a half height increment of the NaBH_4 signal. This increment is due to symmetry loss passes from 1.5 ppm to 5 ppm.

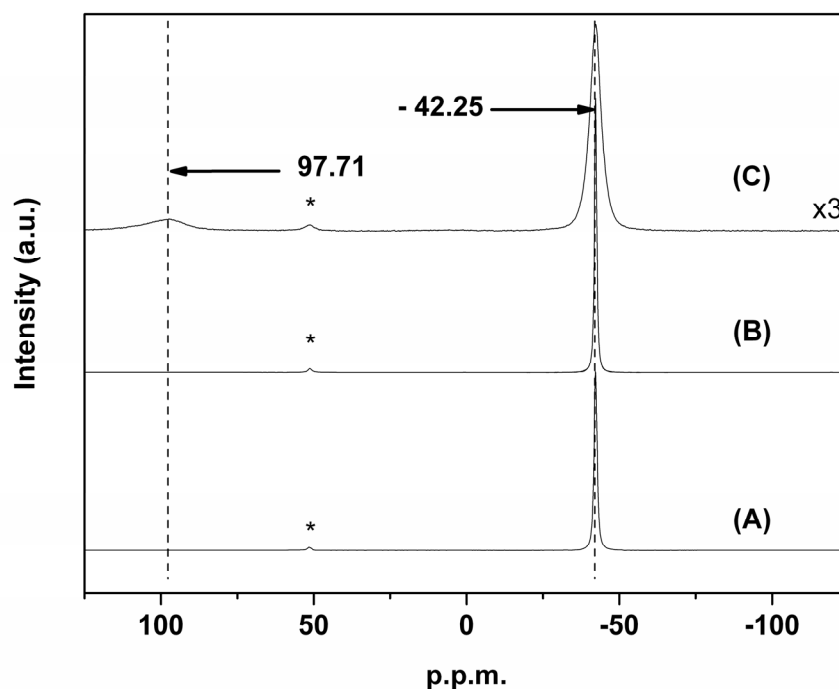


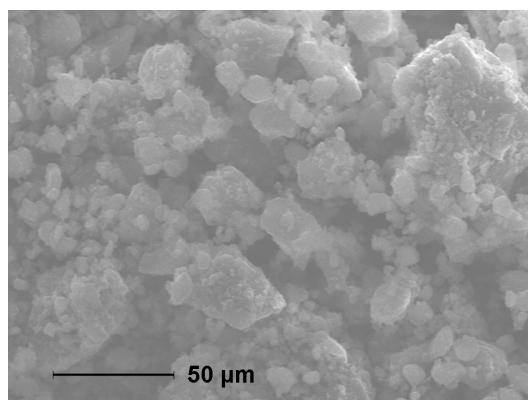
Figure 3.31: A) $^{11}\text{B}\{^1\text{H}\}$ MAS (12 kHz) NMR spectrum of: as milled NaBH_4 , B) heat-hydrogen treated $2\text{NaBH}_4+\text{MgH}_2$, C) heat-hydrogen treated $2\text{NaBH}_4+\text{MgH}_2$ partially desorbed in vacuum at 450°C .

3.4.2.4 Morphological and microstructural characterization

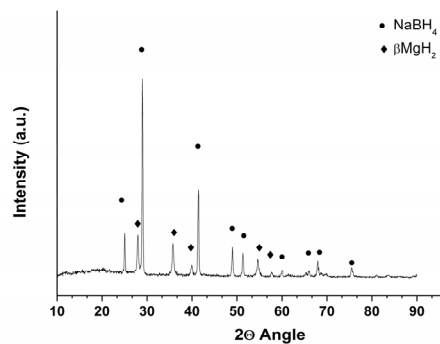
The results of the morphological investigations on the heat-hydrogen treated material and on desorbed specimens are presented in this section.

The SEM and XRD analysis of the as milled material after heat-hydrogen treatment are reported in figure 3.32 A and B respectively. Like for the as milled material (section 3.4.1.1), the particle size distribution of the heat hydrogen treated material appears to be divided into two main domains. Although, a small portion of the sample still shows a particle dimension similar to the smaller particle sizes observed for the only milled material (between 5 and 10 μm) the most of the sample consists of very large particles (between 30 and 50 μm). This new particle size distribution is most probably consequence of the particle aggregation upon heating. In figure 3.32 b, a further consequence of the heat-hydrogen treatment is visible. The treated material does not contain $\gamma\text{-MgH}_2$ anymore. In addition, the calculated crystallite size for both NaBH_4 and $\beta\text{-MgH}_2$ shows a substantial value increment. This increment is more marked for $\beta\text{-MgH}_2$ where the crystallite size increases from 17 to 60 nm, whereas for NaBH_4 it increases from 105 to 150 nm only.

The morphological analysis of the heat-hydrogen treated material heated up to 370 $^\circ\text{C}$ under static vacuum (starting value 10^{-2} bar) is shown in figure 3.33 a and b. The SEM analysis of figure 3.33 a shows the presence of a fraction of material which has a particle dimension smaller than that observed in the only heat-hydrogen treated material. In fact, though particles with an average dimension of 10 μm or more are still clearly visible (figure 3.33 a), a large fraction of material with sizes lower than 5 μm is present (figure 3.33 a). For this material the TEM analysis (figure 3.33 b) reveals the presence of hexagonal particle of pure Mg with a diameter of several hundreds of nm.

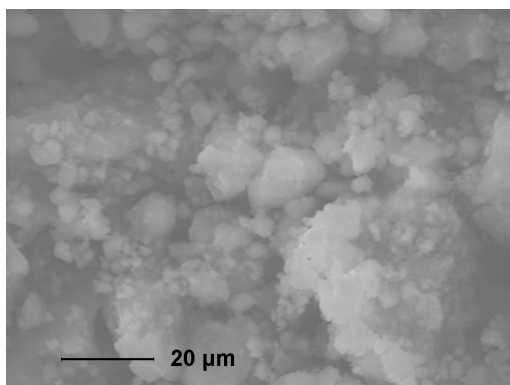


(a) SEM image

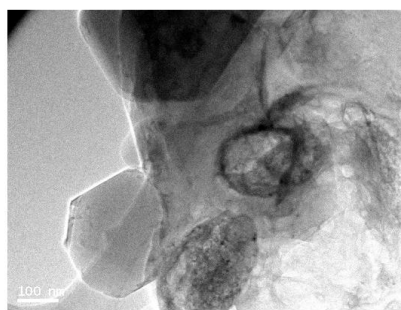


(b) XRD pattern

Figure 3.32: SEM image and XRD pattern of as milled $2\text{NaBH}_4+\text{MgH}_2$ system after heat hydrogen treatment.

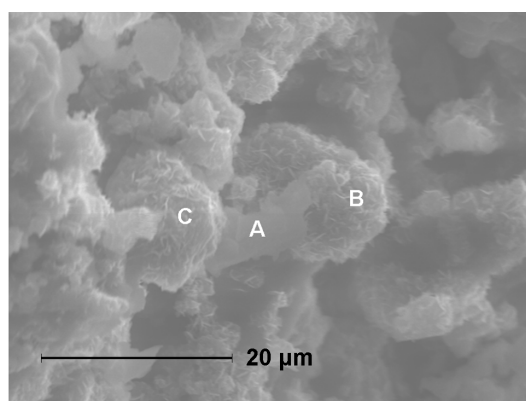


(a) SEM image

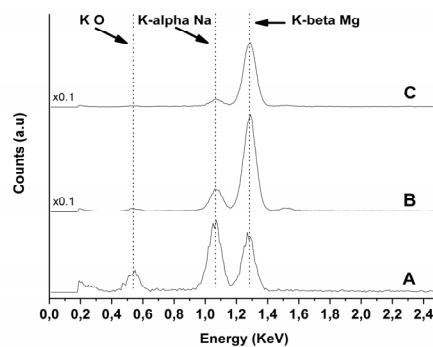


(b) TEM image

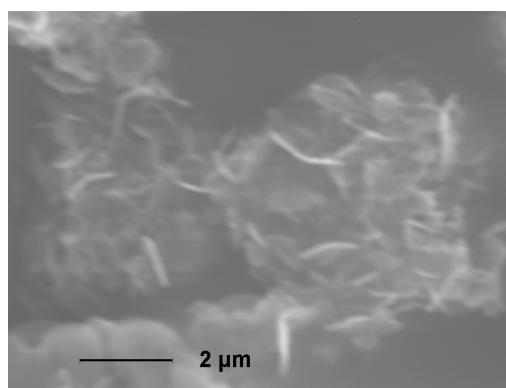
Figure 3.33: SEM image and TEM image of the heat-hydrogen treated $2\text{NaBH}_4+\text{MgH}_2$ system heated to $370\text{ }^\circ\text{C}$ in static vacuum.



(a) SEM image



(b) EDX analysis



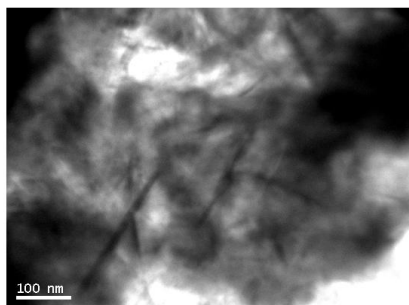
(c) SEM image

Figure 3.34: SEM-EDX analysis of the heat-hydrogen treated $2\text{NaBH}_4+\text{MgH}_2$ system fully desorbed at $450\text{ }^\circ\text{C}$ in static vacuum.

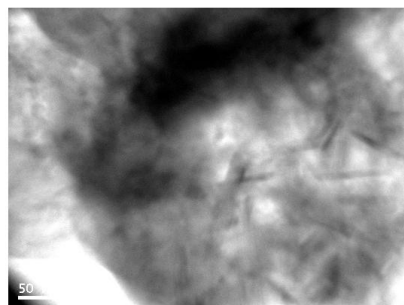
A major change in the surface morphology of the $2\text{NaBH}_4+\text{MgH}_2$ composite is observed for the material fully desorbed (figure 3.34 a, 3.34 b, 3.35 a, 3.35 b). The SEM analysis presented in figure 3.34 a shows the presence of two morphological different portions of the sample. The particles indicated with the letters B and C appear to have a highly disordered surface constructed with stacked micro-sheets of $\sim 2 \mu\text{m}$ in length and $\sim 100 \text{ nm}$ in thickness. The second type of structure is epitomized by the particle indicated with the letter A in figure 3.34. The surface of these formations appears smooth and regular. In addition, these regions show a low stability under the electron beam, whereas the regions B and C are stable. The elemental characterization of the three regions indicated by the letters A, B and C (figure 3.34 a) was performed by EDX technique (figure 3.34 b). The EDX spectra A, B and C in figure 3.34 b correspond to the analysis performed respectively on the regions A, B and C of figure 3.34 a. All three spectra (A, B and C figure 3.34 b) show the presence of three main signals with maximum at 0.54, 1.064, and 1.28 keV. According to literature these peaks correspond to oxygen, sodium and magnesium (K edge oxygen = 0.537 keV ^[44], K-alpha edge sodium = 1.041 keV ^[44] and K-beta magnesium = 1.297 keV ^[44]). In spectrum A (figure 3.34 b) the sodium appears to be the main element present in region A (figure 3.34 a), whereas for the spectra B and C magnesium is clearly the main present element. Unfortunately, due to its low atomic number the boron is not easily detectable by EDX analysis. Based on above results, it is possible to conclude that the particles having irregular surface consist mostly of MgB_2 and the smooth particles of NaH. In fact, although spectrum A (figure 3.34 b) shows the presence of Mg together with Na, this is most probably due to the surrounding MgB_2 particles.

The structural characterization of the completely desorbed material in the nanometer scale was performed by TEM and the results are shown in figure 3.35. Similarly to the SEM analysis, the morphology of the material appears to be organized in two different structures. A part of the material presents an irregular surface, whereas the second structure shows a disordered nano-sheets organization. According to the previously described SEM analysis (figure 3.34 a) this last structure can be referenced to the presence of MgB_2 clusters. In fact, though the structure observed in the figures 3.35 a and 3.35 b appear to have a needle-like shape (length comprised between 50 nm and several hundreds of nm and a thickness of roughly 10 nm) this can be justified by a possible orientation of the MgB_2 sheets parallel to the TEM incident electron beam. This structure similarly to that previously observed in figure 3.34 a shows a high stability under the electron beam whereas the surrounding material

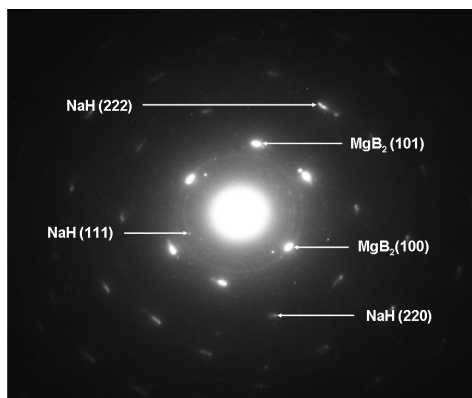
clearly undergoes to a melting-decomposition process. The electron diffraction pattern measured for the material completely desorbed (figure 3.35 c), shows the presence of NaH and MgB₂ as only desorption products. Although the diffraction image reveals the typical patterns of highly crystalline materials, for the MgB₂ reflections the presence of diffuse rings corresponding to a smaller nanocrystallite size is also visible.



(a) TEM image



(b) TEM image



(c) XRD pattern

Figure 3.35: TEM analysis of the heat-hydrogen treated $2\text{NaBH}_4+\text{MgH}_2$ system fully desorbed at 450 °C in static vacuum.

3.4.3 Hydrogen desorption properties of the material exposed to the moist atmosphere

In this section the possibility to enhance the hydrogen desorption properties of the as milled $2\text{NaBH}_4+\text{MgH}_2$ by improving the contact area between NaBH_4 and MgH_2 is reported. In order to achieve such an improvement, two batches of as milled material were exposed to water saturated atmosphere for 1 and 2 hours respectively and subsequently dried. The reasons for exposing the material to the water saturated atmosphere will be discussed in detail in section 4.2.2.

3.4.3.1 Volumetric analysis

Figure 3.36 shows the desorption kinetics registered for the material exposed for increasing time to the water saturated atmosphere. The samples were heated with a constant heating rate of $3\text{ }^\circ\text{C}/\text{min}$ from room temperature to $450\text{ }^\circ\text{C}$ and then kept at constant temperature for several hours. Although the desorption kinetic of the as milled material was already described in section 3.4.1.2 it is here reported again for comparison purpose (curve A). In contrast to the as milled material the desorption kinetics of the material exposed for one hour to the water saturated atmosphere (curve B) shows a two steps desorption reaction. The first step starts roughly at $280\text{ }^\circ\text{C}$, then after desorbing $1.8\text{ wt.}\%$ hydrogen at $420\text{ }^\circ\text{C}$ the second step starts and continues until it reaches an amount of hydrogen equal to $3.4\text{ wt.}\%$. Curve C shows the desorption kinetics of the as milled $2\text{NaBH}_4+\text{MgH}_2$ exposed to the water saturated atmosphere for two hours. Similarly to curve B, curve C also shows a two steps desorption reaction, however, the onset temperatures of the desorption reaction results to be shifted toward higher temperatures. In fact the first desorption step starts at $350\text{ }^\circ\text{C}$ and reaches an amount of released hydrogen equal to $1.8\text{ wt.}\%$ at roughly $420\text{ }^\circ\text{C}$. The second desorption step starts at $450\text{ }^\circ\text{C}$ and continues until after 6 hours an amount of hydrogen equal to $7.8\text{ wt.}\%$ is desorbed.

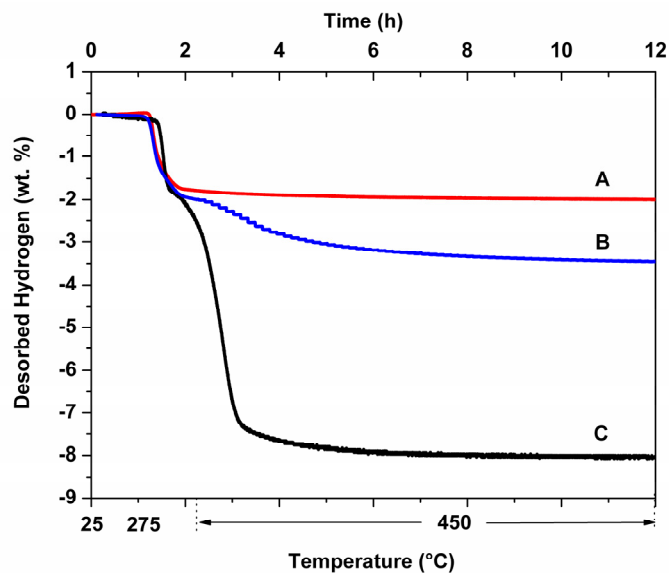


Figure 3.36: Hydrogen desorption kinetics measured in a Sievert's -Type apparatus of as milled $2\text{NaH}+\text{MgB}_2$ measured in a Sievert's -Type apparatus. The samples as milled $2\text{NaBH}_4+\text{MgH}_2$ (curve A), as milled $2\text{NaBH}_4+\text{MgH}_2$ exposed for 1 hour to the water saturated atmosphere (curve B), as milled $2\text{NaBH}_4+\text{MgH}_2$ exposed for 2 hour to the water saturated atmosphere (curve C) were heated under static vacuum from RT to 450°C .

3.4.3.2 MAS NMR analysis

In order to understand the effect of the moisture exposure on the chemical state of the as milled $2\text{NaBH}_4+\text{MgH}_2$, the material was exposed to the moistened atmosphere for two hours and investigated by means of $^{11}\text{B}\{\text{H}\}$ MAS NMR (figure 3.37). The two spectra reported in figure 3.37 are respectively those of the as milled $2\text{NaBH}_4+\text{MgH}_2$ (spectrum A) and as milled $2\text{NaBH}_4+\text{MgH}_2$ after being exposed to the water saturated atmosphere (spectrum B). As for the material as milled the spectrum B shows only the presence of NaBH_4 as B-containing phase (main peak at -42.25 ppm, side band at 55.21 ppm). This result clearly demonstrates that NaBH_4 does not undergo oxidation during the material exposure to the moistened atmosphere.

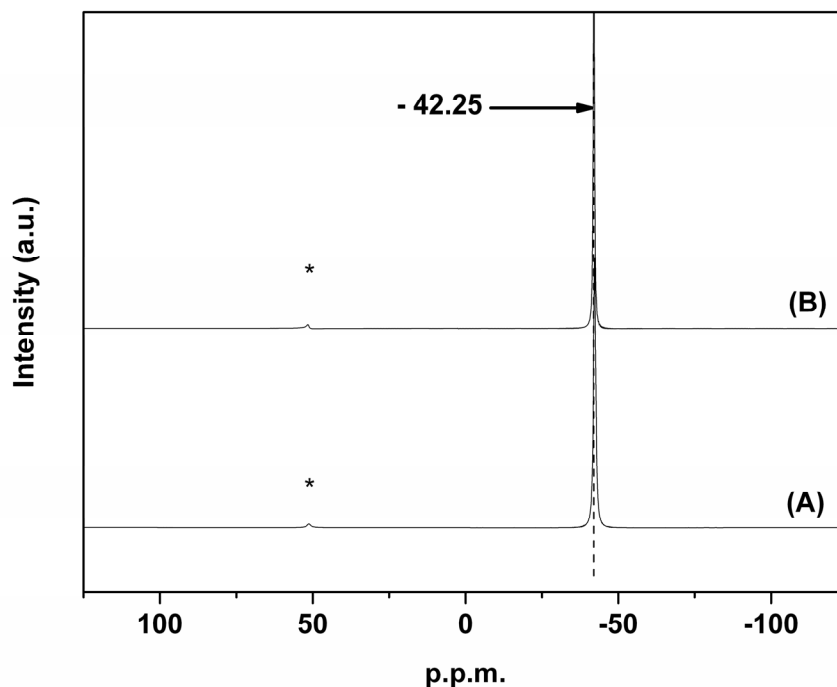


Figure 3.37: A) $^{11}\text{B}\{^1\text{H}\}$ MAS (12 kHz) NMR spectrum of: as milled NaBH_4 , B) as milled $2\text{NaBH}_4+\text{MgH}_2$ exposed for 2 hour to the water saturated atmosphere.

3.4.3.3 Microstructure and phase distribution

Figure 3.38 a shows the SEM picture of the as milled $2\text{NaBH}_4 + \text{MgH}_2$ after two hours of exposure to the water saturated atmosphere and subsequent drying procedure. The morphology and particle size distribution of the material appear deeply changed in comparison with those observed in the only as milled $2\text{NaBH}_4+\text{MgH}_2$ (see figure 3.24 a). Due to the fact that NaBH_4 is partially soluble in water, the surface of the powder particles looks smoother and the average particle size distribution sensibly increased. In order to further investigate the effects of the water exposure on the material, the exposed samples were also characterized by XRD method (figure 3.38 b). Figure 3.38 b shows the diffraction pattern of the as milled material (pattern A), and the respective samples after one and two hours of exposure time to the water saturated atmosphere (respectively pattern B and C). The

reflections associated with the presence of NaBH_4 , $\beta\text{-MgH}_2$ are observed in all three patterns. Although due to the low resolution of the patterns $\gamma\text{-MgH}_2$ is not visible in figure 3.38 b. Its presence is confirmed by the SR-PXD analysis shown in figure 3.40. It must be noticed that for the material exposed to the water saturated atmosphere it is not possible to observe any reflections of possible decomposition or oxidation products.

The Rietveld's analysis performed on the diffraction patterns of the exposed material reveals a progressive increment of the NaBH_4 crystallite size. In fact the NaBH_4 crystallite size in the as milled material was equal to 105 nm, whereas for the material after 1 hour exposure time is equal to 120 nm and to 199 nm for the material after 2 hours exposure time. Differently from the NaBH_4 , the crystallite size of the $\beta\text{-MgH}_2$ does not undergo any changes. Although for values of crystallite sizes higher than 100 nm due to instrumental limitations the accuracy of the measured values is low, these values irrefutably show an increase of the NaBH_4 crystallite size directly related to the increasing exposure time to water saturated atmosphere.

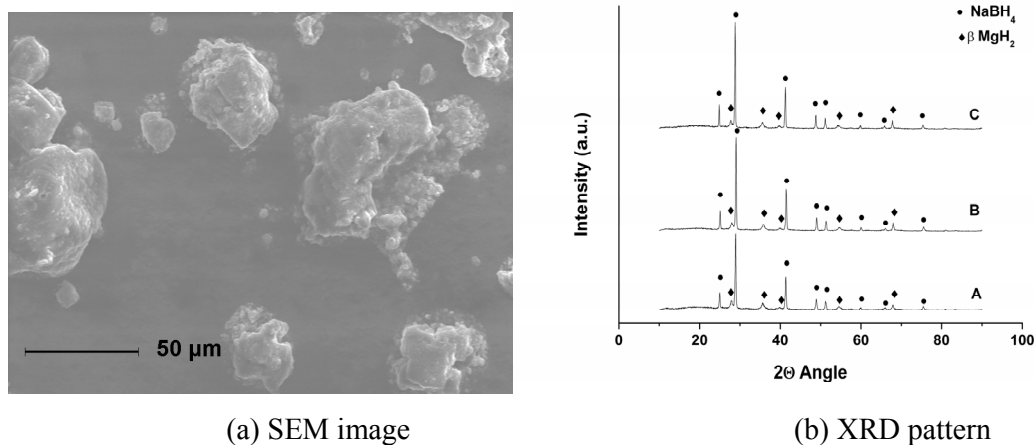


Figure 3.38: SEM image of as milled $2\text{NaBH}_4+\text{MgH}_2$ system after two hours exposure to the water saturated atmosphere and XRD pattern of as milled material (A), as milled material after one hour exposure to the water saturated atmosphere (B) and as milled material after two hours exposure to the water saturated atmosphere (C).

Aiming to understand the reason of the different hydrogen desorptions, the desorbed materials were investigated by XRD (figure 3.39). Pattern A shows the presence of NaBH_4 and free Mg as final products of the desorption reaction for the as milled material. The XRD pattern of the material exposed for 1 hour to the water saturated atmosphere is given by pattern B and shows

the presence of NaBH_4 and Mg plus small amounts of MgB_2 and NaH. This clearly explains the higher amount of desorbed hydrogen of this sample (figure 3.36). The presence of only MgB_2 and NaH in pattern C confirms for the $2\text{NaBH}_4+\text{MgH}_2$ exposed 2 hours to the water saturated atmosphere the achieved complete hydrogen desorption.

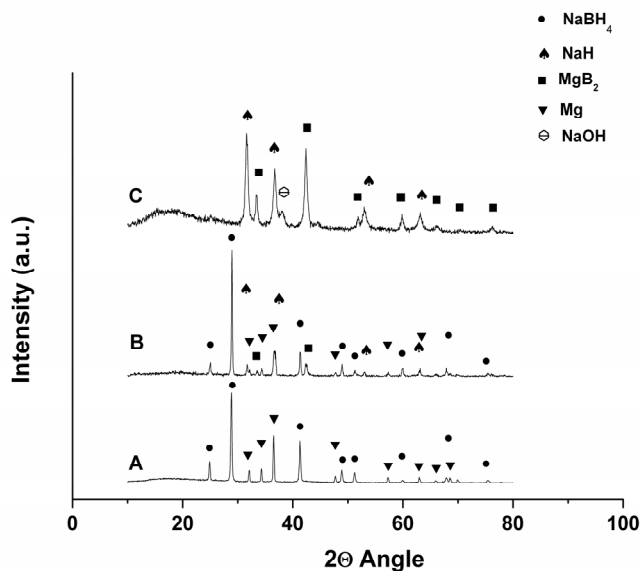


Figure 3.39: XRD pattern of $2\text{NaBH}_4+\text{MgH}_2$ desorbed under static vacuum at 450 °C (wavelength = 0.154184 nm): as milled $2\text{NaBH}_4+\text{MgH}_2$ (pattern A), as milled $2\text{NaBH}_4+\text{MgH}_2$ exposed for 1 hour to the water saturated atmosphere (pattern B), as milled $2\text{NaBH}_4+\text{MgH}_2$ exposed for 2 hour to the water saturated atmosphere (pattern C).

3.4.3.4 In situ SR-PXD characterization

In the attempt of providing a deeper insight regarding the effects of water exposure on the $2\text{NaBH}_4+\text{MgH}_2$ system, the desorption reaction of the material was characterized by *in situ* SR-PXD measurements (figure 3.40). In particular the decomposition reaction of the material with an exposure time of two hours was investigated in detail. The measurement was performed under static vacuum (starting value 10^{-2} bar), heating the material from room temperature to 400 °C (heating rate 3 °C/min), and then keeping it at 400 °C. As previously observed for the as milled material (see section 3.4.1.4), the starting material contains NaBH_4 , $\beta\text{-MgH}_2$, $\gamma\text{-MgH}_2$ and little MgO. Upon heating, the temperature range of room temperature and 230 °C is characterized by the simultaneous intensity decrement of both NaBH_4 and

MgH₂ phases. At 240 °C the $\gamma \rightarrow \beta$ MgH₂ conversion starts and is completed at 280 °C. At 300 °C the decomposition of MgH₂ and the simultaneous formation of Mg occurs. In the temperature range of 300 to 400 °C no other significant event is observed. Then at 400 °C MgB₂ starts to form, and continues during the isothermal period at 400 °C. At the same time the NaBH₄ reflections completely disappear. After an isothermal period of 3 hours the measurement was interrupted without achieving complete hydrogen desorption as clearly demonstrated by the presence of not reacted Mg (see figure 3.40).

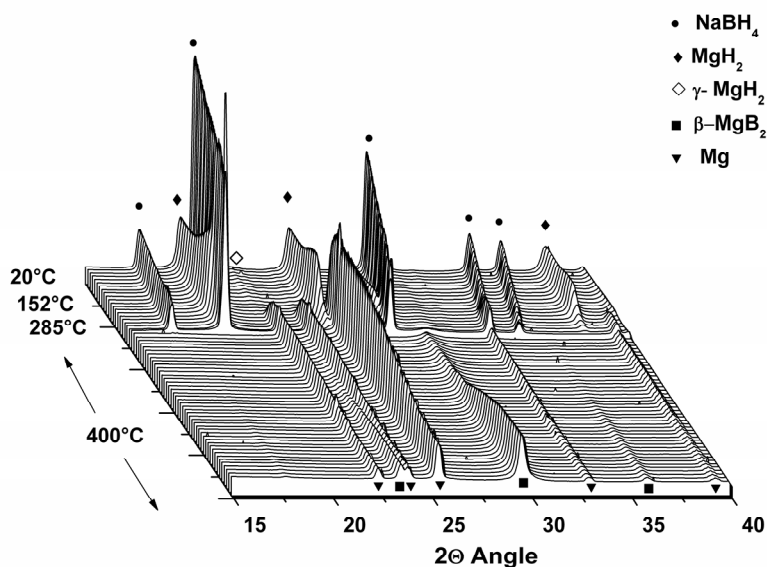


Figure 3.40: Series of SR-PXD patterns of the 2NaBH₄+MgH₂ exposed for two hours to the water saturated atmosphere (and subsequently dried) heated static vacuum from RT to 400 °C and kept under isothermal condition (5 °C/min, wavelength = 0.109719 nm). The measurement was obtained at the beamline I711 at the Max II synchrotron in Lund.

4 Discussion

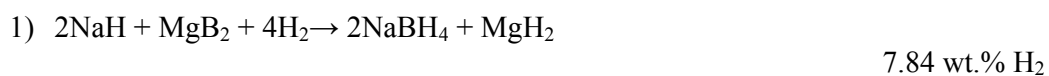
In the following section the sorption properties of the composite system $2\text{NaH}+\text{MgB}_2$ are discussed with regard to the experimental data reported in section 3. Firstly, the $2\text{NaH}+\text{MgB}_2$ hydrogen absorption reaction mechanism is described for an applied hydrogen pressure of 50 and 5 bar respectively. Then for a pressure of 50 bar the reaction mechanism is evaluated as a function of the NaH/MgB_2 ratio present in the starting material. As conclusion of this first part the boundary conditions and the effect on the absorption reaction of the observed intermediate phases is also discussed.

The second part focuses on the desorption reaction mechanism of the ball milled $2\text{NaBH}_4+\text{MgH}_2$ system. In this section the beneficial effect of the heat hydrogen treatment and water exposure on the hydrogen desorption reaction will be also discussed.

4.1 Hydrogen absorption mechanism

In this chapter the absorption reaction processes of the system $2\text{NaH}+\text{MgB}_2$ performed at a hydrogen pressure of 50 and 5 bar are discussed. In addition, for an applied hydrogen pressure of 50 bar the absorption processes of the systems, $1.5\text{NaBH}_4/\text{NaH}$, NaBH_4/NaH and $0.5\text{NaBH}_4/\text{NaH}$ will be also evaluated.

Assuming the complete conversion of the starting reactants into NaBH_4 and MgH_2 for the absorption of the system $2\text{NaH}+\text{MgB}_2$, the reaction was expected to proceed as follow:



However, as reported in section 3, the absorption reaction follows a sensibly different hydrogenation path. Proof of this is the formation of several intermediate phases at an applied hydrogen pressure of 50 bar besides the formation of NaBH_4 . In order to give an exact description of the desorption mechanism, a cross-check between the *in situ* SR-PXD analysis

and HP-DSC, DSC, MAS NMR, TEM and volumetric measurements has been performed as shown in chapter 3. As first step the features of the absorption reaction mechanism are discussed in detail.

Due to its characteristics, the 2NaH/MgB₂ hydrogen absorption kinetics measured at a pressure of 50 bar (figure 3.1) can be divided into two different parts. The first part includes the complete first absorption step from 0 wt.% up to 0.6 wt.%. The second part comprises the complete second step starting at 0.6 wt.% until the measurement stops.

Regarding the first part of the absorption reaction, the comparison of the *in situ* SR-PXD measurement in figure 3.6 with the HP-DSC trace in figure 3.4 allows correlating the first absorption step to the formation of the observed unknown crystalline phase (marked in figure 3.6 with question mark) and NaMgH₃. Based on the ¹¹B{¹H} and ²³Na{¹H} MAS NMR analysis performed on the material heated up to 310 °C at 50 bar H₂, it is possible to draw some conclusions regarding the nature of this observed unknown crystalline phase. The analysis of the data shown in figure 3.10 and figure 3.11 indicates that most probably this unknown phase contains in its structure two not equivalent Na atoms (²³Na{¹H} NMR peaks at -11.71 and -15.97 ppm.), and as suggested by the presence of a signal at -42 ppm in the ¹¹B{¹H} MAS NMR analysis (figure 3.10 B) also boron bonded with hydrogen atoms possibly in form of [BH₄]⁻ anions. The possibility of this phases being Na₂B₁₂H₁₂ or Na₃BH₆ was also checked. However based on the MAS NMR analysis and first principle calculations it is possible to exclude it. In fact, the MAS NMR spectra for the phases Na₂B₁₂H₁₂ gives a signal at -15 ppm, and the calculated energy of formation for Na₃BH₆ is largely positive. Although, the presence of Mg atoms in this phase is also presumable, first ab initio calculations (here not reported) seem to exclude this scenario ^[45]. Comparing the MAS NMR analysis performed for the material hydrogenated under 50 bar (fig. 3.10 and 3.11) with those obtained for the material charged at 5 bar (fig. 3.17 and 3.18) it is clearly visible that along with the formation of NaMgH₃ also other phases not visible in the *in situ* SR-PXD measurements are formed (figure 3.11 C signals at 2.67 ppm and figure 3.10 C signal at 3, 6, 18 and - 15.8 ppm). Among these phases, the presence of amorphous boron is suggested by a broad peak having maximum at 3 ppm in the ¹¹B{¹H} MAS NMR trace of figure 3.10 C. In addition, the CDP analysis of figure 3.12, points out that also the other additional phases formed along with NaMgH₃ do not contain hydrogen. This restricts the spectrum of possible compounds to Mg/B containing phases (different from MgB₂) and Na/B phases only.

Analyzing the second part of the $2\text{NaH}/\text{MgB}_2$ absorption reaction (figure 3.1), it is possible to relate the endothermic peak with its maximum at $330\text{ }^\circ\text{C}$ and the exothermic signal starting at $353\text{ }^\circ\text{C}$ in the HP-DSC trace of figure 3.4 with the disappearing of the unknown crystalline phase reflections at $325\text{ }^\circ\text{C}$ and the formation of NaBH_4 at $370\text{ }^\circ\text{C}$ in the SR-PXD analysis of figure 3.6. By further comparing the *in situ* SR-PXD measurement of figure 3.6 and the HP-DSC of figure 3.4 it is possible to assign the two exothermic peaks observed upon cooling at 367 and $316\text{ }^\circ\text{C}$ respectively to the NaBH_4 - NaH crystallization and re-crystallization of the unknown phase (see figure 3.6).

In section 3.1 we concluded from the appearance of the material after absorption that one or more reaction steps could take place in the liquid state. This assumption is further confirmed by the appearance of the amorphous background at $19.50\text{ }2\theta$ angle in the SR-PXD data (figure 3.6 and 3.7). Therefore, assuming that the two exothermic signals observed upon cooling are due to the precipitation from the melt of NaBH_4 plus NaH at $367\text{ }^\circ\text{C}$ and the unknown crystalline phase at $316\text{ }^\circ\text{C}$ (figure 3.6), we can conclude that the two phases in the liquid form coexist together in the observed molten phase. However, this coexistence as clearly shown by the HP-DSC trace of figure 3.5 is only temporary. In fact, the HP-DSC trace of the material kept 90 minutes at $400\text{ }^\circ\text{C}$ and 50 bar of hydrogen pressure shows during cooling the presence of the NaBH_4 - NaH crystallization peak at $367\text{ }^\circ\text{C}$ only. This suggests a progressive consumption or decomposition of the unknown phase in favour of the molten NaBH_4 - NaH phase. The NaBH_4 - NaH molten phase, which so far has been observed in all measurements, presumably comprises only a molten salt mixture of NaH and NaBH_4 . In fact, both these phases reappear in the SR-PXD analysis of figure 3.6 once the temperature decreases below $370\text{ }^\circ\text{C}$. Moreover, further experiments performed on a 1:1 mixture of NaH and NaBH_4 show upon heating a melting point of $383\text{ }^\circ\text{C}$ and a solidification point of $383\text{ }^\circ\text{C}$ during cooling for a range of investigated H_2 pressures between 5 and 50 bar (figure 4.1). This temperature is lower than the melting points of both single compounds ($T_m(\text{NaH}) = >400\text{ }^\circ\text{C}$ ^[46] and $T_m(\text{NaBH}_4) = 505\text{ }^\circ\text{C}$ ^[47]). In addition, this measurement confirms a reaction which involves the two phases (NaH and NaBH_4), and suggests the formation of a eutectic melting between NaH and NaBH_4 .

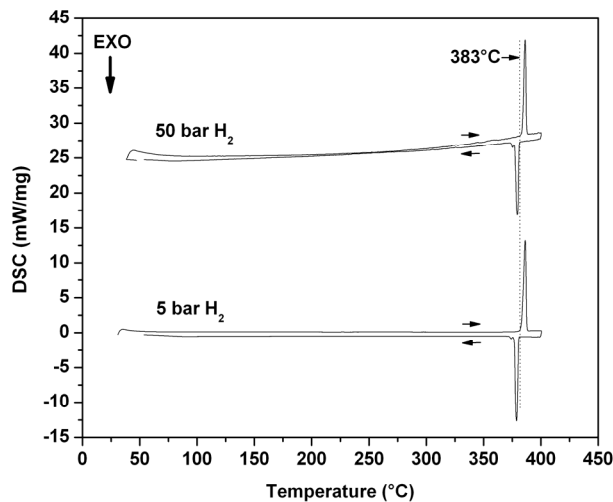


Figure 4.1: HP-DSC traces of a 1:1 mixture of NaH and NaBH₄, measured at 5 and 50 bar of hydrogen pressure from RT to 450 °C and subsequently cooled (5 °C/min heating/cooling rate).

The hydrogen uptake for the measurement performed at 50 bar H₂ shown in figure 3.1 stops after 3 hours. The *in situ* SR-PXD analysis of figure 3.7 suggests for this measurement as final state a mixture of MgB₂, NaMgH₃, NaBH₄, Mg and the NaBH₄-NaH molten phase. However, this final composition is most probably caused by the kinetic constraints which are depending on the preparation of the material, the amount of material investigated and sample holder design and of course the applied external parameters like temperature and pressure. In fact a further absorption measurement performed for the system 2NaH/MgB₂ under the same temperature and pressure conditions, but using another Sievert's apparatus with differently designed sample holder (see section 2.3), leads to different results as can be seen in figure 3.19 and 3.21). Figure 3.19 A shows the absorption measurement of the system 2NaH/MgB₂ measured at the JRC's Institute for Energy under 50 bar of pressure at 400 °C (heating rate 3 °C/min). The first part of the curve (figure 3.19 A) exactly traces out the absorption measurement performed at the Helmholtz-Zentrum Geesthacht. This indicates that the first step of the absorption, the absorption behavior of the material in the solid state, is independent from the utilized apparatus. However, in contrast to the results shown in figure 3.1 the second part of the absorption (figure 3.19 A), does not stop after 3 hours but continues until it reaches

in two separate steps a total storage capacity of almost 6 wt.%. The presence of NaBH₄ and free Mg as only products of this absorption (see figure 3.21 A) clearly justifies the observed different absorption behavior. Therefore, for the system 2NaH/MgB₂ the reproducibility of the absorption measurement (for the temperature and pressure conditions investigated in this work) is strictly dependent on the design of the used sample holder. The absence of NaMgH₃ in the XRD analysis of figure 3.21 it is due to a progressive consumption of NaMgH₃ in favor of the NaBH₄-NaH molten phase and NaBH₄ which takes place in the region between 3 and 5.75 wt.% of stored hydrogen. That Mg is not hydrogenated under the applied conditions is unexpected and weird. According to what has been found in this thesis about the presence of a eutectic NaBH₄-NaH molten phase it can be concluded that this phase which coexists with NaBH₄ and Mg affects the hydrogen diffusion according to a mechanism that will be discussed in section 4.1.2 and thereby hinders the hydrogenation of Mg.

From the above mentioned follows that for the 2NaH+MgB₂ absorption reaction performed under 50 bar H₂ the reaction mechanism can be resumed by the following scheme (figure 4.2):

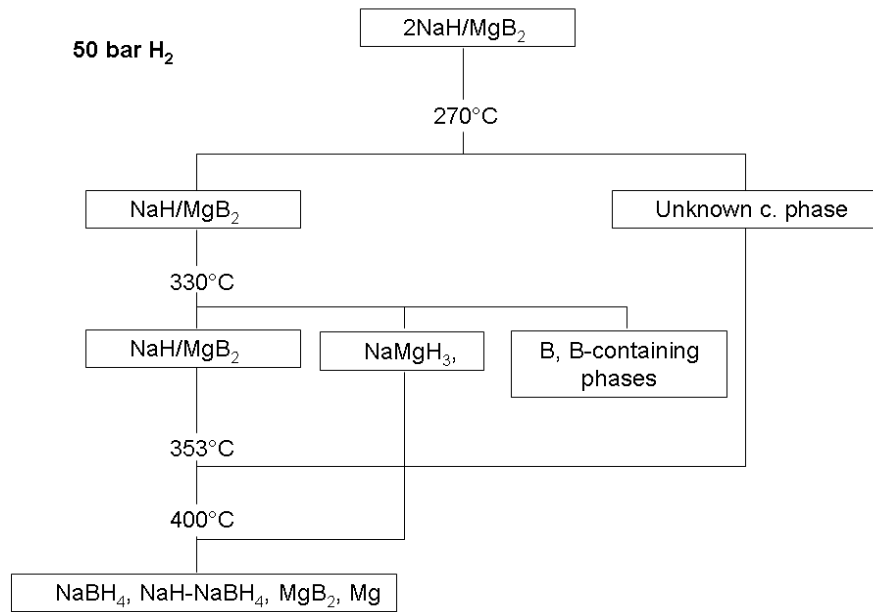


Figure 4.2: Hydrogen absorption reaction scheme of the system 2NaH+MgB₂ at 50 bar H₂ pressure.

In section 3.3 the absorption reaction mechanism under a pressure of 50 bar H₂, was shown to strongly depend on the NaH-MgB₂ ratio of the starting material. The effect of the

NaH-MgB₂ ratio is clearly visible in the volumetric analysis of figure 3.19. In fact, though all measured absorption kinetics show an identical first absorption step, they strongly differ in the manner the hydrogen absorptions proceeds. In particular, sensible differences are observed between the systems 2NaH/MgB₂ and 0.5NaH/MgB₂ (figure 3.19 curves A and D), whereas the absorption curves of the systems 1.5NaH/MgB₂ and 1NaH/MgB₂ are rather similar to those of 2NaH/MgB₂ and 0.5NaH/MgB₂, respectively. Differences are also visible on the XRD analysis of the absorbed materials (figure 3.21). The absorbed 1.5NaH/MgB₂ (pattern B) shows the presence of NaBH₄ and free Mg plus unreacted MgB₂, whereas the absorbed 1NaH/MgB₂ and 0.5NaH/MgB₂ (figure 3.21 C and 3.21 D) contain NaBH₄, MgH₂ and MgB₂, though in different ratios.

Clear differences between the absorption reaction of the systems 2NaH/MgB₂, 1.5NaH/MgB₂, 1NaH/MgB₂ and 0.5NaH/MgB₂ are also visible in the calorimetric analyses of figure 3.22 (curve A, B, C and D). The onset temperature of the first exothermic peak of the traces B, C and D (peaks attributed to the formation of the unknown crystalline phase and of the NaMgH₃ phase) following the decrement of the NaH amount, sensibly shift towards lower temperature. This, indicates a direct relation between the earlier beginning of the absorption reaction and the amount of NaH contained in the system. A possible explanation for this phenomenon can be given based on the crystallite sizes of NaH and MgB₂. In section 3.3.2 (table 3.2) we reported that the crystallite sizes of both NaH and MgB₂ in the milled material decreases with the reduction of the amount of NaH in the NaH-MgB₂ system. This crystallite size decrement leads to a shortening of the diffusion paths in the composite. Therefore, as result of this shortening of diffusion distances, kinetics improve and accordingly the onset temperature of the hydrogen absorption reaction is lowered. This is also valid for the NaBH₄ formation. In fact, in the case of the 0.5NaH/MgB₂ system the formation of NaBH₄ starts at 325 °C (see figure 3.22 D), which is by about 30 °C lower than in the reference system 2NaH/MgB₂ (see figure 3.22 A). Another effect of the reduction of the NaH content is observed in the HP-DSC analysis of figure 3.22, where an intensity drop of the endothermic signal related to the melting of the unknown crystalline phase at 330 °C is observed. This decrement is particularly significant for the composition NaH/MgB₂ and 0.5NaH/MgB₂ (respectively figure 3.22 C and 3.22 D) whereas for the composition 1.5 NaH/MgB₂ (figure 3.22 B) it is not. According to the in-situ XRD measurement shown in figure 3.23 the unknown crystalline phase and NaMgH₃ are the only sources of Na in the system in the

moment when NaBH_4 starts to form and they start to be consumed before the temperature reaches $330\text{ }^\circ\text{C}$. This explains also the absence of the exothermic peak at $316\text{ }^\circ\text{C}$ in the HP-DSC traces C and D of figure 3.22 during cooling.

In the temperature range between $330\text{ }^\circ\text{C}$ and $400\text{ }^\circ\text{C}$, the absorption reaction mechanisms of the four investigated stoichiometries reveal further differences. These differences are more marked in the cases of the systems NaH/MgB_2 and 0.5NaH/MgB_2 (figure 3.22 C and 3.22 D). In fact, whereas for the systems 2NaH/MgB_2 and 1.5 NaH/MgB_2 (figure 3.22 A and 3.22 B) only a single exothermic signal is visible, the systems NaH/MgB_2 (figure 3.22 C) and 0.5 NaH/MgB_2 (figure 3.22 D) show the presence of a broad peak split into two and three parts respectively. These differences in respect to the reference system 2NaH/MgB_2 are due to the continued hydrogen absorption reaction towards the formation of NaBH_4 , MgH_2 and disappearance of NaMgH_3 as clearly visible in the SR-PXD analysis of figure 3.23. In addition, the absence of additional peaks in the cooling period of the traces C and D of figure 3.22 is an evidence of the completeness of the absorption reaction (see figure 3.21). As already mentioned in section 3.3.4, differently from the 2NaH/MgB_2 system the absorption reaction performed for 0.5 NaH/MgB_2 (see figure 3.23) does not lead to the formation of the NaH/NaBH_4 liquid phase. This is due to the fact that in the system 0.5 NaH/MgB_2 the formation of NaBH_4 starts after NaH (initially present in the system) is completely consumed by the previous formation of the unknown crystalline phase and NaMgH_3 . The absorption measurements performed at 50 bar pressure for the systems NaH/MgB_2 and 0.5NaH/MgB_2 show a hydrogen uptake of significantly less than the theoretical values (5.4 and $3.36\text{ wt.}\%$ respectively). This can be explained by the possible formation of small amounts of amorphous boron and other species containing Na and B or Mg and B as previously observed for the system 2NaH/MgB_2 . The hydrogen absorption reaction path for $0.5\text{ NaH}+\text{MgB}_2$ can be resumed as follow (figure 4.3):

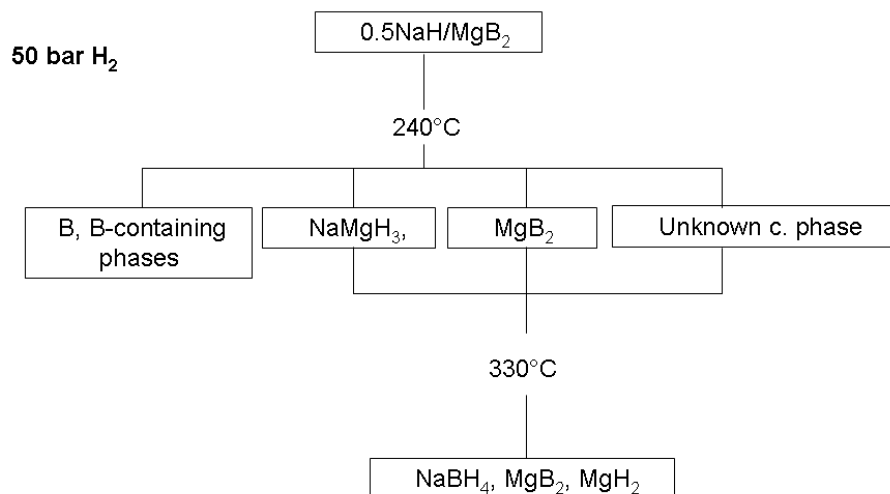


Figure 4.3: Hydrogen absorption reaction scheme of the system $0.5\text{NaH}+\text{MgB}_2$ at 50 bar H_2 pressure.

Hereunder, the absorption reaction mechanism of the $2\text{NaH}+\text{MgB}_2$ system is described for an applied hydrogen pressure of 5 bar . The hydrogenation process at 5 bar H_2 , though still leading to the liquid phase, does not allow NaMgH_3 as well as the unknown crystalline phase to form (figure 3.16). This finding suggests that the formation of these two phases strongly depends on the applied hydrogen pressure. Comparing the calorimetric analysis of figure 3.15 C to the *in situ* SR-PXD measurements performed under 5 bar of hydrogen pressure (figure 3.16), it is possible to assign the broad exothermic signal with onset at 320°C (figure 3.15) to the formation of the amorphous background starting at 320°C (figure 3.16). In addition, the exothermic peak observed at 367°C during cooling has to be related to the formation of NaBH_4 and partial formation of NaH (figure 3.16). It must be noted, that in contrast to the HP-DSC analysis carried out at a pressure of 50 and 25 bar (figure 3.15 traces A and B), the measurement performed at 5 bar does not show the exothermic signal at 316°C upon cooling. This is due to the fact that the unknown crystalline phase is not formed under these conditions. For the system $2\text{NaH}+\text{MgB}_2$ the hydrogenation reaction at 5 bar H_2 can be resumed by the following scheme (figure 4.4):

5 bar H₂

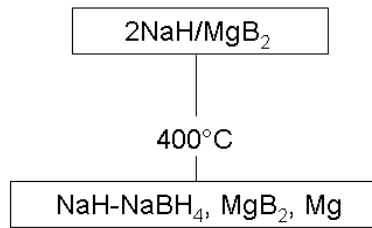


Figure 4.4: Hydrogen absorption reaction scheme of the system $2\text{NaH}+\text{MgB}_2$ at 5 bar H₂ pressure.

Unfortunately, because of the missing composition of some of the intermediate phases and of the unknown amount of material involved in each single step, it is not possible to give a more exact description of the events taking place during the absorption measurements at 50 and 5 bar H₂ pressure.

In this section the hydrogen absorption process of the NaH-MgB₂ composite was described. The reasons of NaMgH₃ and NaH-NaBH₄ molten phase formation as well as their influence on the overall absorption process will be addressed in the next two sections.

4.1.1 MgH₂ and NaMgH₃ formation

A peculiarity in all the absorption measurements reported in this work is the lack of MgH₂ even though its formation is thermodynamically favored in the experiments performed at 50 and 25 bar H₂. Moreover for the 2NaH+MgB₂ absorption reaction the MgH₂ formation has been observed by Barkhordarian et al. [26] and Mao et al. [48] using setups different from the one used for this work. In the experiments presented in this work NaMgH₃ and free Mg are found only. Recently Ikeda et al. [49] reported that NaMgH₃ can be synthesized by mechanical milling of NaH and MgH₂ mixture, at ambient temperature and inert atmosphere. Considering that the experiments performed in this work were carried out at relatively high temperatures a possible explanation for the missing MgH₂ formation can be given by the fact that as soon as MgH₂ is formed it reacts with remaining NaH to form NaMgH₃. In order to prove this assumption, an absorption measurement was performed at conditions of hydrogen pressure and temperature at which the MgH₂ formation is thermodynamically not possible, but where NaMgH₃ is stable. Based on the van't Hoff equation the equilibrium H₂ pressure of MgH₂ was calculated to be about 45 bar at 450 °C (assuming an enthalpy of formation ΔH_F equal to -74.4 kJmol⁻¹ [50] and entropy of formation ΔS_F of -135 Jmol⁻¹K⁻¹ [50] for the range of temperatures between 314 and 576 °C). In contrast NaMgH₃ was found to be thermally stable up to 500 °C at a hydrogen pressure of 10 bar [51]. Consequently we performed a hydrogen absorption measurement at a constant temperature of 450 °C and 20 bar hydrogen pressure of the as milled 2NaH+MgB₂ mixture (figure 4.5).

The initial phase of the absorption reaction was characterized by a fast hydrogen uptake until the hydrogen stored in the system reached a value of 2.5 wt.%. Then the absorption continued reaching asymptotically a total amount of 5.45 wt.% after 17.5 hours. Note, that since at these experimental conditions MgH₂ should not be formed, a maximal H₂ capacity of 6 wt.% is expected if the formation of NaBH₄ is considered. During cooling, at a temperature of 360 °C the hydrogen absorption started again charging a further 0.1 wt.% of hydrogen. The XRD analysis of the material as above synthesized is shown in figure 4.6. The diffraction pattern shows the presence of NaBH₄, Mg, NaH, MgB₂ and only a tiny amount of NaMgH₃. We suppose that this NaMgH₃ is formed during cooling, where the system crosses conditions of temperature and pressure favorable for MgH₂ formation. (at 360 °C, $p_{eq}(\text{MgH}_2) = 8.44$ bar

H₂, assuming an enthalpy of formation ΔH_F equal to -74.4 kJmol^{-1} [50], and entropy of formation ΔS_F of $-135 \text{ Jmol}^{-1}\text{K}^{-1}$ [50])

These results underline the supposition that NaMgH₃ is formed by a two phase reaction of MgH₂ and NaH only, moreover they also explain the reason why, in presence of NaH, it has never been possible to observe MgH₂ as final absorption product since the formation of NaMgH₃ is thermodynamically much more favorable. This indicates that the kinetic boundary conditions for the NaMgH₃ formation in the system NaH-MgB₂ are identical to the thermodynamic boundary conditions of MgH₂. In addition, the above discussion justifies the lack of NaMgH₃ formation in the hydrogen absorption measurements performed at 5 bar of hydrogen pressure and during the desorption of the 2NaBH₄ + MgH₂ in vacuum. In fact, $p_{eq}(\text{MgH}_2) = 5 \text{ bar}$ at 350 °C, thus MgH₂ formation is possible only in short range of temperature (and time), which very likely is not sufficient to lead to a significant formation of MgH₂. Consequently, since MgH₂ is not formed, it is not possible to observe NaMgH₃ among the final products neither during absorption at 5 bar of hydrogen pressure nor during the desorption in vacuum, even if it is known to be stable under these temperature and pressure conditions [51].

On the basis of the combined Sievert's and ex-situ X-ray diffraction measurements it is possible to conclude that the formation of NaMgH₃ has a detrimental effect on the absorption reaction. In fact the formation of NaMgH₃ removes NaH from the system, which is not available for the formation of NaBH₄. Recently Shane et al. [52] demonstrated that atomic hydrogen can easily diffuse into the NaMgH₃ structure, however, the formation of such a hydride might affect the diffusion of species different from H. A likely scenario is that NaMgH₃ forms around MgB₂ particles enveloping them and consequently disturbing the borohydride formation by blocking any direct contact between NaH and MgB₂, with a mechanism mirroring the one explained by Stander [7] for the MgH₂ formation. This would explain why absorption at lower H₂ pressures (where NaMgH₃ formation is suppressed) yields higher amounts of hydrogen uptake. This hypothesis is corroborated by results of TEM measurements performed on material which was hydrogenated at 50 bar of hydrogen pressure and 400 °C (figure 3.9 b). Here a high overlapping between the lattice planes of MgB₂ and those of NaMgH₃ and NaBH₄ is observed. This particular plane disposition can be interpreted as a shield structure of superimposed different hydride phases.

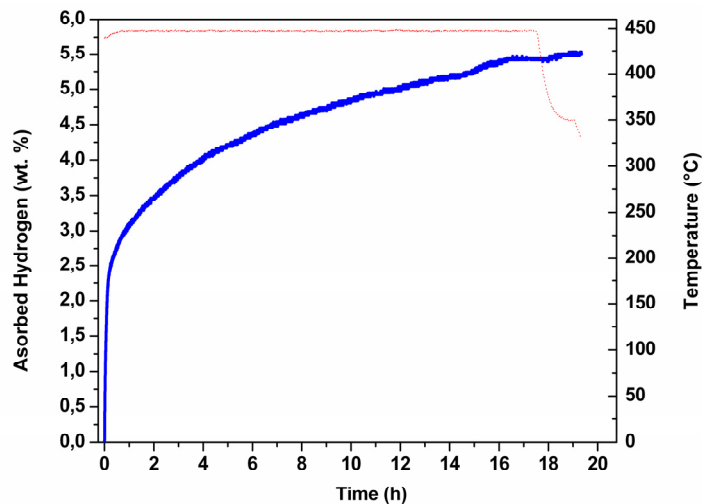


Figure 4.5: Absorption kinetic of the material $2\text{NaH}+\text{MgB}_2$ as milled measured in a Sievert's-Type apparatus. The measurement was performed at $400\text{ }^\circ\text{C}$ under 20 bar of hydrogen pressure. Thick line shows hydrogen uptake while thin dots line refer to the temperature of the powder bed.

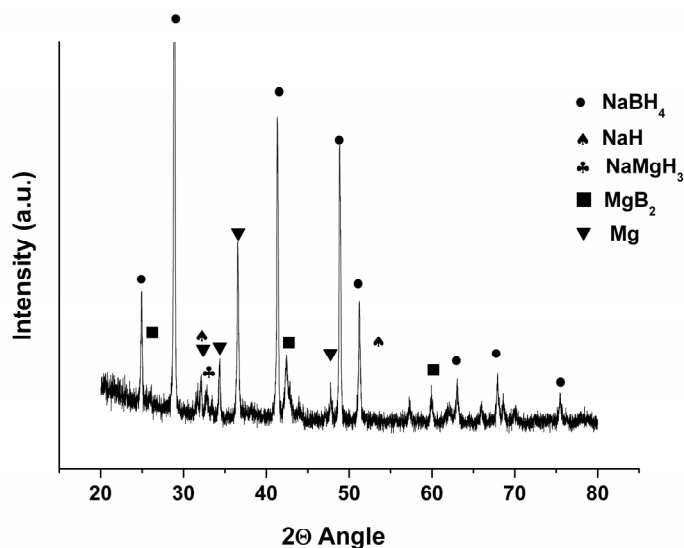


Figure 4.6: XRD patterns of the $2\text{NaH}+\text{MgB}_2$ after absorption under 20 bar of hydrogen pressure at $450\text{ }^\circ\text{C}$ (wavelength = 0.154184 nm).

Similarly to the system $\text{NaH}-\text{MgB}_2$, the formation of a ternary hydride ($\text{Ca}_4\text{Mg}_3\text{H}_{14}$) is also observed in $\text{CaH}_2-\text{MgB}_2$ during the desorption of the hydrogenated products ^[43] and in $\text{CaH}_2-\text{CaB}_6-\text{Mg}$ ^[53] during the absorption and most likely also during the desorption. The

formation of $\text{Ca}_4\text{Mg}_3\text{H}_{14}$ influences the sorption properties of the systems $\text{CaH}_2\text{-MgB}_2$ and $\text{CaH}_2\text{-CaB}_6\text{-Mg}$ differently than NaMgH_3 affects the system NaH-MgB_2 . Whereas the formation of NaMgH_3 on the absorption reaction of the system NaH-MgB_2 has a detrimental effect, the formation of the phase $\text{Ca}_4\text{Mg}_3\text{H}_{14}$ in the system $\text{CaH}_2\text{-CaB}_6\text{-Mg}$ plays an important role in increasing the absorption reaction kinetics and it allows the system to be reversible. As in case of NaMgH_3 the formation of $\text{Ca}_4\text{Mg}_3\text{H}_{14}$ during the dehydrogenation of $\text{Ca}(\text{BH}_4)_2\text{-MgH}_2$ increases the overall desorption temperature of the system. In fact, CaH_2 formed in the first step of the reaction, reacts with MgH_2 forming the more stable hydride $\text{Ca}_4\text{Mg}_3\text{H}_{14}$.

4.1.2 Effect of the NaH-NaBH₄ molten phase on the absorption reaction

The last issue regarding the hydrogen absorption process not yet fully addressed is to explain the presence of elemental Mg among the final absorption products. As observed in figure 3.7 the appearance of free Mg with the consequent inhibition of the growth of NaMgH_3 phase follows the formation of the NaH-NaBH_4 molten phase. In order to see if the appearance of free Mg is related to the formation of the above mentioned molten phase an *in situ* SR-PXD measurement was performed at 50 bar H_2 restricting the maximum temperature to 300 °C (Figure 4.8). In fact at this temperature all the reactants and products should remain in the solid state.

As already observed for the previous SR-PXD measurement performed under 50 bar of pressure the formation of the unknown crystalline phase is found to take place at roughly 270 °C. No further phase formation is observed until the temperature reaches 300 °C. After reaching the constant temperature of 300 °C the formation of NaMgH_3 starts, followed later by the formation of NaBH_4 . Due to the decreased measurement temperature the formation of the amorphous background can not be observed, hence confirming an “all solid state” reaction. None of the free Mg reflections can be observed which clearly demonstrates that the NaH-NaBH_4 molten phase represents a barrier for the hydrogen diffusion into the system.

Regarding the diffusion of hydrogen in hydride systems, a deep knowledge of this issue exists for metal hydrides. However, little is known regarding the H diffusion in “complex” metal hydrides. In fact the differences in the electronic structure between the two families of hydrides lead to completely different diffusion mechanisms. Recent studies on hydrogen diffusion in borohydrides demonstrate that for this class of hydrides the hydrogen diffusion follows two different paths. The main one involves the diffusion of intact $[\text{BH}_4]^-$ units ^[54] and has to be considered valid for both for the solid state and the molten state. Secondly, the hydrogen can diffuse as individual H atom between not diffusing (or only slowly diffusing) borohydride units ($[\text{BH}_4]^-$) ^[55-57]. Consequently, the diffusion of hydrogen through the molten NaH-NaBH₄ phase should be possible if $[\text{BH}_4]^-$ units are present in the phase.

In order to further elucidate the reaction mechanism of this molten phase the determination of the chemical composition is mandatory. For this reason the Rietveld’s analysis of the diffraction patterns shown in figure 3.16 has been performed. In fact the SR-PXD patterns collected at 5 bar hydrogen pressure (figure 3.16) during the isothermal period at 400 °C shows the presence of free Mg and remaining MgB₂ together with an amorphous background due to the presence of the NaH-NaBH₄ molten mixture. Bragg reflections related to the possible presence of NaH and NaBH₄ can not be observed. Consequently, assuming that no hydrogen exchange takes place during the NaH-NaBH₄ melting/crystallization, by calculating the amount of NaH and NaBH₄ formed during the cooling period it is possible to obtain information concerning the composition of the molten phase. The mentioned calculation was obtained by Rietveld’s refinement of the diffraction pattern of figure 3.16 collected at a temperature of 60 °C during cooling. The results of the fitting procedure performed by the MAUD program are shown in figure 4.7. The calculated weight fraction for the present phases is the following: 11 wt.% NaH, 43 wt.% MgB₂, 28 wt.% NaBH₄ and 18 wt.% Mg. In conclusion, two possible explanations can be given to elucidate the molten phase hydrogen isolating mechanism. The molten salt mixture has an ionic character and this must be taken in account. In fact, although the measurements were performed at high temperatures and high hydrogen pressures, for an un-polar gas such as H₂, the diffusion through an ionic liquid media (e.g. NaH-NaBH₄ molten phase) is rather difficult. However, this can not be the only reason. In fact, as mentioned above, in the case of molten borohydride the hydrogen can diffuse by means of intact $[\text{BH}_4]^-$ units diffusion and by H atoms. This shows a certain degree

of mobility for $[\text{BH}_4]^-$ units. At this point the presence of B and H atom containing phases different from $[\text{BH}_4]^-$ units and with consequently different features is very likely. Moreover, the incapacity of the free Mg to remove hydrogen from the surrounding molten phase suggests that the stability of the hydrogen bonded in the liquid phase is higher than that bonded in the MgH_2 .

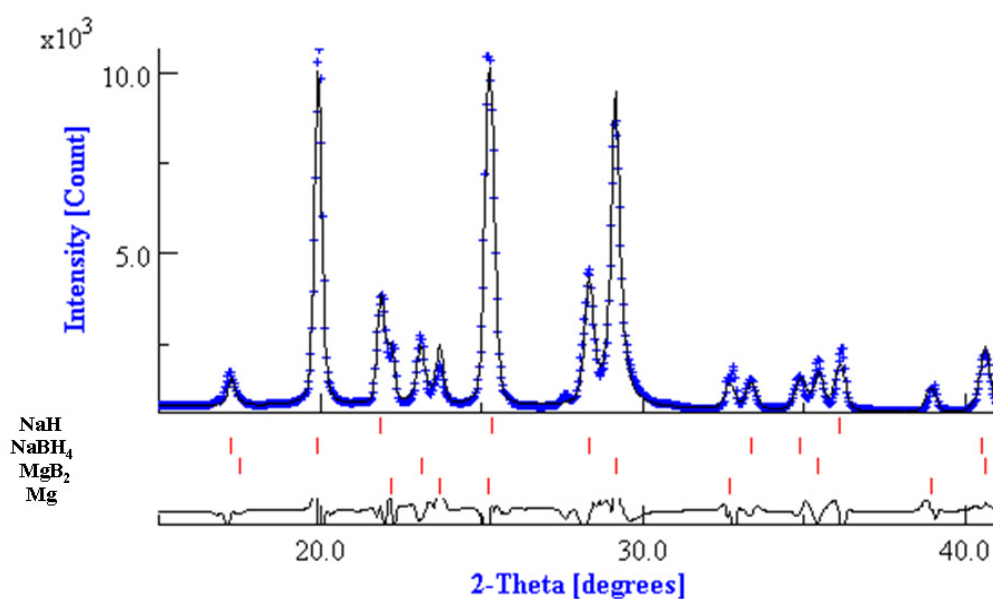


Figure 4.7: Rietveld refinement of the SR-PXD pattern relative to the $2\text{NaH}+\text{MgB}_2$ hydrogenated under 5 bar and $400\text{ }^\circ\text{C}$ cooled down to $60\text{ }^\circ\text{C}$.

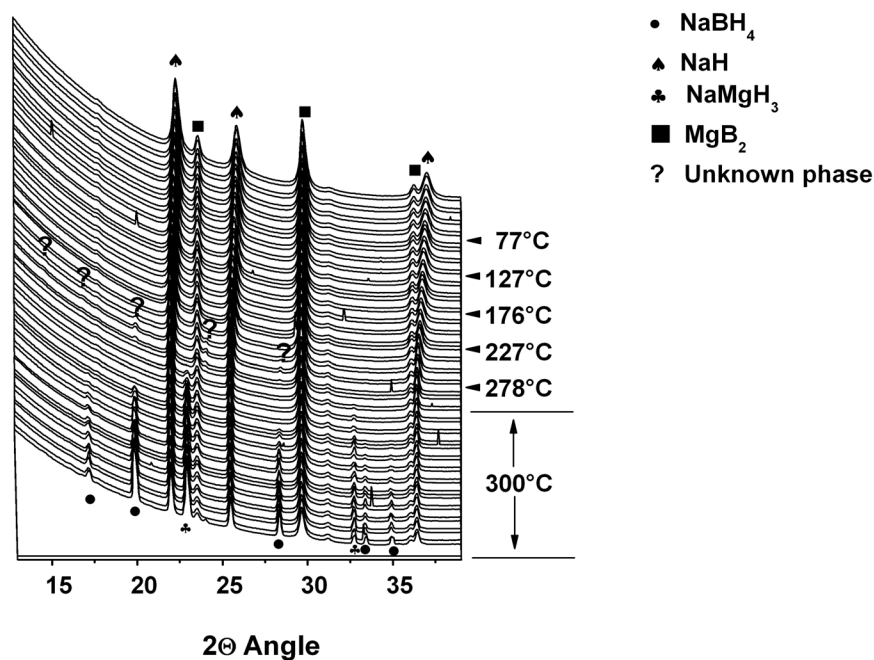
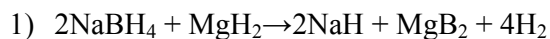


Figure 4.8: Series of SR-PXD patterns of the $2\text{NaH}+\text{MgB}_2$ system heated at 50 bar hydrogen pressure from RT to 300 °C and kept under isothermal condition (5 °C/min, wavelength = 0.109719 nm). The measurement was obtained at the beamline I711 at the Max II synchrotron in Lund.

4.2 Hydrogen desorption mechanism

In this section the hydrogen desorption mechanism observed for the composite system $2\text{NaBH}_4/\text{MgH}_2$ under static vacuum conditions is described. When at first the possibility to synthesize $2\text{NaBH}_4+\text{MgH}_2$ starting from NaH, MgB_2 and H_2 was demonstrated ^[26], a single step desorption reaction path was expected according to the following equation:



However, the results presented in this work demonstrate clearly that the desorption reaction of the system $2\text{NaBH}_4+\text{MgH}_2$ proceeds via a multi-step reaction. Recently, this has been confirmed by several publications ^[31, 48, 58, 59].

Differently from the results reported in literature, in our measurements the complete hydrogen desorption for the pure as milled $2\text{NaBH}_4+\text{MgH}_2$ was never achieved at temperature $T \leq 450$ °C. Full hydrogen desorption was obtained only for the material annealed under hydrogen atmosphere and for that exposed to a moistened atmosphere. In order to shed more light on the observed reaction mechanism of the system $2\text{NaBH}_4+\text{MgH}_2$ a comparison of the DSC, *in situ* SR-PXD, MAS NMR and volumetric analysis is reported below.

The hydrogen desorption reaction of the as milled $2\text{NaBH}_4+\text{MgH}_2$ recorded under static vacuum (initial pressure value 10^{-2} bar) and $T \leq 450$ °C shows a single step desorption path (figure 3.25). According to the *in situ* SR-PXD analysis (figure 3.27) this first step involves the desorption of the hydrogen from $\gamma\text{-MgH}_2$ and $\beta\text{-MgH}_2$ as seen also in the DSC-MS analysis of figure 3.26. In spite of the $\gamma \rightarrow \beta\text{-MgH}_2$ partial conversion observed in figure 3.27, no visible calorimetric signal related to this conversion is observed in the DSC analysis of figure 3.26. Although, the volumetric analysis (figure 3.25) and the *in situ* SR-PXD characterization (figure 3.27) do not show further signs of hydrogen desorption, the results shown in figure 3.26 hint towards it. In fact at 400 °C in the DSC trace A (figure 3.26), an endothermic signal is present related to a small hydrogen release (figure 3.26 trace B). Most probably this signal is due to a restricted decomposition of NaBH_4 and formation of NaH and MgB_2 taking place on the grain boundaries between Mg and NaBH_4 . This supposition finds a confirmation in the work of Czujko et al. ^[58], where for the composite system $\text{MgH}_2 + 20$ wt.% NaBH_4 the decomposition of NaBH_4 and consequent formation of MgB_2 was found to takes place at 405 °C. In addition, the reaction between free Mg and NaBH_4 to form NaH and MgB_2 was observed also to take place at 400 °C for both the heat-hydrogen treated material (section 3.4.1.4) and for the material exposed to the water atmosphere (section 3.4.3.4). As observed in section 3.4.2.4 the morphology of the newly formed MgB_2 shows a highly irregular surface, made of sheets stacked together to form globular agglomerates (figure 3.34). The possibility to obtain MgB_2 with a plate-like structure was early reported by Sergey Lee ^[60]. Recently, Bösenberg et al. ^[61] reported on the formation of this particular structure of MgB_2 during the $2\text{LiBH}_4+\text{MgH}_2$ desorption reaction. However, this is the first time that the formation of MgB_2 plate-like structures is observed in the desorbed $2\text{NaBH}_4+\text{MgH}_2$ system. This particular MgB_2 organization mirrors the anisotropic nature of the material which results in a restricted growth of the MgB_2 particles along the c-axis. The SEM and TEM analyses in section 3.4.2.4 show a size distribution of the MgB_2 plates which is in the range few hundreds

of nm to $\sim 2\mu\text{m}$. This wide range of the MgB_2 particle size distribution may be qualitatively explained by the presence of a temperature gradient ^[60]. In fact as supposed above, the formation of MgB_2 occurs in two different temperature regimes. It starts upon heating at roughly $400\text{ }^\circ\text{C}$ (figure 3.26) and then it continues later at a final temperature of $450\text{ }^\circ\text{C}$.

For the materials annealed under hydrogen and those exposed to moistened atmosphere, the NaBH_4 decomposition is followed by the formation of an amorphous background which is visible in the SR-PXD patterns shown in figure 3.29 and 3.40. Likely, the formation of the amorphous background is caused by the reaction of NaH (produced from NaBH_4 decomposition) and NaBH_4 , leading to the NaH-NaBH_4 molten phase as previously described in the sections 3.1-3.3. This assumption is confirmed by the presence of a nonlinear trend between the disappearing of the Mg and the formation of MgB_2 observed in the temperature range of 350 to $400\text{ }^\circ\text{C}$ (figure 3.30). The DSC trace A (figure 3.26) shows two further endothermic signals with onset temperatures at 450 and $475\text{ }^\circ\text{C}$ respectively, both associated with release of hydrogen (see figure 3.26 B). Considering that the peak with onset at $450\text{ }^\circ\text{C}$ (figure 3.26 A) appears rather narrow and the associated amount of released hydrogen is small, we assume this signal to result from the melting of the still present NaBH_4 . The signal starting at $475\text{ }^\circ\text{C}$ involves a considerable release of hydrogen. This is most probably due to the decomposition of the molten NaBH_4 . It is known from literature that NaBH_4 melts at $505\text{ }^\circ\text{C}$ and decomposes at temperatures above $600\text{ }^\circ\text{C}$ ^[47, 62] (hydrogen pressure 1-10 bar), therefore, it can be concluded that the presence of free Mg not only lowers the melting temperature of NaBH_4 but reacting with the molten NaBH_4 it also decreases the NaBH_4 decomposition temperature.

It is well established that the decomposition reaction of various metal borohydrides ($\text{M}(\text{BH}_4)_n$) is often followed by the formation of stable of boron and hydrogen containing species as $[\text{B}_{12}\text{H}_{12}]^{2-}$ ^[38, 63-65]. Based on the volumetric measurements and MAS NMR analysis performed on the partially decomposed $2\text{NaBH}_4+\text{MgH}_2$ samples collected in this work the formation of B-containing species different from MgB_2 seems not likely. However, further analyses are needed in order to give a more accurate answer to this issue.

It follows from the above led discussion that for the composite system $2\text{NaBH}_4+\text{MgH}_2$ the hydrogen desorption reaction can be summarized in the following scheme (figure 4.9):

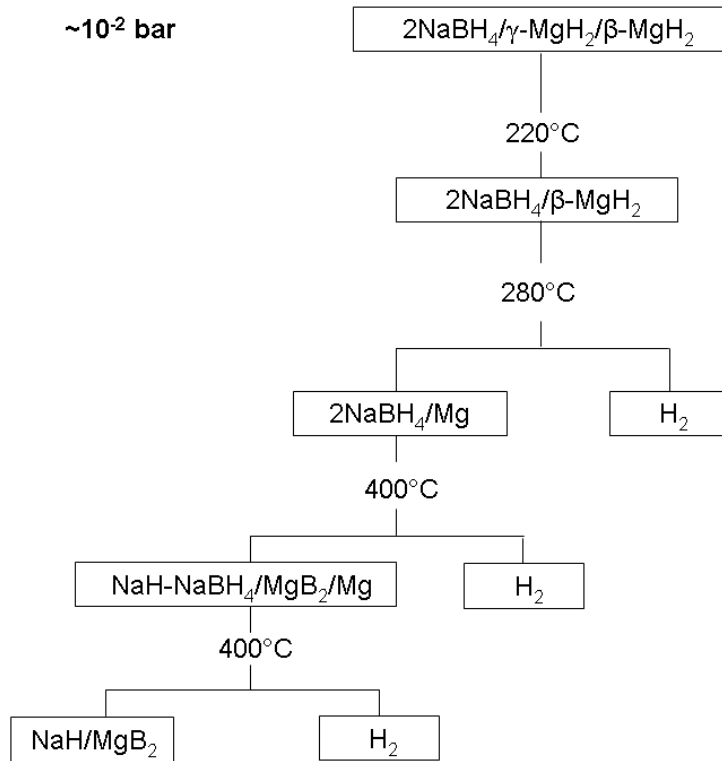


Figure 4.9: Hydrogen desorption reaction scheme of the system $2\text{NaBH}_4+\text{MgH}_2$ under static vacuum condition ($\sim 10^{-2}$ bar).

4.2.1 Hydrogen treatment effect

In section 3.4.2 the considerable influence of the heat-hydrogen treatment (one hour at $300\text{ }^\circ\text{C}$ and 50 bar H_2) on the desorption kinetic of the composite system $2\text{NaBH}_4+\text{MgH}_2$ was reported. However, although the beneficial effects which this treatment entails are evident, there is no clear explanation for this behavior. In order to understand this phenomenon the heat-hydrogen treatment of the as milled material was characterized by in-situ SR-PXD measurements (figure 4.10 a and 4.10 b). The reflections in figure 4.10 collected at room

temperature are associated to the presence of NaBH_4 , $\beta\text{-MgH}_2$, $\gamma\text{-MgH}_2$ and MgO in the starting material. During the heating, the $\gamma\text{-MgH}_2$ is observed to be stable in the range of RT to 220 °C, whereas in the range 220-290 °C it completely disappears. Coupled with the $\gamma\text{-MgH}_2$ disappearance the intensity of the $\beta\text{-MgH}_2$ peaks sensibly increases (figure 4.10 a), thus indicating a complete conversion of the $\gamma\text{-MgH}_2$ into $\beta\text{-MgH}_2$ (see figure 4.10 b). A further consequence of the treatment at 300 °C comes to light from the Rietveld's analysis of the material before and after the treatment. This analysis shows a crystallite size increment of both NaBH_4 and MgH_2 due to the annealing from 105 to 130 nm and from 17 to 55 nm respectively.

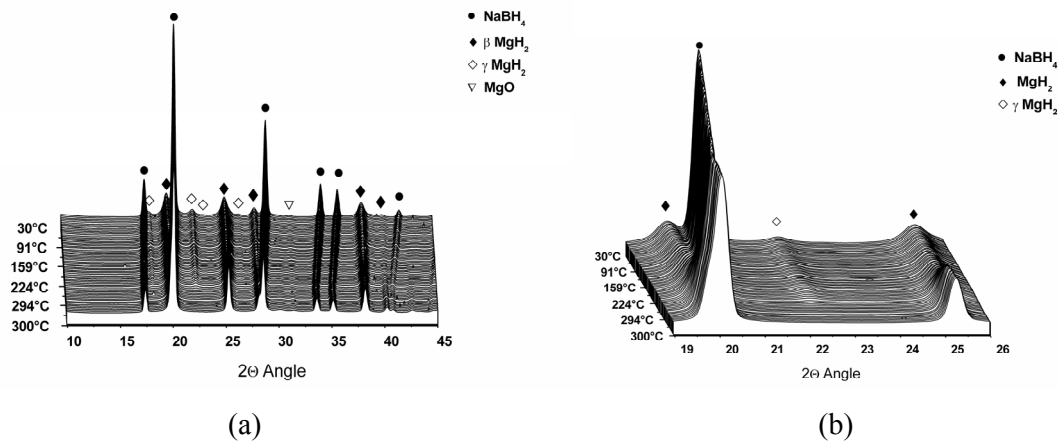


Figure 4.10: Series of SR-PXD patterns of the $2\text{NaBH}_4+\text{MgH}_2$ heat-hydrogen treatment, performed under 50 bar hydrogen pressure heating the sample from RT to 300 °C (5 °C/min, wavelength = 0.109719 nm). The measurement was obtained at the beamline I711 at the Max II synchrotron in Lund.

There are two different mechanisms which can cause an improvement of the sorption properties.

Nucleation of new phases is often dominated by defect sites ^[66-69]. During the $\gamma\rightarrow\beta$ phase transformation the volume of the involved MgH_2 increases by 1.6 % ^[70]. This volume expansion leads to the formation of additional defects in the heat-hydrogen treated material which might act as heterogeneous nucleation sites.

The presence of passivating oxide/hydroxide layers on the particle surfaces and especially at the interphases can act as diffusion barrier between MgH_2 and NaBH_4 . Although

the material was stored under continuously purified argon atmosphere, the presence of a thin passivating oxide layer like NaB_2O on top of the NaBH_4 particles cannot be avoided. Recently, the conversion of NaB_2O in NaBH_4 has been the object of several studies ^[71-74]. In particular the reaction between NaBO_2 and Mg or MgH_2 to form NaBH_4 and MgO has been investigated. In this process MgH_2 was used as reducing agent to produce NaBH_4 from NaBO_2 . This reaction was reported to have a high yield either if it is performed by mechanical milling in inert atmosphere or annealing in H_2 atmosphere. Based on these works, it is possible to imagine a conversion of the NaBO_2 layers present at the surface of the NaBH_4 particle into fresh NaBH_4 and MgO as possible effect of the annealing in hydrogen atmosphere.

4.2.2 Exposure to the moist atmosphere effect

In this section the effects of exposing the milled material to moistened atmosphere are discussed. Aiming to understand the possible reasons which lay behind the $2\text{NaBH}_4+\text{MgH}_2$ sorption properties enhancement, a brief discussion on the reactivity of the single components towards the water is necessary. In recent years, due to the possibility to generate hydrogen with purity meeting the standard necessary for fuel cells applications, the hydrolysis reactions of several hydrides with NaBH_4 ^[75-81] and MgH_2 ^[82-85] being among the most important were investigated. From these studies we know that magnesium hydride partially reacts with the water to form $\text{Mg}(\text{OH})_2$ and hydrogen. This reaction is hindered by the formation of a protective $\text{Mg}(\text{OH})_2$ layer which preserves the material from further reacting ^[86, 87]. However, as previously mentioned in section 3.4.1.1, the MgH_2 particles in the system $2\text{NaBH}_4+\text{MgH}_2$ appear to be surrounded by NaBH_4 . This results in a not direct exposure of MgH_2 to the moistened atmosphere.

NaBH_4 , on the other hand, reacts slowly with the water forming a hydrate which decomposes in sodium metaborate and hydrogen with a rate which depends on several factors such as pH value, temperature and the presence of selected catalysts. For example an un-catalyzed solution of NaBH_4 has a half life time of 430 days if kept at 25 °C and pH 14, whereas at low pH (e.g. < 7) it has a half life time of a few minutes only ^[81]. However, as clearly visible in

the in the MAS NMR analysis of figure 3.37 and in the situ SR-PXD patterns of figure 3.40 the limited amount of water to which the composite system $2\text{NaBH}_4+\text{MgH}_2$ was exposed and the reduced exposure time did not lead to a detectable degradation of the reactants. In spite of the apparently unchanged chemical state of the reactants, significant morphological and microstructural differences are observed. From the Rietveld's analysis of the diffraction pattern shown in figure 3.38 b (section 3.4.3.3) a progressive growth of the NaBH_4 crystallite size linked to the increasing exposure time is observed. In addition the material morphology (figure 3.38 A) appears deeply changed in respect to the as milled material (figure 3.24). These two main effects are due to the progressive moisturizing and formation of a NaBH_4 slurry, which involves an increasing portion of material exposed to the moistened atmosphere. Then, during the drying procedure subsequent to the material "soaking", the fraction of NaBH_4 in slurry form re-crystallizes with structural properties depending on the exposure time and applied drying conditions.

In solid-solid reactions the nature of the contact between reactants is of crucial importance for the reaction to establish a stable growth. Differently from solid-liquid, solid-gas etc. where one reactant is immersed in a flow partner, in the solid-solid reaction the reactants are in a stagnant state. Consequently, whereas for heterogeneous reactions the interface area reaches the possible maximum value, in the solid-solid reaction the effective contact area is restricted only to the contact points between reactants. The exposure of the system $2\text{NaBH}_4+\text{MgH}_2$ to the moistened atmosphere leads to a partial reproduction of the contact conditions encountered by the reactants in solid-liquid reactions. In fact, whereas MgH_2 remains solid for the whole length of the treatment, the slurry of NaBH_4 formed as a consequence of the NaBH_4 moisturizing "wets" the surface of the MgH_2 particles. Then, these advanced interface conditions are conserved in the solid state during the drying procedure. In spite of several attempts, the characterization of the NaBH_4 - MgH_2 interface area by transmission electron microscopy (TEM) has not been possible. In fact the instability of the material during long time exposure to the electron beam leads to the decomposition of the specimens before acquiring significant information. Few attempts of characterizing the material surface were also carried out by X-ray photoelectron spectroscopy (XPS). However, the impossibility to transfer the material to the XPS apparatus completely avoiding the air contamination nullifies all the efforts. At this point, considering the data presented in thesis, the key factor to explain the sorption properties enhancement is the achieved advanced

interface conditions between MgH_2 and NaBH_4 . At the best of our knowledge this is the first time that the possibility to enhance the effective contact area between reactants by dissolution and re-crystallization of one or more selected compounds is reported in literature. These results demonstrate a novel approach to significantly improve the kinetic of hydrogen storage material.

Recently several articles regarding the sorption properties of the system $2\text{NaBH}_4+\text{MgH}_2$ were published by Garroni et al. ^[31, 59] and Mao et al. ^[48]. In these works they reported the possibility to completely desorb the system $2\text{NaBH}_4+\text{MgH}_2$ to Na and MgB_2 under static vacuum (initial pressure 10^{-1} bar) and 450°C . Clearly these findings contrast with the results presented in this thesis. However, a possible explanation can be found in the different ball milling procedure followed in the different laboratories. Whereas in the case of this PhD work the whole material handling and milling was carried out inside a glovebox under continuously purified argon atmosphere, milling apparatuses used by Garroni et al. and Mao et al. were placed outside the glove box. Therefore, it is likely that the material was contaminated by oxygen and moisture during the milling. This hypothesis is supported by the marked presence of MgO in their diffraction patterns. Although as discussed in section 3.4.1.4 MgO appears not to influence the $2\text{NaBH}_4+\text{MgH}_2$ sorption properties, the contamination by the moisture clearly does. This explains the difference between the $2\text{NaBH}_4+\text{MgH}_2$ sorption properties measured in the different laboratories.

5 Outlook

One of the aims of this work was to study the system NaH-MgH₂ in order to contribute to the fundamental understanding of the sorptive properties of the reactive hydride composites based on MgB₂ (i.e. LiH-MgB₂ and CaH₂-MgB₂). As conclusion of this work, it is possible to state that a direct transfer of knowledge between different reactive hydride composites appears difficult. In fact, the nature of the phases involved in the absorption and desorption reactions (e.g. alkali hydrides, complex hydrides, materials in the elemental state), their reactivity and stability are too different to be synthesized in a single general scheme. However, some of the features observed for the system NaH-MgB₂ are common to the other systems. These features will be discussed hereunder.

In this work the effect of the applied conditions (hydrogen pressure and temperature) on the absorption reaction of the system NaH-MgB₂ was deeply investigated (section 3.2 and 4.1.2). It was observed that the formation of intermediate phases or undesired side products is tightly related to the applied hydrogen pressure. This aspect is of great importance because often the overall sorption properties of a system depend on the formation of such phases (i.e. NaMgH₃ and NaH-NaBH₄ molten phase). A clear example is the effect of the applied hydrogen pressure on the formation of MgB₂ during the desorption of the system LiBH₄-MgH₂. The use of specific hydrogen pressure and temperature conditions is therefore necessary in order to direct the course of the absorption and desorption reactions of the reactive hydride composites toward the formation of the desired products. For reaction which involves the formation of several intermediate phases as in the case of NaH-MgB₂, the use of a multi-step pressure temperature process should be considered.

It is well established that the steadiness of the material composition upon cycling is one of the major requirements for the applicability of the reactive hydride composites as reversible hydrogen storage materials. In section 3.1.1 it was reported that the composition in the batch of hydrogenated material was locally not homogeneous. In particular, the material at the top of the sample holder significantly differs in composition from that at the bottom (table 3.1). The same phenomenon was observed also in the desorption products of the system $2\text{NaBH}_4 + \text{MgH}_2$ by Garroni et al. ^[59]. These material inhomogeneities are most likely linked to the simultaneous coexistence of portions of material in the solid state and others in the liquid state during the absorption/desorption processes. Clearly the observed material disproportions do not impose severe cyclability limitations only to the system studied in this work, but it might also affect other reactive hydride composites systems, which during the absorption/desorption processes undergo formation of molten phases (e.g. $\text{LiBH}_4\text{-MgH}_2$). In addition, insight of a future implementation of the reactive hydride composites for onboard applications, the observed phenomena also raises serious security concerns. The tendency of the molten phases to occupy specific area of the container (as observed in section 3.1.1) might lead to an unexpected local stress concentration and consequent structural downfall of the container. The study of the material distribution in the hydrogen tank by techniques such as the tomography should be considered in the process of design and development of future reactive hydride composites tanks. In this direction, at the Helmholtz-Zentrum Geesthacht and at the University of Pavia, a systematic study of the sorption properties of the system NaH-MgB_2 in relation to the material microstructure and phase distributions is carried out. Special emphasis is also put on the study of the cyclability of the material. The compositions under investigation are 2NaH/MgB_2 , 1.5NaH/MgB_2 , NaH/MgB_2 , 0.5NaH/MgB_2 . A second step of this work will involve the optimization of the material properties by the addition of suitable additives.

In section 3.3 and 4.1 the effect of the NaH/MgB_2 ratio on the absorption properties of the system NaH-MgB_2 was discussed. It was observed that moving from the ideal NaH/MgB_2 ratio of 2:1 to the ratio 0.5:1, the hydrogenation reaction proceeds further toward the formation of the absorption products NaBH_4 and MgH_2 . Recently, Garroni et al. ^[59] studied the effect of the starting reactant ratio on the desorption properties of the system $\text{NaBH}_4/\text{MgH}_2$. The $\text{NaBH}_4/\text{MgH}_2$ ratios investigated in Garroni's work were 2:1 and 0.5:1.

As conclusion of this study they reported that the desorption reaction in the MgH_2 -rich system (composition 0.5:1) was sensibly faster than that of the NaBH_4 -rich system (composition 2:1).

Due to the NaMgH_3 , NaH-NaBH_4 molten phase formation and consequent impossibility to achieve the theoretical hydrogen storage capacity upon absorption, the NaH-MgB_2 systems with a NaH/MgH_2 ratio higher than 2:1 were not investigated. However, among the NaH rich systems $3\text{NaH}+\text{MgB}_2$ appears promising. Assuming the formation of two moles of NaBH_4 and one mole of NaMgH_3 as the only absorption products, this system has a theoretical gravimetric hydrogen capacity of 6.4 wt.%. Based on the thermodynamic data reported on the HSC Chemistry 6.12 database it is possible to calculate for this system an equilibrium pressure of 1 bar H_2 at 320 °C (30 °C lower than that of the system 2NaH/MgB_2). This temperature value is particularly interesting because it lies well below the observed melting point of the NaH-NaBH_4 eutectic mixture (383 °C). Therefore it might be possible to perform both absorption and desorption measurements avoiding the kinetic constraints related to the formation of the eutectic molten phase.

The ratio of the starting reactants appears to be an important factor also for the other systems. Price et al. ^[34] demonstrated that the stoichiometry of the $\text{LiBD}_4\text{-MgD}_2$ mixtures plays an important role in the desorption reaction pathway and cyclability of the system. The effect of the stoichiometry on the sorption properties of the reactive hydride composites is mostly connected to the mass transport and formation of diffusion barriers at the interface between reactants (e.g. layers of hydrogenated products, encapsulation of the reactants within stable side products). Thus, similar behaviours are likely to be found also in other systems (e.g. $\text{Ca}(\text{BH}_4)_2\text{-MgH}_2$, $\text{CaH}_2\text{-CaB}_6\text{-Mg}$ and etc.).

The critical role of the contact area between reactants in the desorption reaction of the system $2\text{NaBH}_4+\text{MgH}_2$ was previously discussed (see section 4.2.2). The initial contact conditions between NaBH_4 and MgH_2 were improved taking advantage of the fact that NaBH_4 , when exposed to a moist atmosphere, forms a slurry which “wets” the surface of the MgH_2 particles. These enhanced contact conditions were then conserved in the solid state by drying procedure. The crucial aspect of this method is that the contact conditions encountered by the reactants in solid–liquid systems can be partially reproduced in a solid system. In section 4.1 the occurrence of a eutectic melting between NaH and NaBH_4 was reported. Formations of eutectic melting are known to take place in several hydride/borohydride and borohydride mixtures (e.g. NaH-KBH_4 , KH-KBH_4 , $\text{KBH}_4\text{-LiBH}_4$, $\text{KBH}_4\text{-NaBH}_4$, $\text{NaBH}_4\text{-$

LiBH₄, LiBH₄-Mg(BH₄)₂, LiBH₄-Ca(BH₄)₂ and etc.). At the light of the previously discussed results, the targeted employment of eutectic hydride/borohydride or borohydride mixtures might result in an efficient method for increasing the contact between reactants *in situ*. In fact, the addition of a small amount of a selected borohydride to hydride mixtures such as 2NaBH₄+MgH₂, 2LiBH₄+MgH₂ and Ca(BH₄)₂+MgH₂ would lead to the liquefaction of a fraction of material already at low temperature. The presence of the eutectic melt at the interface will ensure a better contact between borohydride and MgH₂/Mg particles and will facilitate the diffusion of the B-containing species in the material.

6 Summary

In the present work, the sorption properties of the composite system $2\text{NaBH}_4+\text{MgH}_2$ were investigated in detail. This system, due to the exothermic formation of MgB_2 alongside with the NaBH_4 decomposition shows a reduced desorption reaction enthalpy in respect to pure NaBH_4 , while the gravimetric hydrogen capacity of the system remains high (7.8 wt.%). Although this system, due to the still high reaction enthalpy is considered not suitable for automotive purpose, its study is of primary importance for understanding the key parameters which influence the sorption properties of the Reactive Hydride Composite.

The absorption measurements performed on the system $2\text{NaH}+\text{MgB}_2$ revealed a marked dependence of the sorption process on the applied hydrogen pressure at which the experiment is carried out. For an applied hydrogen pressure of 50, 25 and 5 bar two different multi-step reaction mechanisms were observed. In particular, at 50 and 25 bar the formation of NaBH_4 was preceded by the appearance of an unknown crystalline hydride phase containing Na, B and hydrogen, NaMgH_3 , amorphous boron, unidentified B-containing phases and a molten NaH-NaBH_4 salt mixture. The application of just 5 bar H_2 led first to the formation of the NaH-NaBH_4 molten salt mixture and then of NaBH_4 . For all the investigated experimental conditions it was not possible to observe MgH_2 among the final absorption products, instead NaMgH_3 and free Mg were found. Due to the complexity of the NaH-MgB_2 absorption and desorption process, the determination of thermodynamic and kinetic boundary conditions for all the observed phases was not possible. However, the formations of NaMgH_3 and of the NaH-NaBH_4 molten salt mixtures were unambiguously explained. Based on the assumption that NaMgH_3 is formed by direct reaction between NaH and MgH_2 ^[49], a further absorption measurement was performed. The hydrogen pressure and temperature chosen for this experiment were those at which the MgH_2 formation is thermodynamically not possible, but where NaMgH_3 is stable. The applied conditions were 450 °C and 20 bar of hydrogen pressure. For this measurement the diffraction pattern of the synthesized material showed the presence of NaBH_4 , Mg, NaH, MgB_2 and only of a tiny amount of NaMgH_3 most likely

formed during cooling. These results confirm that NaMgH_3 is formed by reaction between MgH_2 and NaH . Moreover they indicate that the kinetic boundary conditions for the NaMgH_3 formation in this system are identical to the thermodynamic boundary conditions of MgH_2 . In addition, based on the Sievert's and ex situ X-ray diffraction measurements it was possible to state that the formation of NaMgH_3 has a detrimental effect on the absorption reaction. In fact, on the one hand it removes NaH from the system, which is not available for forming NaBH_4 and on the other hand it appears to slow down the reaction process. To better explain the effect of NaMgH_3 on the absorption reaction a depictive model was reported. Regarding the observed formation of the NaH - NaBH_4 molten salts mixture it was found that it takes place independently from the applied hydrogen pressure at a fixed temperature (383 °C for a 1:1 NaH - NaBH_4 mixture). This finding not only confirms that the formation of a liquid phase during absorption involves only NaH and NaBH_4 , but also suggests the possibility of eutectic melting between these two components. The formation of this molten salt phase entails a drastic reduction of the hydrogen diffusion into the system. This behavior was explained by both the ionic character of the molten phase and by the possibility of an organization of the B-H units different from the classic $[\text{BH}_4]^-$.

The absorption process of the NaH - MgB_2 composite at the hydrogen pressure of 50 bar was also investigated as a function of the NaH - MgB_2 ratio. In particular the compositions $1.5\text{NaH}/\text{MgB}_2$, $1\text{NaH}/\text{MgB}_2$ and $0.5\text{NaH}/\text{MgB}_2$ were studied. It was observed that reducing the amount of NaH in the system NaH - MgB_2 the onset temperatures of the absorption reaction were sensibly lowered. Moreover, a further consequence of the NaH content decrement is the prosecuting of the hydrogen absorption reaction towards the formation of NaBH_4 and MgH_2 . This reduces the formation of NaMgH_3 and the NaH - NaBH_4 molten salts phase.

As for the hydrogen absorption, also the desorption reaction is a multi-step process. For the as milled $2\text{NaBH}_4+\text{MgH}_2$, based on the volumetric and *in situ* SR-PXD analysis performed under static vacuum condition ($\sim 10^{-2}$ bar) at a final temperature of 450 °C, it is possible to observe the decomposition of the only MgH_2 phases. However, although not visible in the SR-PXD measurements, the combined DSC-MS analysis suggests for this material also a restricted MgB_2 nucleation, which most likely takes place at the Mg - NaBH_4 interfaces.

Considerable kinetic improvements were achieved by pre-treating the as milled material at 300 °C in hydrogen atmosphere. For this material, differently from the as milled one, the desorption of an amount of hydrogen equal to 7.8 wt.% was achieved through a two steps desorption reaction. The first step starts at roughly 340 °C and involves the release of hydrogen from the only MgH₂, whereas the second step leads to the complete NaBH₄ decomposition and subsequent MgB₂ formation. Associated to this last reaction step the formation of a liquid phase was observed. As for the absorption reaction, likely this liquid phase contains initially a molten salt mixture of NaH and NaBH₄. No formation of stable [B₁₂H₁₂]⁻ containing species was observed to follow the decomposition of NaBH₄. The beneficial effect of the heat-hydrogen treatment is the improved contact between particles, achieved as a consequence of the $\gamma \rightarrow \beta$ -MgH₂ conversion. Further explanations involve the reduction of the Mg(OH)₂ layer present at the topmost surface layer of the magnesium hydride particles, and the possible formation of MgB₂ nucleation base.

In this work the possibility to improve the desorption reaction by an innovative method of enhancing the effective contact area between reactants is also proposed. This method was based on the kinetic enhancement observed for the desorption reaction of the system 2NaBH₄+MgH₂ exposed for increasing time to a moistened atmosphere. This method opens a new path for the kinetic enhancement of multi-compound reaction in the solid state.

7 Bibliography

- [1] I. E. Agency, **2004**.
- [2] K. Aleklett, M. Hook, K. Jakobsson, M. Lardelli, S. Snowden, B. Soderbergh, *Energy Policy* **2008**, *38*, 1398.
- [3] R. Monastersky, *Nature* **2009**, *458*, 1091.
- [4] G. Schmidt, D. Archer, *Nature* **2009**, *458*, 1117.
- [5] T. Graham, *Philosophical Transactions of the Royal Society* **1866**, *32*, 401.
- [6] L. Schlapbach, A. Seiler, F. Stucki, H. C. Siegmann, *Journal of the Less-Common Metals* **1980**, *73*, 145.
- [7] C. M. Stander, *Zeitschrift Fur Physikalische Chemie-Frankfurt* **1977**, *104*, 229.
- [8] C. M. Stander, *Journal of Inorganic & Nuclear Chemistry* **1977**, *39*, 221.
- [9] B. Vigeholm, J. Kjoller, B. Larsen, A. S. Pedersen, *Journal of the Less-Common Metals* **1983**, *89*, 135.
- [10] J. Huot, G. Liang, S. Boily, A. Van Neste, R. Schulz, *Journal of Alloys and Compounds* **1999**, *293*, 495.
- [11] N. Hanada, T. Ichikawa, H. Fujii, *Journal of Physical Chemistry B* **2005**, *109*, 7188.
- [12] M. Yamauchi, R. Ikeda, H. Kitagawa, M. Takata, *Journal of Physical Chemistry C* **2008**, *112*, 3294.
- [13] S. Kishore, J. A. Nelson, J. H. Adair, P. C. Eklund, *Journal of Alloys and Compounds* **2005**, *389*, 234.
- [14] A. Pundt, C. Sachs, M. Winter, M. T. Reetz, D. Fritsch, R. Kirchheim, *Journal of Alloys and Compounds* **1999**, *293*, 480.
- [15] R. J. Wolf, M. W. Lee, J. R. Ray, *Physical Review Letters* **1994**, *73*, 557.

- [16] B. Bogdanovic, M. Schwickardi, *Journal of Alloys and Compounds* **1997**, 253, 1.
- [17] P. Chen, Z. T. Xiong, J. Z. Luo, J. Y. Lin, K. L. Tan, *Nature* **2002**, 420, 302.
- [18] A. Zuttel, A. Borgschulte, S. I. Orimo, *Scripta Materialia* **2007**, 56, 823.
- [19] A. Stock, in *Hydrides of Boron and Silicon*, Cornell University Press, Ithaca, New York, **1933**.
- [20] A. Stock, C. Nassenz, *Berichte* **1912**, 45.
- [21] T. N. Dymova, Y. M. Dergachev, V. A. Sokolov, N. A. Grechanaya, *Doklady Akademii Nauk Sssr* **1975**, 224, 591.
- [22] T. N. Dymova, N. G. Eliseeva, S. I. Bakum, Dergache.Ym, *Doklady Akademii Nauk Sssr* **1974**, 215, 1369.
- [23] J. J. Reilly, R. H. Wiswall, *Inorganic Chemistry* **1968**, 7, 2254.
- [24] P. Chen, Z. Xiong, J. Luo, J. Lin, K. L. Tan, *Nature* **2002**, 420, 302.
- [25] J. J. Vajo, F. Mertens, C. C. Ahn, R. C. Bowman, B. Fultz, *The Journal of Physical Chemistry B* **2004**, 108, 13977.
- [26] G. Barkhordarian, T. Klassen, M. Dornheim, R. Bormann, *Journal of Alloys and Compounds* **2007**, 440, L18.
- [27] J. Urgnani, F. J. Torres, M. Palumbo, M. Baricco, *International Journal of Hydrogen Energy* **2008**, 33, 3111.
- [28] A. F. Gross, J. J. Vajo, S. L. Van Atta, G. L. Olson, *The Journal of Physical Chemistry C* **2008**, 112, 5651.
- [29] S. Y. Zheng, F. Fang, G. Y. Zhou, G. R. Chen, L. Z. Ouyang, M. Zhu, D. L. Sun, *Chemistry of Materials* **2008**, 20, 3954.
- [30] C. Liu, F. Li, L. P. Ma, H. M. Cheng, *Advanced Materials* **2010**, 22, E28.
- [31] S. Garroni, C. Pistidda, M. Brunelli, G. B. M. Vaughan, S. Surinach, M. D. Baro, *Scripta Materialia* **2009**, 60, 1129.
- [32] J. J. Vajo, G. L. Olson, *Scripta Materialia* **2007**, 56, 829.
- [33] U. Bosenberg, S. Doppiu, L. Mosegaard, G. Barkhordarian, N. Eigen, A. Borgschulte, T. R. Jensen, Y. Cerenius, O. Gutfleisch, T. Klassen, M. Dornheim, R. Bormann, *Acta Materialia* **2007**, 55, 3951.

- [34] T. E. C. Price, D. M. Grant, V. Legrand, G. S. Walker, *International Journal of Hydrogen Energy* **2010**, *35*, 4154.
- [35] Y. Cerenius, K. Stahl, L. A. Svensson, T. Ursby, A. Oskarsson, J. Albertsson, A. Liljas, *Journal of Synchrotron Radiation* **2000**, *7*, 203.
- [36] B. S. Clausen, G. Steffensen, B. Fabius, J. Villadsen, R. Feidenhansl, H. Topsoe, *Journal of Catalysis* **1991**, *132*, 524.
- [37] J. A. Rodriguez, J. C. Hanson, A. I. Frenkel, J. Y. Kim, M. Perez, *Journal of the American Chemical Society* **2002**, *124*, 346.
- [38] S.-J. Hwang, R. C. Bowman, J. W. Reiter, Rijssenbeek, G. L. Soloveichik, J.-C. Zhao, H. Kabbour, C. C. Ahn, *The Journal of Physical Chemistry C* **2008**, *112*, 3164.
- [39] G. L. Soloveichik, Y. Gao, J. Rijssenbeek, M. Andrus, S. Kniajanski, R. C. Bowman, S. J. Hwan, J. C. Zhao, *International Journal of Hydrogen Energy* **2009**, *34*, 916.
- [40] J. C. Zhao, D. A. Knight, G. M. Brown, C. Kim, S. J. Hwang, J. W. Reiter, R. C. Bowman, J. A. Zan, J. G. Kulleck, *Journal of Physical Chemistry C* **2009**, *113*, 2.
- [41] A. E. Bennett, C. M. Rienstra, M. Auger, K. V. Lakshmi, R. G. Griffin, *Journal of Chemical Physics* **1995**, *103*, 6951.
- [42] A. San-Martin, F. D. Manchester, in *Phase Diagrams of Binary Magnesium Alloys* (Eds.: N.-H. A.A, C. J.B.), ASM International, **1999**, pp. 142.
- [43] G. Barkhordarian, T. R. Jensen, S. Doppiu, U. Bosenberg, A. Borgschulte, R. Gremaud, Y. Cerenius, M. Dornheim, T. Klassen, R. Bormann, *The Journal of Physical Chemistry C* **2008**, *112*, 2743.
- [44] <http://csrri.iit.edu/periodic-table.html>.
- [45] R. Caputo, **2010**.
- [46] A. San-Martin, F. D. Manchester, *Journal of Phase Equilibria* **1990**, *11*, 287.
- [47] D. S. Stasinevich, G. A. Egorenko, *Russian Journal of Inorganic Chemistry* **1968**, *13(3)*, 341.
- [48] J. F. Mao, X. B. Yu, Z. P. Guo, H. K. Liu, Z. Wu, J. Ni, *Journal of Alloys and Compounds* **2009**, *479*, 619.
- [49] K. Ikeda, Y. Nakamori, S. Orimo, *Acta Materialia* **2005**, *53*, 3453.
- [50] K. Zeng, T. Klassen, W. Oelerich, R. Bormann, *International Journal of Hydrogen Energy* **1999**, *24*, 989.

- [51] K. Ikeda, Y. Kogure, Y. Nakamori, S. Orimo, *Scripta Materialia* **2005**, *53*, 319.
- [52] D. T. Shane, R. L. Corey, R. C. Bowman, R. Zidan, A. C. Stowe, S. J. Hwang, C. Kim, M. S. Conradi, *Journal of Physical Chemistry C* **2009**, *113*, 18414.
- [53] Y. Kim, D. Reed, Y.-S. Lee, J.-H. Shim, H. N. Han, D. Book, Y. W. Cho, *Journal of Alloys and Compounds* **2010**, *492*, 597.
- [54] D. T. Shane, R. C. Bowman, M. S. Conradi, *Journal of Physical Chemistry C* **2009**, *113*, 5039.
- [55] R. L. Corey, D. T. Shane, R. C. Bowman, M. S. Conradi, *Journal of Physical Chemistry C* **2008**, *112*, 18706.
- [56] A. Borgschulte, A. Züttel, P. Hug, A. M. Racu, J. Schoenes, *Journal of Physical Chemistry A* **2008**, *112*, 4749.
- [57] A. Remhof, Z. Lodziana, F. Buchter, P. Martelli, F. Pendolino, O. Friedrichs, A. Züttel, J. P. Embs, *Journal of Physical Chemistry C* **2009**, *113*, 16834.
- [58] T. Czujko, R. A. Varin, Z. Wronski, Z. Zaranski, T. Durejko, *Journal of Alloys and Compounds* **2007**, *427*, 291.
- [59] S. Garroni, C. Milanese, A. Girella, A. Marini, G. Mulas, E. Menéndez, C. Pistidda, M. Dornheim, S. Suriñach, M. D. Baró, *International Journal of Hydrogen Energy, In Press, Corrected Proof*.
- [60] S. Lee, *Physica C-Superconductivity and Its Applications* **2003**, *385*, 31.
- [61] U. Bosenberg, J. W. Kim, D. Gossler, N. Eigen, T. R. Jensen, J. M. B. von Colbe, Y. Zhou, M. Dahms, D. H. Kim, R. Gunther, Y. W. Cho, K. H. Oh, T. Klassen, R. Bormann, M. Dornheim, *Acta Materialia* **2010**, *58*, 3381.
- [62] S. Orimo, Y. Nakamori, A. Züttel, *Materials Science and Engineering B* **2004**, *108*, 51.
- [63] J. E. Huheey, E. A. Keiter, R. Keiter, *Inorganic Chemistry* 4th ed., HarperCollins Publishers, **1993**.
- [64] A. R. Pitochelli, F. M. Hawthorne, *Journal of the American Chemical Society* **1960**, *82*, 3228.
- [65] N. Ohba, K. Miwa, M. Aoki, T. Noritake, S.-i. Towata, Y. Nakamori, S.-i. Orimo, A. Züttel, *Physical Review B* **2006**, *74*, 075110.
- [66] J. H. Harding, A. M. Stoneham, J. A. Venables, *Physical Review B* **1998**, *57*, 6715.

- [67] G. Haas, A. Menck, H. Brune, J. V. Barth, J. A. Venables, K. Kern, *Physical Review B* **2000**, *61*, 11105.
- [68] J. A. Venables, L. Giordano, J. H. Harding, *Journal of Physics-Condensed Matter* **2006**, *18*, S411.
- [69] J. A. Venables, J. H. Harding, *Journal of Crystal Growth* **2000**, *211*, 27.
- [70] P. Vajeeston, P. Ravindran, A. Kjekshus, H. Fjellvag, *Physical Review Letters* **2002**, *89*.
- [71] C.-L. Hsueh, C.-H. Liu, B.-H. Chen, C.-Y. Chen, Y.-C. Kuo, K.-J. Hwang, J.-R. Ku, *International Journal of Hydrogen Energy* **2009**, *34*, 1717.
- [72] Y. Kojima, T. Haga, *International Journal of Hydrogen Energy* **2003**, *28*, 989.
- [73] S. Suda, N. Morigasaki, Y. Iwase, Z. P. Li, *Journal of Alloys and Compounds* **2005**, *404-406*, 643.
- [74] Z. P. Li, B. H. Liu, J. K. Zhu, N. Morigasaki, S. Suda, *Journal of Alloys and Compounds* **2007**, *437*, 311.
- [75] S. C. Amendola, S. L. Sharp-Goldman, M. S. Janjua, N. C. Spencer, M. T. Kelly, P. J. Petillo, M. Binder, *International Journal of Hydrogen Energy* **2000**, *25*, 969.
- [76] R. E. Davis, *Journal of the American Chemical Society* **1962**, *84*, 892.
- [77] U. B. Demirci, O. Akdim, J. Andrieux, J. Hannauer, R. Chamoun, P. Miele, *Fuel Cells* **2010**, *10*, 335.
- [78] R. Fernandes, N. Patel, A. Miotello, *Applied Catalysis B: Environmental* **2009**, *92*, 68.
- [79] K. N. Mochalov, K. V. Shifrin, A. S. Bogonostsev, *Zhurnal Fizicheskoi Khimii* **1963**, *37*, 2404.
- [80] N. Patel, R. Fernandes, A. Miotello, *Journal of Power Sources* **2009**, *188*, 411.
- [81] H. I. Schlesinger, H. C. Brown, A. E. Finholt, J. R. Gilbreath, H. R. Hoekstra, E. K. Hyde, *Journal of the American Chemical Society* **1953**, *75*, 215.
- [82] M. H. Grosjean, M. Zidoune, L. Roué, J. Y. Huot, *International Journal of Hydrogen Energy* **2006**, *31*, 109.
- [83] Y. Kojima, K. I. Suzuki, Y. Kawai, *Journal of Materials Science* **2004**, *39*, 2227.
- [84] J. P. Tessier, P. Palau, J. Huot, R. Schulz, D. Guay, *Journal of Alloys and Compounds* **2004**, *376*, 180.
- [85] R. A. Varin, S. Li, A. Calka, *Journal of Alloys and Compounds* **2004**, *376*, 222.

- [86] O. Friedrichs, J. C. Sánchez-López, C. López-Cartes, M. Dornheim, T. Klassen, R. Bormann, A. Fernández, *Applied Surface Science* **2006**, 252, 2334.
- [87] J. Huot, G. Liang, R. Schulz, *Journal of Alloys and Compounds* **2003**, 353, L12.